UNITED NATIONS EDUCATIONAL, SCIENTIFIC AND CULTURAL ORGANIZATION
INTERNATIONAL ATOMIC ENERGY AGENCY
INTERNATIONAL CENTRE FOR THEORETICAL PHYSICS
I.C.T.P., P.O. BOX 586, 34100 TRIESTE, ITALY, CABLE: CENTRATOM TRIESTE

H4.SMR/1058-4

WINTER COLLEGE ON OPTICS

9 - 27 February 1998

Guided Wave Optics on Silicon: Physics and Technology

B. P. Pal

Physics Department, Indian Institute of Technology Delhi, India

GUIDED WAVE OPTICS ON SILICON: PHYSICS AND TECHNOLOGY

Background material for the talks to be delivered at the Winter College on Optics, February 9-27, 1998 at ICTP, Trieste, Italy

BISHNU PAL*
PHYSICS DEPARTMENT
INDIAN INSTITUTE OF TECHNOLOGY DELHI
NEW DELHI 110 016
INDIA

* Fax : +91-11-686 2037/686 5039
email : bppal@physics.iitd.ernet.in

E. WOLF, PROGRESS IN OPTICS XXXII
1993 ELSEVIER SCIENCE PUBLISHERS B.V.

I

GUIDED-WAVE OPTICS ON SILICON: PHYSICS, TECHNOLOGY, AND STATUS*

BY

B. P. PAL**

Electromagnetic Technology Division,
National Institute of Standards and Technology,
325 Broadway,
Boulder, CO 80303, USA

CONTENTS

§ 1. Introduction

The aim of integrated optics is to combine discrete miniature components on a common substrate by means of optical waveguides, much like the integrated-circuit technology combines electronic devices on a single substrate. In fact, the term *integrated optics* was coined by Miller [1969] from this analogy. As an example, Miller proposed a miniature optical repeater that would use guided-wave optics to integrate an optical detector, an amplifier, and a light source on a common substrate. However, there is one essential difference between optical and electronic technologies. Integrated-optical circuits usually require a relatively large length-to-width ratio for a usable device. These are typically a few optical wavelengths in width, but several millimeters to centimeters in length (Papuchon [1986]). However, monolithic integration of several optical components requires key devices like source, detector, modulator, and switch all built around a single material. To fulfill these functions simultaneously, the material must

(i) possess a direct band gap,
(ii) exhibit strong absorption at the wavelengths of interest,
(iii) be optically active, and
(iv) have a large electro-optic or acousto-optic coefficient.

Since any such single material was unavailable in the 1970s, research and development efforts concentrated on a hybrid technology instead of a monolithic technology. In the hybrid technology, several guided-wave components are built around different materials and then assembled and operated as an integral system.

Integrated optics is also often generically, although somewhat loosely, used to refer to any discrete-device-like modulator, e.g., a directional coupler, which has been formed out of optical waveguides. The last two decades have witnessed demonstrations of a variety of guided-wave optical devices, such as wavelength division multiplexers/demultiplexers (Aiki, Nakamura and Umeda [1977]), spectrum analyzers (Mergerian, Malarkey, Pautienus, Bradley, Marx, Hutcheson and Kellner [1980], Thylen and Stensland [1982]), analog-to-digital converters (Taylor [1978], Leonberger, Woodward and Spears [1979], Chang and Tsai [1983]), digital correlators (Verber,

Kenan and Busch [1983]), switches and modulators (Schmidt and Alferness [1979]), directional couplers (Papuchon, Combemale, Mathieu, Ostrowsky, Reiber, Roy, Sejourne and Werner [1975], Schmidt and Alferness [1979]), filters (Schmidt and Alferness [1979], Alferness and Buhl [1982]), and signal samplers (Izutsu, Haga and Sueta [1983]). Those ranged from passive to active devices and were based on insulators such as $LiNbO_3$, glass, semiconductors like GaAs/AlGaAs, InGaAsP/InP, thin films of silica, or doped silica on silicon. Out of these, InGaAsP/InP offers a good choice for monolithic integration of several devices (Merz, Yuan and Vawter [1985]).

During the 1980s much effort was spent in realizing guided-wave optical components based on semiconductors, although the technologies based on $LiNbO_3$ (Korotky and Alferness [1987]) and glass (Findalky [1985], Ramaswamy and Srivastava [1988], Hashizume, Seki and Nakoma [1989], Nissim, Beguin, Jansen and Laborde [1989]) developed at a much faster pace. Since high-performance discrete devices are now available from these technologies, a question about the rationale behind integration is sometimes raised. The rationale for integration can be appreciated from the following example. Through a monolithic optoelectronic integrated circuit, a detector-amplifier can be connected with a capacitance as low as 0.2 pF as opposed to about 1 pF required by the combination of a discrete photodiode and a discrete amplifier (Carney and Hutcheson [1987]). This five-fold decrease in capacitance would yield a corresponding increase in detector bandwidth, since the RC time constant related bandwidth of a detector is given by $(2\pi RC)^{-1}$, where R and C represent the resistance and the capacitance of the detector circuit. Thus optical integration of different devices is expected to yield higher performance due to lower parasitic capacitances and inductances, and fewer interconnecting discrete components.

Furthermore, integration can achieve an increase in the density of functional devices and, often, a lower manufacturing cost. Considerable research activity in this direction recently has been concerned with integration of optical and electronic components on a single III–V semiconductor substrate such as GaAs and InP or ternary/quarternary compounds lattice-matched to these semiconductors and grown on these substrates. This has led to the emergence of optoelectronic integrated circuits (Koren [1989]) in which all optical and electronic functional components are built on a single substrate such as InP, GaAs, Si, Ge, or GaAs on Si.

A second option is a hybrid approach in which different functional units can be surface-mounted on a common substrate with guided-wave components as interconnections between them. Due to the maturity of the silicon technology, which is extensively used for forming large-scale and very large-scale integrated circuits in the area of microelectronics, silica on silicon is a good choice for such hybrid integration. The attractive features of silicon include the following:

- An established electronic substrate for integrated circuit technology. Thus, integrated optics on silicon is synergetic with microelectronics.
- Availability in excellent quality.
- Availability of relatively large silicon wafers (up to about 16 or 20 cm), making it suitable for integrating a number of components on a common substrate.
- Relatively high thermal conductivity (1.6 $cm^{-1} K^{-1}$), enabling surface-mounting of active components like III–V compound laser diodes.
- Transparency over infrared wavelengths ranging from 1.2 to 1.6 μm, which is the lowest loss wavelength transmission window of silica-based optical fibers. Thus, optical waveguide components on silicon are suitable for efficient coupling to optical fibers in the important wavelength range. Furthermore, since the materials are similar, easy design procedures are allowed to match guided-mode spot sizes between an optical waveguide and a fiber.
- Amenability to anisotropic etching (Bean [1978], Kendall [1979], Peterson [1982], Matsuo [1978], Matsuo [1980]), enabling easy fiber attachment through etched mechanical fixtures like V- or U-grooves (Boyd and Sriram [1978], Grand, Denis and Valette [1991]).
- Amenability to dry etching, which allows flexibility in component integration technology.
- Highly developed technology for etching, cutting and dicing, polishing, and photolithography, yielding the potential for mass production.
- Availability at lower costs than III–V compounds.
- Less toxic than III- V compounds.
- Well-developed silica deposition technologies for waveguide fabrication are available.

Despite these attractive features, silicon was not seriously viewed as a potential candidate for integrated optics until recently (Stutius and Streifer [1977], Boyd, Chang, Fan and Ramey [1981], Willander [1983a], Falco, Botineau, Azema, De Micheli and Ostrowsky [1983], Willander [1983b], Kawachi, Yasu and Kobayashi [1983], Boyd, Wu, Zelmon, Neumaan and Timlin [1984], Yamada, Kawachi, Yasu and Kobayashi [1984a, 1984b], Kawachi, Yamada, Yasu and Kobayashi [1985], Lee, Henry, Kazarinov and

Orlowsky [1987], Aarnio, Honkanen and Leppihalme [1987], Hall [1987], Valette [1987, 1988], Hickernell [1988], Soref and Lorenzo [1988], Valette, Renard, Denis, Jadot, Fournier, Philippe, Gidon, Grouillet and Desgranges [1989], Soref and Ritter [1990], Baba, Kokubun and Watanabe [1990], Pal, Singh, Ghatak and Bhattacharya [1990], Kawachi [1990], Valette, Renard, Jadot, Gidon and Erbeia [1990], Tewari, Singh and Pal [1990], Takagi, Jinguji and Kawachi [1991], Adams, Shani, Henry, Kistler, Blonder and Olsson [1991], Kawachi, Miya and Ohmori [1991], Welbourn, Beaumont and Nield [1991], Kokubun, Tamura and Kondo [1991], Henry [1991], Okamoto [1991], Kawachi [1991]). The subject is important because future optical networks will require a large variety of optical components for switching, branching, combining, and wavelength multiplexing and demultiplexing of optical signals and data. The intense interest in this technology prompted this attempt to present a unified description of guided-wave optics on silicon.

§ 2. Physics and Analysis of Optical Waveguides

2.1. PLANAR WAVEGUIDES

The physics of an optical waveguide is best illustrated through a planar or slab geometry. As shown in fig. 1, it involves a guiding region of refractive index n_1 surrounded by a cover and a substrate of refractive indices n_c and n_s on each side with $n_c, n_s < n_1$ (Marcuse [1974], Sodha and Ghatak [1977], Adams [1981], Ghatak [1986], Ghatak and Thyagarajan [1989], Pal

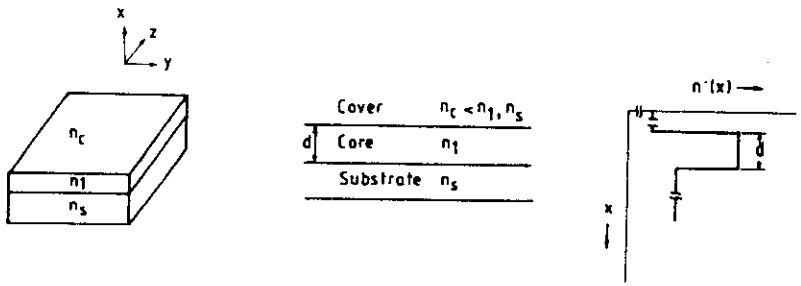

Fig. 1. Schematic of a planar optical waveguide in which a core of uniform refractive index n_1 is surrounded by a cover of refractive index n_c and a substrate of refractive index n_s; the refractive index distribution $n(x)$ is also shown.

[1987]). If $n_c = n_s$, the waveguide is called a symmetric waveguide. We assume the refractive index to be varying only along x as

$$\begin{aligned} n^2(x) &= n_c^2 \quad x \geqslant d \qquad \text{(cover)}, \\ &= n_1^2 \quad 0 < x < d \quad \text{(core)}, \\ &= n_s^2 \quad x \leqslant 0 \qquad \text{(substrate)}. \end{aligned} \tag{2.1}$$

The governing wave equation is (Ghatak [1986])

$$\nabla^2 \Psi + \varepsilon_0 \mu_0 n^2(x) \frac{\partial^2 \Psi}{\partial t^2} = 0, \tag{2.2}$$

where ε_0 and μ_0 are the free-space dielectric permittivity and the magnetic permeability (the media are assumed to be nonmagnetic), respectively. Here Ψ stands for either $\mathscr{E}$ or $\mathscr{H}$, and it encompasses both the spatial and temporal variations of the electric and magnetic fields. If we choose the z-axis as the direction of propagation (fig. 1), without any loss of generality, spatial variations of the fields will be confined to the xz plane. If the time dependence is $e^{i\omega t}$, the solution of eq. (2.2) is

$$\begin{aligned} \Psi(x, y, z, t) &= E_j(x)\, e^{i(\omega t - \beta z)}, \\ &= H_j(x)\, e^{i(\omega t - \beta z)} \quad j = x, y, z, \end{aligned} \tag{2.3}$$

where β represents the propagation constant. Values of β are dictated by the waveguide parameters. The boundary conditions allow only a discrete set of β's. The transverse field distributions $E_j(x)$ and $H_j(x)$ (which remain invariant with propagation) corresponding to these discrete β's constitute the guided or bound modes of the waveguide. Any arbitrary electromagnetic field incident at the input end of the waveguide can be expanded into a sum over the waveguide's allowed discrete (or guided) modes and a continuum of radiation modes (Marcuse [1974], Ghatak and Thyagarajan [1989]):

$$\Psi(x, y, z, t) = \sum_p a_p \psi_p(x)\, e^{i(\omega t - \beta_p z)} + \int a(\beta) \psi_\beta(x)\, e^{i(\omega t - \beta z)}\, d\beta. \tag{2.4}$$

In eq.(2.4), ψ on the right-hand side stands for either E or H, and p labels a particular mode; the coefficient a_p is such that power in the pth mode is proportional to $|a_p|^2$. Furthermore, these guided modes are mutually orthogonal and are normalized so they satisfy the orthonormality condition (Ghatak and Thyagarajan [1989])

$$\int_{-\infty}^{\infty} \psi_p^*(x)\, \psi_q(x)\, dx = \delta_{pq}, \tag{2.5}$$

where δ_{pq} is the Kronecker delta function:

$$\delta_{pq} = 0 \quad \text{for } p \neq q,$$
$$= 1 \quad \text{for } p = q. \tag{2.6}$$

The orthonormality condition normalizes the power carried by each mode to 1. The radiation modes also form an orthogonal set, although the orthonormality condition is required to be defined appropriately in terms of the Dirac delta function (Ghatak and Thyagarajan [1989]).

For the index distribution given by eq. (2.1), the structure (fig. 1) will support both TE and TM modes. For the TE modes, E_y, H_x, and H_z are the only nonzero field components, whereas for the TM modes, corresponding nonzero field components are H_y, E_x, and E_z. The TE modes satisfy the wave equation (Pal [1987])

$$\frac{d^2 E_y(x)}{dx^2} + \kappa_p^2 E_y(x) = 0, \tag{2.7}$$

where

$$\kappa_p = \sqrt{k^2(x) - \beta_p^2} \tag{2.8}$$

represents transverse component of the plane wave vector $k(x)$ $(= k_0 n(x))$. Solutions of eq. (2.7) for the index distribution (eq. (2.1)) can be written as (Pal [1987])

$$\begin{aligned} E_y &= A\, e^{-\gamma_c x} && x \geqslant d, \\ &= B\, e^{-i\kappa_p x} + C\, e^{+i\kappa_p x} && 0 < x < d, \\ &= D\, e^{\gamma_s x} && x \leqslant 0, \end{aligned} \tag{2.9}$$

where

$$\gamma_c^2 = \beta_p^2 - k_0^2 n_c^2, \qquad \kappa_p^2 = k_0^2 n_1^2 - \beta_p^2, \qquad \gamma_s^2 = \beta_p^2 - k_0^2 n_s^2. \tag{2.10}$$

For a guided mode the field is oscillatory within the core, and is exponentially decaying in the cover and substrate. Accordingly, γ_c, κ_p, and γ_s, are all real and positive. Hence, for a guided mode

$$k_0 n_1 > \beta_p > k_0 n_s > k_0 n_c, \tag{2.11}$$

where it is assumed that n_c is less than n_s. The portion of the field outside the core, which exponentially decays in the cover and the substrate (eq. (2.9)), is known as the evanescent tail of a guided mode, which is used in practice to construct a number of waveguide components, such as directional couplers

and polarizers. The continuity of E_y and H_z across the film–cover and film–substrate interfaces leads to the following eigenvalue or characteristic equation (Pal [1987])

$$\tan(\kappa_p d) = \frac{\gamma_c/\kappa_p + \gamma_s/\kappa_p}{1 - \gamma_c \gamma_s/\kappa_p^2}, \tag{2.12}$$

or

$$\kappa_p = (\phi_s + \phi_c + p\pi)/d, \quad p = 0, 1, 2, \ldots, \tag{2.13}$$

where $\tan\phi_s = \gamma_s/\kappa_p$ and $\tan\phi_c = \gamma_c/\kappa_p$. Solutions of eq. (2.13) yield $\beta_0, \beta_1, \beta_2, \ldots$, which correspond to the $TE_0, TE_1, TE_2, \ldots$, modes of the waveguide. For a symmetric waveguide, eq. (2.12) is transformed to (Pal [1987])

$$\tan(\kappa_p d) = \frac{2\gamma_s/\kappa_p}{1 - \gamma_s^2/\kappa_p^2}. \tag{2.14}$$

Since $\tan(\kappa_p d)$ can be expanded as $2\tan(\frac{1}{2}\kappa_p d)/[1 - \tan^2(\frac{1}{2}\kappa_p d)]$, eq. (2.14) may be recast as a quadratic equation in $\tan(\frac{1}{2}\kappa_p d)$, the solution of which yields (Pal [1987])

$$\tfrac{1}{2}\kappa_p d \tan(\tfrac{1}{2}\kappa_p d) = \tfrac{1}{2}\gamma_2 d, \tag{2.15a}$$

or

$$\tfrac{1}{2}\kappa_p d/2 \cot(\tfrac{1}{2}\kappa_p d) = -\tfrac{1}{2}\gamma_2 d, \tag{2.15b}$$

where $\gamma_2^2 = \beta_p^2 - k_0^2 n_2^2$, and $n_c = n_s = n_2$. The modal field associated with the propagation constants yielded by solutions of eq. (2.15a) is (Pal [1987])

$$E_y(x) = \frac{D}{\cos(\frac{1}{2}\kappa_p d)} \cos[\kappa_p(x - \tfrac{1}{2}d)], \tag{2.16}$$

which is symmetric in x about the mid-plane of the core. The corresponding modal field associated with the propagation constants yielded by solutions of eq. (2.15b) is

$$E_y(x) = \frac{D}{\sin(\frac{1}{2}\kappa_p d)} \sin(\kappa_p(\tfrac{1}{2}d - x)). \tag{2.17}$$

Thus, in a symmetric waveguide the guided TE modes will, in general, consist of symmetric (eq. (2.16)) and antisymmetric (eq. (2.17)) modes. For a quantitative evaluation of the modal fields of a given planar waveguide one must solve the transcendental equation, eq. (2.15), for β either graphically or

numerically. We introduce two dimensionless parameters

$$V^2 = \tfrac{1}{4}(\kappa_p^2 + \gamma_2^2)d^2 = \tfrac{1}{4}k_0^2 d^2(n_1^2 - n_2^2) \tag{2.18a}$$

and

$$b = \frac{\beta^2/k_0^2 - n_2^2}{n_1^2 - n_2^2}. \tag{2.18b}$$

In view of eq. (2.11),

$$0 \leqslant b \leqslant 1. \tag{2.19}$$

In terms of V and b, eqs. (2.15a) and (2.15b) can be rewritten as

$$\tan(V\sqrt{1-b}) = \sqrt{b/(1-b)} \qquad \text{(symmetric modes)} \tag{2.20a}$$

and

$$\tan(V\sqrt{1-b}) = -\sqrt{(1-b)/b} \quad \text{(antisymmetric modes).} \tag{2.20b}$$

For a given waveguide and operating wavelength, V is known. For that V, a plot of the left- and right-hand sides of eqs. (2.20) as a function of b in the range defined by eq. (2.19) on the same figure will yield b (hence β) through their intersections. The number of intersections also determines the number of modes. As an example, consider a symmetric planar waveguide formed from silicon nitride (Si_3N_4) as the core layer with silica (SiO_2) as the surrounding medium. If we assume the operating wavelength to be 0.6328 μm, the refractive index of Si_3N_4 is 2.014 and that of SiO_2 is 1.458. Since λ, n_1, and n_2 are fixed, different values of V correspond to different widths (d) of the waveguide. For example, for a $V = 1$, $d \approx 0.14$ μm in such a nitride ($SiO_2/Si_3N_4/SiO_2$) planar waveguide. Figure 2 shows universal dispersion curves depicting b as a function of V of the TE modes in a symmetric planar waveguide; values of b at different values of V are obtained by solving eqs. (2.20a) and (2.20b). We find from fig. 2 that for $V = 1$, which corresponds to a $d \simeq 0.14$ μm, a silicon nitride waveguide will support only one TE mode at 0.6328 μm wavelength. If d is increased to $\simeq 0.73$ μm, V increases to $\simeq 5$, and the silicon nitride waveguide will support two symmetric and one antisymmetric TE modes at 0.6823 μm wavelength. We may state that for $V = 1$, all modes except the TE_0 mode are cut off in a planar waveguide. By definition a mode is cut off in a symmetric waveguide when the propagation constant β_p equals $k_0 n_2$, which implies that $b = 0$. Thus at cutoff, eq. (2.13a) becomes (Pal [1987])

$$V_c = \tfrac{1}{2}p\pi, \quad p = 0, 1, 2, \ldots \tag{2.21a}$$

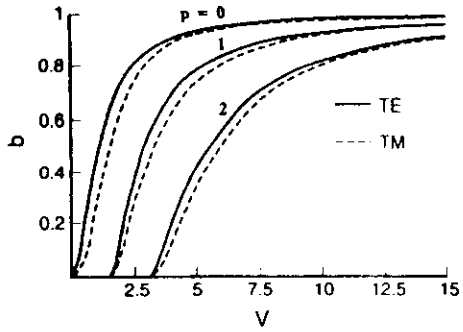

Fig. 2. Normalized b–V dispersion curve of a symmetric planar waveguide. The full curve (——) corresponds to universal curves for TE modes, and the dashed curve (- - -) corresponds to TM modes of a $SiO_2/Si_3N_4/SiO_2$ symmetric waveguide for which the refractive index of SiO_2 and Si_3N_4 are 1.458 and 2.014, respectively, at 0.6328 μm.

where V_c stands for normalized cutoff frequency, i.e., the V-number at which a mode is cut off. Even values of p correspond to symmetric TE modes, and odd values to antisymmetric modes. Equation (2.21a) shows that the TE_0 mode is never cut off in a symmetric planar waveguide. For design purposes the cutoff condition, eq. (2.21a), can be rewritten in a more useful form (Pal [1987])

$$\left(\frac{d}{\lambda}\right)_c = \frac{1}{2}\frac{p}{(n_1^2 - n_2^2)^{1/2}}. \tag{2.21b}$$

This condition implies that the smallest ratio (d/λ) for the pth mode to be supported in a waveguide is given by eq. (2.21b). For example, for any d/λ less than 0.35, a silicon nitride planar waveguide will function as a single-mode (only TE_0 mode) waveguide.

These calculations can be repeated for the TM modes of an asymmetric planar waveguide. The eigenvalue equation is

$$\tan(\kappa_p d) = \frac{\left(\frac{n_1^2}{n_s^2}\right)\frac{\gamma_s}{\kappa_p} + \left(\frac{n_1^2}{n_c^2}\right)\frac{\gamma_c}{\kappa_p}}{1 - \left(\frac{n_1^4}{n_c^2 n_s^2}\right)\frac{\gamma_c \gamma_s}{\kappa_p^2}}. \tag{2.22}$$

For a symmetric planar waveguide the eigenvalue equations for the TM modes are

$$\tan(V\sqrt{1-b}) = (n_1^2/n_2^2)\sqrt{b/(1-b)} \qquad \text{(symmetric modes)} \tag{2.23a}$$

TABLE I

	TE modes		TM modes	
	Asymmetric waveguide	Symmetric waveguide	Asymmetric waveguide	Symmetric waveguide
Eigenvalue equation	Eqs. (2.12) or (2.13)	Eqs. (2.20a) and (2.20b)	Eq. (2.22)	Eqs. (2.23a) and (2.23b)
Cutoff frequency V_c	$\tan^{-1}\sqrt{a}+\frac{1}{2}p\pi$ $(p=0,1,2,\ldots)$	$\frac{1}{2}p\pi$ $(p=0,1,2,\ldots)$	$\tan^{-1}\left(\frac{n_1^2\sqrt{a}}{n_c^2}\right)+\frac{1}{2}p\pi$ $(p=0,1,2,\ldots)$	$\frac{1}{2}p\pi$ $(p=0,1,2,\ldots)$

and

$$\tan(V\sqrt{1-b}) = -(n_1^2/n_2^2)\sqrt{(1-b)/b} \quad \text{(antisymmetric modes).} \tag{2.23b}$$

The b–V dispersion curves for the TM modes of a silicon nitride planar waveguide are shown in fig. 2 as dashed curves. The ratio of the core-to-cladding refractive index at 0.6328 μm wavelength is about 1.38 in such a waveguide. We list important results for the TE and TM modes of a planar waveguide in table 1. For an asymmetric waveguide, V_c^{TM} is greater than V_c^{TE}. For the lowest order mode (Ghatak [1986]),

$$V_c^{TE} = \tan^{-1}\sqrt{a} \quad \text{and} \quad V_c^{TM} = \tan^{-1}(n_1^2\sqrt{a}/n_s^2).$$

Here a represents the asymmetry parameter, and it is defined as $a=(n_s^2-n_c^2)/(n_1^2-n_s^2)$. Thus, for $\tan^{-1}\sqrt{a} < V < \tan^{-1}(n_1^2\sqrt{a}/n_s^2)$, only the TE_0 mode is supported in an asymmetric planar waveguide. Such a waveguide, in which all modes except the TE_0 mode are cut off, is called a single-polarization, single-mode waveguide (Ghatak [1986], Ghatak and Thyagarajan [1989]). In the case of weakly guiding waveguides, for which $n_1 \approx n_s$, TE and TM modes are nearly degenerate.

2.2. POWER CARRIED BY A GUIDED MODE IN A PLANAR WAVEGUIDE

The energy density associated with the electromagnetic field, by definition, is given by the time average of the corresponding Poynting vector (S),

$$\langle S\rangle = \langle \mathscr{E}\times\mathscr{H}\rangle = \tfrac{1}{2}\,\mathrm{Re}(\mathscr{E}\times\mathscr{H}), \tag{2.24}$$

where $\langle\ldots\rangle$ implies time average. In eq. (2.24) both temporal and spatial dependences are assumed to have been included in the field components. As an example, we consider only symmetric TE modes. Simple algebraic manipulations lead to an expression for the net power carried by a symmetric TE mode along z-direction per unit length along y (Pal [1987])

$$P_z = \tfrac{1}{2}\int_{-\infty}^{\infty} \mathrm{Re}(\mathscr{E}\times\mathscr{H})\cdot\hat{z}\,dx$$

$$= \frac{\beta_p D^2}{4\omega\mu_0\cos^2\xi}\left[d+\frac{2}{\gamma_2}\right], \tag{2.25}$$

where $\xi = \frac{1}{2}\kappa_p d$ and $\hat{z}$ is the unit vector along z. Equation (2.25) shows that the guided-mode power is confined to an effective guide half-width of $(\frac{1}{2}d + 1/\gamma_2)$. We can thus ascribe a confinement factor Γ to each mode by the following definition (Pal [1987])

$$\Gamma = \frac{\text{optical power inside the core}}{\text{total optical power}}$$

$$= \frac{\xi+\sin\xi\cos\xi}{\xi+\kappa_p/\gamma_2}. \tag{2.26}$$

At mode cutoff, $\beta = k_0 n_2$, so $\gamma_2 = 0$, and hence $\Gamma = 0$; the mode, therefore, ceases to be guided inside the core.

2.3. WAVEGUIDING IN THREE-DIMENSIONAL STRUCTURES

The density of guided-wave components on a substrate can be greatly increased by confining the guided optical energy in both the x and y directions. In contrast to the planar geometry, three-dimensional waveguides (fig. 3) consist of rectangular or near-rectangular cores, which are difficult to analyze. Studies of propagation effects in them generally require extensive

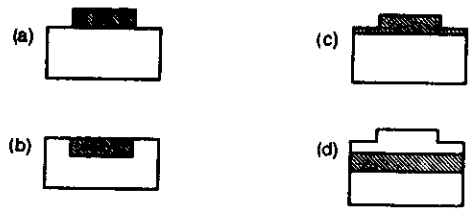

Fig. 3. Some examples of three-dimensional waveguide geometries: (a) raised strip, (b) embedded strip, (c) rib, (d) strip-loaded; in all these geometries the shaded region represents the core.

numerical analyses (Marcatili [1969], Goell [1969]). Hocker and Burns [1977] have, however, proposed a relatively simple and approximate approach, which is called the effective-index method (Knox and Toulios [1970]). This method can be illustrated through the example of an embedded strip waveguide (fig. 3b), in which a core that has dimension $d_a \times d_b$ and refractive index n_1 and has on its three sides a medium of refractive index n_3. The core is assumed to be covered by a medium of refractive index n_2. The method starts with the assumption that the waveguide extends infinitely along y. We then find the modes of an asymmetric slab waveguide (fig. 4a) in the xz plane consisting of a core of width d_a that has index n_1, and is sandwiched between two media of refractive indices n_2 and n_3. The analysis presented in § 2.1 can be extended to obtain the propagation constant β_p from the mode dispersion curve: b versus V of the guided modes for this asymmetric waveguide. Depending on polarization of the input beam, either TE (electric field along y) or TM (magnetic field along y) modes will be excited. An effective index $n_p^{\text{eff}} (= \beta_p / k_0)$ can be associated with the pth mode of this waveguide. At the next step the method assumes that the entire asymmetric waveguide along x can be replaced by a core material of index n_p^{eff}. In the yz plane we thus obtain a symmetric planar pseudo-waveguide of core refractive index n_p^{eff} and of width d_b surrounded by a medium of index n_3 (fig. 4b). Thus, we can study propagation in such a symmetric pseudo-waveguide by finding the propagation constants β_q of different modes from the mode dispersion curve (fig. 2). For each value of p there will be q solutions for the effective waveguide structure in the yz plane. Thus, in the effective-index model, each mode is designated with a pair of subscripts: p and q. According to Hocker and Burns [1977], the agreement in the values of β_{pq} found for the effective-index method and more nearly exact numerical

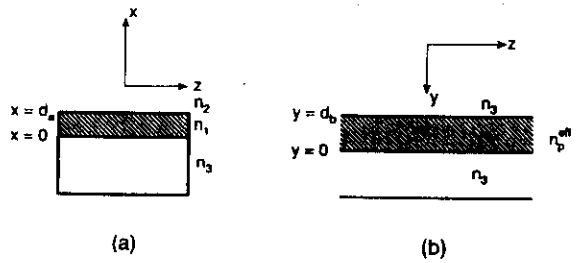

Fig. 4. Effective-index model: (a) an asymmetric planar waveguide of width d_a in the xz plane with a core of refractive index n_1 sandwiched between a cover and a substrate of refractive index n_2 and n_3, respectively; (b) a symmetric planar waveguide of width d_b in the yz plane with a core of refractive index n_p^{eff} surrounded by a medium of refractive index n_3.

methods is quite good for the lowest-order modes and for large aspect ratios (Marcatili [1969], Goell [1969]). In particular, the agreement is extremely good far from cutoff. In view of this and the simplicity of the model, the effective-index method is used extensively in the literature to model propagation in three-dimensional waveguides.

In the mid-1980s an alternate and relatively simple technique (Kumar, Thyagarajan and Ghatak [1983]) based on perturbation theory was proposed to deal with such rectangular geometries. This technique was applied to a number of integrated-optical waveguide geometries and devices (Kumar, Thyagarajan and Ghatak [1983], Kumar, Kaul and Ghatak [1985], Varshney and Kumar [1988]). The method relies on choosing a fictitious rectangular optical waveguide, the index profile of which is separable in x and y coordinates, and which closely resembles the actual waveguide except at the corners. Since the index profile is separable in x and y, the modal solution to the fictitious waveguide becomes extremely simple. Furthermore, since the real index profile differs little from the hypothetical profile, simple perturbation theory is then applied to obtain the propagation characteristics, and hence the b–V dispersion curves of the real waveguide. As an example, consider the ridge waveguide of fig. 5a. It can be approximated as a fictitious waveguide of the form shown in fig. 5b, with index profile (Varshney and

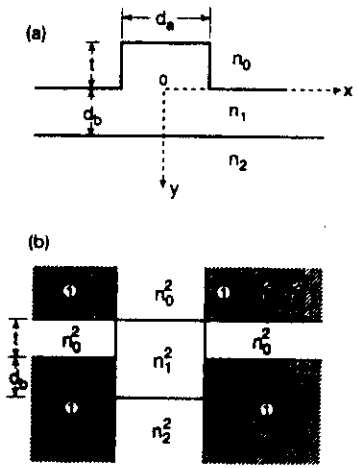

Fig. 5. Perturbation theory model to analyze a three-dimensional waveguide: (a) real waveguide (adapted with permission of IEEE from Varshney and Kumar [1988], © 1988 IEEE); (b) fictitious waveguide with a dielectric constant profile separable in x and y coordinates; the dielectric constant profile of the fictitious waveguide differs from the real waveguide only in the shaded regions.

Kumar [1988])

$$n^2(x, y) = n_{\mathrm{I}}^2(x) + n_{\mathrm{II}}^2(y) - n_1^2, \tag{2.27}$$

where

$$\begin{aligned} n_{\mathrm{I}}^2(x) &= n_1^2, \quad |x| < \tfrac{1}{2}d_{\mathrm{a}}, \\ &= n_0^2, \quad |x| > \tfrac{1}{2}d_{\mathrm{a}}, \end{aligned} \tag{2.28a}$$

and

$$\begin{aligned} n_{\mathrm{II}}^2(y) &= n_2^2, \quad y > d_{\mathrm{b}}, \\ &= n_1^2, \quad -t < y < d_{\mathrm{b}}, \\ &= n_0^2, \quad y < -t. \end{aligned} \tag{2.28b}$$

The dielectric profile (eq. (2.27)) matches the dielectric profile of the real waveguide everywhere except at the shaded regions shown in fig. 5b. The modal solution to the fictitious waveguide is given by a solution of the scalar wave equation (Kumar, Thyagarajan and Ghatak [1983], Varshney and Kumar [1988])

$$\left[\frac{\partial^2}{\partial x^2} + \frac{\partial^2}{\partial y^2} + (k_0^2 n^2(x, y) - \beta_0^2)\right]\psi(x, y) = 0, \tag{2.29}$$

where β_0 is the propagation constant. Equation (2.29) can be converted into two independent equations in x and y by substituting $\psi(x, y) = X(x)Y(y)$, and by using the method of separation of variables,

$$\left[\frac{\mathrm{d}^2}{\mathrm{d}x^2} + (k_0^2 n_{\mathrm{I}}^2(x) - \beta_1^2)\right]X = 0 \tag{2.30}$$

and

$$\left[\frac{\mathrm{d}^2}{\mathrm{d}y^2} + (k_0^2 n_{\mathrm{II}}^2(y) - \beta_2^2)\right]Y = 0, \tag{2.31}$$

where $\beta_0^2 = \beta_1^2 + \beta_2^2 - k_0^2 n_1^2$. The solutions to eq. (2.30) in different regions of the waveguide are (Varshney and Kumar [1988])

$$\begin{aligned} X(x) &= A\cos(2\mu_1 x/d_{\mathrm{a}} - \theta), \quad |x| < \tfrac{1}{2}d_{\mathrm{a}}, \\ &= B\,\mathrm{e}^{-2\mu_2|x|/d_{\mathrm{a}}}, \quad |x| > \tfrac{1}{2}d_{\mathrm{a}}, \end{aligned} \tag{2.32}$$

where

$$\begin{aligned} \mu_1 &= \tfrac{1}{2}d_{\mathrm{a}}\sqrt{k_0^2 n_1^2 - \beta_1^2}, \\ \mu_2 &= \sqrt{V_x^2 - \mu_1^2}, \\ V_x &= \tfrac{1}{2}k_0 d_{\mathrm{a}}\sqrt{n_1^2 - n_0^2}. \end{aligned} \tag{2.33}$$

Here, $\theta = 0$ for a mode symmetric in x, and $\theta = \frac{1}{2}\pi$ for a mode antisymmetric in x, and A and B are constants. The solutions to eq. (2.31) in different regions of the waveguide are

$$\begin{aligned} Y(y) &= A_2\exp(-\gamma_2 y/t), && y > d_{\mathrm{b}}, \\ &= A_1\cos(\gamma_1 y/t) + B_1\sin(\gamma_1 y/t), && -t < y < d_{\mathrm{b}}, \\ &= A_0\exp(\gamma_0 y/t), && y < -t, \end{aligned} \tag{2.34}$$

where

$$\gamma_2 = t\sqrt{\beta_2^2 - k_0^2 n_2^2}, \qquad \gamma_1 = \sqrt{V_y^2 - \gamma_2^2}, \qquad V_y = tk_0\sqrt{n_1^2 - n_2^2},$$

$$\gamma_0 = \sqrt{\gamma_2^2 + V_y^2\frac{(n_2^2 - n_0^2)}{2\Delta n_1^2}}, \qquad \Delta = \frac{(n_1^2 - n_2^2)}{2n_1^2}.$$

The consants β_1 and β_2 are determined by satisfying the boundary conditions for the dominant field vector. For example, the E_{pq}^y-mode will approximate a TE mode in the x-direction and a TM mode in the y-direction. The boundary conditions required to be satisfied by $\psi(x, y)$ ($\equiv E_{pq}^y$ mode) are (Varshney and Kumar [1988])

$$\begin{aligned} &\psi, \frac{\partial\psi}{\partial x} && \text{continuous at } x = \pm\tfrac{1}{2}d_{\mathrm{a}}; \\ &n^2\psi, \frac{\partial\psi}{\partial y} && \text{continuous at } y = -t \text{ and } y = d_{\mathrm{b}}. \end{aligned} \tag{2.36}$$

In a similar manner, $\psi(x, y)$ ($\equiv E_{pq}^x$ mode) requires continuity of

$$\begin{aligned} &n^2\psi, \frac{\partial\psi}{\partial x} && \text{at } x = \pm\tfrac{1}{2}d_{\mathrm{a}}; \\ &\psi, \frac{\partial\psi}{\partial y} && \text{at } y = -t \text{ and } y = d_{\mathrm{b}}. \end{aligned} \tag{2.37}$$

These boundary conditions lead to eigenvalue equations for β_1 and β_2 (Varshney and Kumar [1988]):

$$\arctan\left(c\frac{\mu_2}{\mu_1}\right) - \mu_1 + \tfrac{1}{2}(p-1)\pi = 0 \tag{2.38}$$

and

$$\arctan\left(D_{10}\frac{\gamma_0}{\quad}\right) + \arctan\left(D_{1\cdot}\frac{\gamma_2}{\quad}\right) - \gamma_1\left(1 + \frac{d_{\mathrm{b}}}{\quad}\right) + (q-1)\pi = 0 \tag{2.39}$$

where $c = n_1^2/n_0^2$ for the E_{pq}^x mode and $c = 1$ for the E_{pq}^y mode, $D_{ij} = n_i^2/n_j^2$ for the E_{pq}^y mode and $D_{ij} = 1$ for the E_{pq}^x mode, and $i, j = 0, 1, 2$. The solutions of eqs. (2.38) and (2.39) will yield β_1 and β_2, and hence β_0, from the relation $\beta_0^2 = \beta_1^2 + \beta_2^2 - k_0^2 n_1^2$. Thus, from perturbation theory, the propagation constant β of the real waveguide will be

$$\beta^2 = \beta_0^2 + (\Delta\beta)^2, \tag{2.40}$$

where $\Delta\beta$ represents the first-order perturbation correction to β_0,

$$(\Delta\beta)^2 = k_0^2 \frac{\int_{-\infty}^{\infty}\int |\psi(x, y)|^2 \, \delta n^2 \, dx \, dy}{\int_{-\infty}^{\infty}\int |\psi(x, y)|^2 \, dx \, dy}. \tag{2.41}$$

Here, δn^2 is the difference in the dielectric constant distribution between the real and the fictitious waveguides. From figs. 5a and b, we obtain

$$\begin{aligned} \delta n^2 &= n_1^2 - n_0^2 \quad \text{for regions (1),} \\ &= 0 \qquad\quad \text{otherwise.} \end{aligned} \tag{2.42}$$

The perturbation theory yields results that are more accurate than the effective-index method (Kumar, Thyagarajan and Ghatak [1983]). This perturbation technique is useful, in particular, when δn^2 is small. However, it has been shown that even for semiconductor rib waveguides, in which $n_1 = 3.44$ and $n_0 = 1.0$ (i.e. in which $\delta n^2 \simeq 10.8$), the perturbation theory yields results that are in good agreement with other methods, such as the finite-element method or the mode-matching technique (Varshney and Kumar [1988]), which involve extensive numerical analysis. The perturbation results for the variation of n_{eff} of the scalar fundamental mode (E_{11}) of a semiconductor waveguide of width d_a is reproduced in fig. 6 from Varshney and Kumar [1988]. In a realistic silica waveguide the difference δn^2 is small, about 1.13 in the case of a silica-clad phosphosilicate waveguide. Perturbation theory should therefore yield useful results. A comparison between various theories with regard to the coupling length estimation for a silica-based waveguide directional coupler is shown in fig. 7 (Takato, Jinguji, Yasu, Toba and Kawachi [1988]); the agreement between the perturbation results and the experiment is quite good. For a tightly bound mode.

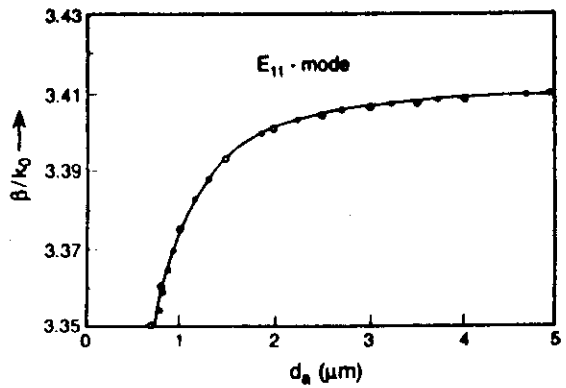

Fig. 6. Effective index of the scalar fundamental mode (E_{11}) versus width (d_a) of a rib waveguide with $n_0 = 1$, $n_1 = 3.44$, $n_2 = 3.35$, $d_b = 0.2$ μm, and $t = 0.8$ μm. (Reproduced with permission of IEEE from Varshney and Kumar [1988], © 1988 IEEE.)

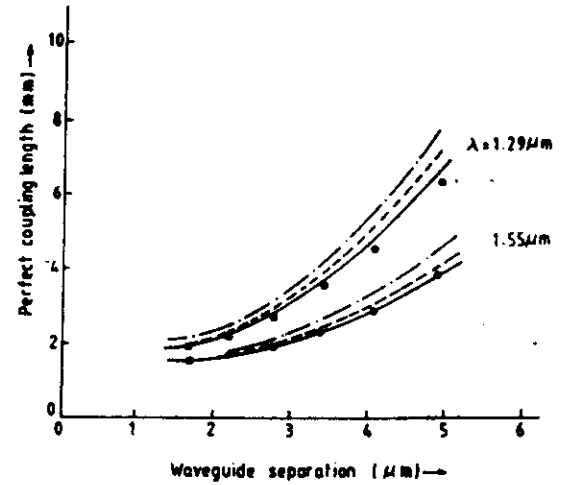

Fig. 7. A comparison of experiments with different theories for the dependence of perfect (i.e., 100%) optical power coupling length in a directional coupler with waveguide separation between two silica channel waveguides (dimension of 10×8 μm^2 each with a relative index difference between the core and cladding of 0.24%) at wavelengths of 1.29 and 1.55 μm; (——) point matching method, (– – –) perturbation analysis (Kumar, Kaul and Ghatak [1985].

nonzero. Thus, the perturbation technique is more accurate when a mode is far from cutoff. Furthermore, any stress-induced birefringence, which may occur in waveguides made of silica on silicon, can be easily incorporated in the perturbation technique, as Kumar, Shenoy and Thyagarajan [1984] showed.

2.4. MULTILAYER WAVEGUIDES

Optical waveguides are difficult to form on silicon due to the lack of another suitable transparent medium of refractive index higher than that of silicon ($n \simeq 3.5$). The difficulty of finding a suitable higher refractive index material compatible to silicon can be overcome by growing a layer of silica on silicon before guiding layers such as glass (Boyd, Wu, Zelmon, Neumaan, Timlin and Jackson [1985]) are deposited; the silica layer acts as a buffer layer. Thus, the refractive index profile of a typical composite structure will be as represented in fig. 8. Because of the high-index silicon substrate, the waveguide behaves as a leaky structure unless the buffer layer is thick enough. To reduce mode leakage loss in such a waveguide, the silica buffer layer is grown thick enough to ensure that the evanescent tail of the guided field will be negligible at the interface between the silica buffer layer and the silicon substrate. To achieve this, typically the silica layer thickness must be greater than 4 μm, requiring a long deposition time. The problem of long deposition time can be overcome in a novel waveguide configuration (Duguay, Kokubun, Koch and Pfeiffer [1986], Kokubun, Baba, Sasaki and Iga [1986]). It involves a multilayer planar configuration known as "ARRO

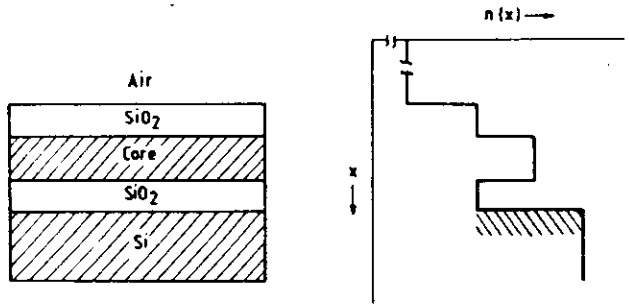

Fig. 8. Schematic of a silicon-based optical waveguide together with its refractive index profile; a buffer SiO_2 layer thick enough to reduce leakage loss of guided light into the silicon substrate is introduced before the core is formed.

waveguides", an acronym for antiresonant reflecting optical waveguide. The layered structure of the waveguide and the corresponding refractive index profile are shown in figs. 9a and b, respectively. The bottom silica layer ($\simeq 2$ μm) is called the second cladding layer, whereas the top silica layer ($\simeq 4$ μm) forms the core of the waveguide. The intermediate high index layer of about 0.1 μm thickness between these two regions is called the first cladding.

Two independent physical phenomena are exploited in this waveguide geometry. The silica–air interface at the top provides a total internal reflecting surface, whereas the high refractive index layer sandwiched between the two silica regions serves as a highly reflecting (>99%) interface. Thus an ARRO waveguide on silicon uses silica as the core like that in an optical fiber. The initial experiments on ARRO waveguides involved poly-silicon (poly-Si) as the thin high refractive index layer. However, for experiments at wavelengths less than 1 μm, poly-Si has been replaced by titania (TiO_2) as the first cladding layer, since silicon is highly absorptive in this wavelength range (Kokubun, Baba, Sasaki and Iga [1986], Baba, Kokubun, Sasaki and Iga [1988]). The thickness of the first cladding layer is chosen to be small to act as a Fabry–Pérot resonator and closely matched the antiresonant condition of the resonator. Antiresonances in a Fabry–Pérot etalon are spectrally broad (Ghatak and Thyagarajan [1989]). From the Fabry–Pérot analogy the waveguide will work over a wide spectral range. Thus the fabrication tolerance is comfortable. Under optimum conditions, reflectivity could be almost 99.96% from the set of two interfaces of poly-Si/TiO_2–SiO_2 and SiO_2–Si (Duguay, Kokubun, Koch and Pfeiffer [1986]). Approximate expressions for optimum thicknesses of the two reflecting layers are (Duguay, Kokubun, Koch and Pfeiffer [1986], Kokubun, Baba, Sasaki and Iga [1986])

$$d_3^{\mathrm{opt}} = \frac{\lambda}{4n_3}(2N+1)\left[1-\left(\frac{n_4}{n_3}\right)^2+\left(\frac{\lambda}{4n_3 d_{\mathrm{eff}}}\right)^2\right]^{-1/2}, \quad N = 0, 1, 2, \ldots \quad (2.43)$$

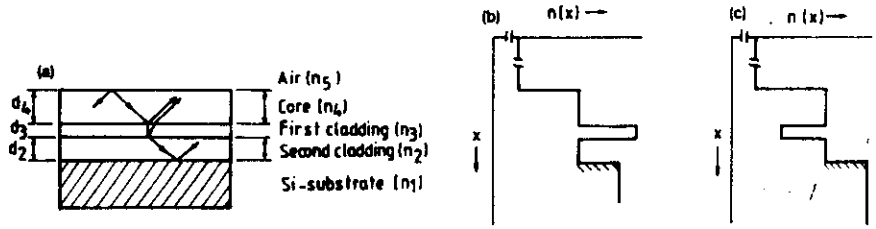

Fig. 9. (a) Schematic of an ARRO waveguide geometry; (b) refractive index profile of an ARRO waveguide; (c) refractive index profile of an ARRO-B waveguide (see text).

and

$$d_2^{opt} \simeq \tfrac{1}{2} d_{eff}(2M+1), \quad M = 0, 1, 2, \ldots, \tag{2.44}$$

where

$$d_{eff} \simeq d_4 \times \zeta \frac{\lambda}{2\pi\sqrt{n_4^2 - n_5^2}},$$

and

$$\begin{aligned} \zeta &= 1 && \text{for TE modes,} \\ &= (n_5^2/n_4^2) && \text{for TM modes;} \end{aligned} \tag{2.45}$$

M, N stand for order of antiresonances. Here, n_3, d_3 and n_2, d_2, represent, respectively, the refractive indices and the widths of the first and second claddings; n_4 and d_4 correspond to refractive index and width of the core; and n_5 is the refractive index of the cover, which is usually air. These results have been derived to yield minimum loss for the fundamental mode in an ARRO waveguide under antiresonant conditions. In an optimum ARRO waveguide configuration, as outlined earlier, the effective index (β/k_0) and loss minimum (α_0^{min}) of the fundamental TE_0 mode, respectively, are (Duguay, Kokubun, Koch and Pfeiffer [1986], Kokubun, Baba, Sasaki and Iga [1986])

$$\beta_1/k_0 \simeq n_4\left[1 - \left(\frac{\lambda}{4n_4 d_{eff}}\right)^2\right]^{1/2}, \tag{2.46}$$

and (Duguay, Kokubun, Koch and Pfeiffer [1986], Kokubun, Baba, Sasaki and Iga [1986], Baba, Kokubun, Sasaki and Iga [1988], Baba and Kokubun [1990, 1991])

$$\alpha_0^{min}\lambda = X \frac{5428.68(\lambda/d_{eff})^5}{n_4\sqrt{1 - \left(\frac{\lambda}{4n_4 d_{eff}}\right)^2}} \frac{1}{\left(n_3^2 - n_4^2 + \left(\frac{\lambda}{4d_{eff}}\right)^2\right)} \times \frac{1}{\sqrt{n_1^2 - n_4^2 + \left(\frac{\lambda}{4d_{eff}}\right)^2}} \cdot \text{(dB/cm)}, \tag{2.47}$$

with

$$\begin{aligned} X &= 1 && \text{for TE mode,} \\ &= (n_3^2 n_1/n_4^3)^2 && \text{for TM mode,} \end{aligned} \tag{2.48}$$

where n_1 is the substrate refractive index, and λ and d_{eff} are measured in micrometers (Baba, Kokubun, Sasaki and Iga [1988]). Equation (2.48) shows that the loss discrepancy between the TE and TM modes is due to the large difference in refractive index between the core and the first cladding, and also between the core and the substrate (Baba, Kokubun, Sasaki and Iga [1988], Baba and Kokubun [1991]).

In an alternative method ARRO waveguides were analyzed through an equivalent transmission line and transverse resonance method (Jiang, Chrostowski and Fontaine [1989]). If the thicknesses d_2 and d_3 satisfy antiresonance conditions, the dispersion relation for the propagation constant of the TE modes is

$$\cot(\gamma_4 d_4) = -\alpha_5/\gamma_4, \tag{2.49}$$

where γ_4 is the imaginary part of the transverse propagation constant in the core, and α_5 is the real part of the transverse propagation constant in air.

More recently a novel matrix approach was used to obtain the propagation characteristics of ARRO waveguides (Tewari, Singh and Pal [1990]). As shown in fig. 10, we call the refractive index of the silicon substrate, the second cladding, the first cladding, the core, and the cover (air) n_1, n_2, n_3, n_4, and n_5, respectively. The thickness of the corresponding regions are d_1, d_2, d_3, d_4, and d_5. The structure has five homogeneous layers, four interfaces, and five different refractive indices. The recipe of the model involves only a few computational steps (Ghatak, Thyagarajan and Shenoy [1987]). As a first step, a plane wave of amplitude E_1^+ is allowed to be incident on the interface between the silicon substrate and the second cladding at some angle of incidence θ. The corresponding amplitude reflection and transmission coefficients at the mth interface for TE and TM polarizations are given by (Ghatak, Thyagarajan and Shenoy [1987], Ghatak and Thyagarajan [1989])

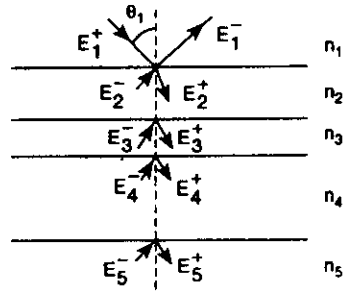

Fig. 10. Matrix method to model the propagation characteristics of an ARRO waveguide

TE polarization:

$$r_m = \frac{n_m \cos\theta_{m+1} - n_{m+1}\cos\theta_{m+1}}{n_m \cos\theta_{m+1} + n_{m+1}\cos\theta_{m+1}},$$

$$t_m = \frac{2n_m \cos\theta_m}{n_m \cos\theta_m + n_{m+1}\cos\theta_{m+1}}; \tag{2.50}$$

TM polarization:

$$r_m = \frac{n_{m+1}\cos\theta_m - n_m \cos\theta_{m+1}}{n_{m+1}\cos\theta_m + n_m \cos\theta_{m+1}},$$

$$t_m = \frac{2n_m \cos\theta_m}{n_{m+1}\cos\theta_{m+1} + n_m \cos\theta_{m+1}}, \tag{2.51}$$

respectively. For individual layers the θ_m's are given by Snell's law at each interface:

$$\beta = k_0 n_1 \sin\theta_1 = k_0 n_2 \sin\theta_2 = k_0 n_3 \sin\theta_3 = k_0 n_4 \sin\theta_4. \tag{2.52}$$

For each θ, the values of r_m and t_m are stored for each interface. Appropriate boundary conditions at each interface lead to the matrix equation

$$\begin{pmatrix} E_1^+ \\ E_1^- \end{pmatrix} = S \begin{pmatrix} E_5^+ \\ E_5^- \end{pmatrix}, \tag{2.53}$$

where + and − signs correspond to transmitted and reflected fields at each interface, and S is the product of 2 × 2 matrices: $S_1, S_2, \ldots, S_4$, with

$$S_m = \frac{1}{t_m}\begin{pmatrix} e^{i\delta_m} & r_m e^{i\delta_m} \\ r_m e^{-i\delta_m} & e^{-i\delta_m} \end{pmatrix} \tag{2.54}$$

and

$$\delta_m = k_m d_m \cos\theta_m; \quad k_m = k_0 n_m. \tag{2.55}$$

In view of eq. (2.52), δ_m can be expressed in terms of θ_1 as

$$\delta_m = k_0 d_m (n_m^2 - n_1^2 \sin^2\theta_1). \tag{2.56}$$

Thus, δ_m, r_m, t_m, and S_m can be calculated for a given θ_1. Since the fifth layer is very thick, the reflected field $E_5^- \cong 0$, and hence from eqs. (2.53)–(2.55) the electric fields in every layer can be obtained in terms of the incident field E_1^+. At the next step the mode excitation efficiency $\eta(\beta) = |E_5^+/E_1^+|^2$ is evaluated for the given θ_1 (i.e., for the given $\beta = k_0 n_1 \sin\theta_1$). The process is repeated by scanning the β-space through a variation in θ. A plot of $\eta(\beta)$

reveals resonant peaks that closely resemble Lorentzian functions in shape. For a single-mode guide there is only one such peak. The value of β at which the peak appears corresponds to the real part of the propagation constant. The full-width-at-half-maximum [FWHM $(= 2\Gamma)$] of the Lorentzian represents the leakage power loss coefficient, where Γ is the imaginary part of the propagation constant (Ghatak, Thyagarajan and Shenoy [1987], Ghatak and Thyagarajan [1989]). With the derived propagation constant the fields throughout the system can be computed by evaluating appropriate matrices (eq. (2.54)). The method can be applied to any multilayer structure in which one or more layers has a complex refractive index (Thyagarajan, Diggavi and Ghatak [1987]). For lossless waveguides, $\Gamma \to 0$. This method was used to design and fabricate ARRO waveguides (Tewari, Singh and Pal [1990], Pal, Singh, Ghatak and Bhattacharya [1990]). Calculation for TE mode losses for various parameters (e.g., thicknesses of the individual layers) can be used to optimize an ARRO waveguide. Some results are shown in figs. 11a,b. An important attribute of this matrix method is that, in addition to giving leakage loss and propagation constant, it allows computation of the corresponding modal field distributions. Feasibility of applying the matrix method to ARRO-B waveguides (Baba and Kokubun [1989]) was also tested (Tewari, Singh and Pal [1990]). These waveguides use a layer of lower refractive index between the two silica layers, rather than a layer of higher refractive index layer (fig. 9c). In contrast to the ARRO waveguides, an ARRO-B waveguide is polarization insensitive.

§ 3. Technology of Silicon-Based Optical Waveguides

The technology of silicon-based waveguides before 1985 was reviewed by Boyd, Wu, Zelmon, Neumaan, Timlin and Jackson [1985]. In the earliest attempts to fabricate optical waveguides on silicon, the silicon surface was first thermally oxidized in order to grow a buffer layer of silica (refractive index $\simeq 1.46$ in the 0.6–0.8 μm wavelength range) before the waveguide core (inorganic polymers or silicon oxynitrides, for example) was formed (Rand and Strandley [1972], Boyd and Chen [1976], Boyd and Chen [1977], Marx, Gottlieb and Brandt [1977]). This silica buffer layer was thick enough to prevent leakage of guided light to the high-index silicon substrate, the complex refractive index of which is about 3.85–i0.077 at the He–Ne wavelength (Stutius and Streifer [1977]). The surface smoothness of the silica buffer layer was usually of about the same quality as the original silicon

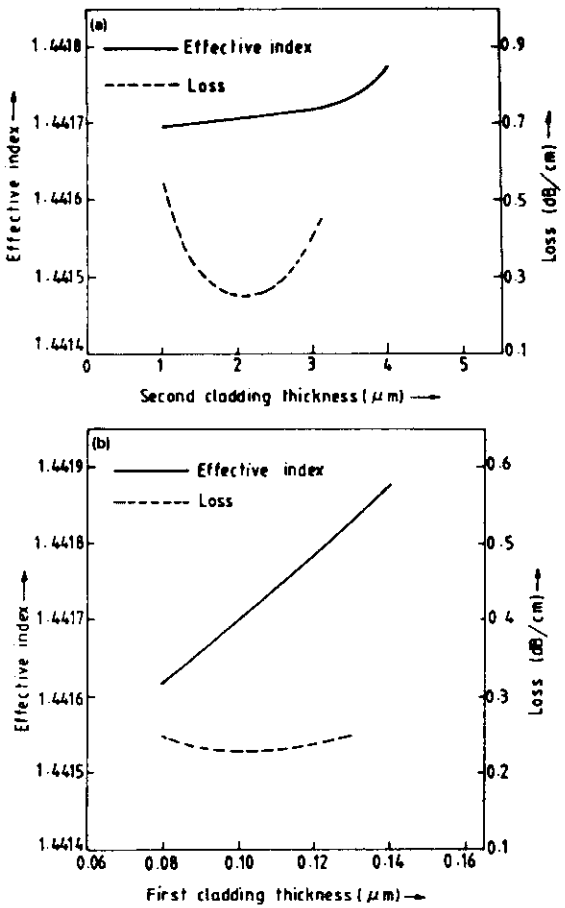

Fig. 11. (a) Effective index and loss of TE_0 mode versus second cladding thickness in the poly-Si ARRO waveguide as obtained by the matrix method (see text). (b) Effective index and loss of TE_0 mode versus first cladding thickness in the poly-Si ARRO waveguide as obtained by the matrix method (see text).

wafer surface (Boyd, Wu, Zelmon, Neumaan, Timlin and Jackson [1985]). The core layers were derived by deposition, for example, by chemical vapor deposition (CVD) or radiofrequency (RF) sputtering. In one of the earliest such waveguides with attenuation less than 0.1 dB/cm (for TE_0 and TM_0 modes at 0.6328 μm), silicon nitride waveguiding film ($\simeq$300 nm thick) of refractive index $\simeq$2.01 was deposited through low pressure CVD (Stutius and Streifer [1977]). The thickness of the silica buffer layer varied from 275 to 820 nm from sample to sample. Other successful attempts involved RF

sputtering of 7059 glass* ($n \simeq 1.5530$) or zinc oxide (ZnO) ($n \sim 2.0$) as the guiding layer (Goell and Strandley [1969], Dutta, Jackson and Boyd [1980], Dutta, Jackson, Boyd, Hickernell and Davis [1981], Dutta, Jackson and Boyd [1981]). Laser annealing of the deposited waveguiding film led to a dramatic reduction of attentuation in such waveguides. Typically, the reduction was by a factor of 250 in ZnO and 80 in the 7059 glass waveguides (Boyd, Wu, Zelmon, Neumaan, Timlin and Jackson [1985]). Improvements in the quality of the interface between the guiding layer and the buffer layer of silica led to a loss of only 0.01 dB/cm (Dutta, Jackson, Boyd, Hickernell and Davis [1981], Dutta, Jackson and Boyd [1981], Chen and Boyd [1981], Dutta, Jackson, Boyd, Davis and Hickernell [1982]). Since ZnO is a piezoelectric material, ZnO-based waveguides enable realization of acousto-optic devices with silica on silicon as the substrate (Hickernell, Davis and Richard [1978], Hickernell [1979], Chubachi [1976], Yao, Anderson and August [1979]). Some success in fabricating spectrum analyzers with ZnO waveguides on silicon-based substrates have been reported in § 4. Fabrication of silicon oxynitride ($Si_xO_yN_z$) core waveguides was reported recently by Gleine and Müller [1991]. The core layer of about 0.25 μm was deposited by low-pressure CVD (LPCVD) at about 3–10 Pa atmosphere from vapor-phase reactions between SiH_2Cl_2 (12–20 mL/min), NH_3 (0–300 mL/min), and O_2 (0–500 mL/min) on top of a 4 μm thick silica layer. The core is finally covered with a silica overlayer. Typically, the losses are less than 0.5 dB/cm at 0.6328 μm. Laser annealing with a pulsed CO_2 laser reduces the loss to some tenth of a dB/cm depending on the irradiation time and intensity of the laser. Laser annealing also led to a decrease in the refractive index of these near oxide films up to about 2% due to a reduction in the stress of the deposited films. This laser-induced reduction in the refractive index of the deposited films can be exploited to trim silicon-based guided-wave components (Gleine and Müller [1991]).

In one study, temperature-independent operation of a single-mode waveguide having the composite structure 7059 glass/SiO_2/Si was demonstrated; the guiding layer thickness was 0.368 μm (Chen and Boyd [1981]). Such temperature-independent waveguide operation has potential applications in interferometric sensors based on optical waveguides.

There is much recent interest in using silica or doped silica as the waveguiding core. Thermal oxidation of silicon for 24–27 hours yielded graded-index

* A proprietory trade name is used to enable the readers to reproduce the experiment; other glasses might work as well or better.

silica waveguides with losses of 0.3–0.4 dB/cm (Zelmon, Jackson, Boyd, Neumaan and Anderson [1983]). The thickness of the grown SiO_2 layers varied from 14.4 to 15.8 μm. For these thicknesses, out-of-plane scattering was very low, and the measured transmission loss was attributed mostly to leakage of light to high index silicon substrate (Zelmon, Jackson, Boyd, Neumaan and Anderson [1983], Boyd, Wu, Zelmon, Neumaan, Timlin and Jackson [1985]). In subsequent works, phosphosilicate glasses were used to form the guiding layer, which were deposited by CVD through co-oxidation of silane and phosphorus at 400 to 500°C under atmospheric pressure (Neumaan and Boyd [1980, 1981]). By doping with phosphorus, the refractive index of silica can be increased by a few percent. Since optical fibers are made from similar host materials (Pal [1979]), it is possible to tailor the mode-field profile of such waveguides to match closely the LP_{01}-mode profile of silica-based optical fibers. This will ensure good power-coupling efficiency between the waveguide and a single-mode fiber. This advantage of phosphosilicate waveguides has motivated extensive investigations of fabrication of low-loss phosphosilicate channel waveguides on silicon (Grand, Jadot, Denis, Valette, Fournier and Grouillet [1990]). The composite structure of these waveguides is Si/SiO_2/P doped-SiO_2/SiO_2 (Valette, Gidon and Jadot [1987], Valette [1987, 1988], Valette, Renard, Denis, Jadot, Fournier, Philippe, Gidon, Grouillet and Desgranges [1989], Grand, Jadot, Denis, Valette, Fournier and Grouillet [1990], Valette, Renard, Jadot, Gidon and Erbeia [1990]). All silica and phosphorus-doped silica layers are deposited through a plasma-enhanced CVD (PECVD) process. Two major attributes of the PECVD technology are that it is a relatively low-temperature process ($\simeq$800°C), compatible with the well-established microelectronics processing, and that it yields a high average deposition rate of about 40 nm/min (Valette, Jadot, Gidon, Renard, Grand, Fournier, Grouillet, Philippe, Denis, Desgranges, Mulatier and Erbeia [1991]). These waveguides exhibited losses less than 0.2 dB/cm at 0.633, 0.8 and 1.3 μm wavelengths. However, to achieve low loss at 1.55 μm, the waveguides require thermal annealing at an elevated temperature of about 1000°C for about 3 h. The reproducibility of the waveguides is achieved by maintaining phosphorus doping (at various levels) during deposition of all the layers. During deposition of the core, phosphorus doping level is kept to 5–10%, whereas for the buffer and cover layers it is between 2 and 3% (Grand, Jadot, Denis, Valette, Fournier and Grouillet [1990]). Typically, a phosphine flow rate of 4 cm^3/min leads to a phosphorus doping of about 3% by mass in silica (Valette, Renard, Denis, Jadot, Fournier, Philippe, Gidon, Grouillet and Desgranges [1989]). Dry

etching of the core layers with CHF_3 has been used to form low-loss channel waveguides using this technology. Modal spot size is optimized for coupling to fibers at 1.55 μm; such an optimized waveguide structure is shown in fig. 12 (Valette, Jadot, Gidon, Renard, Grand, Fournier, Grouillet, Philippe, Denis, Desgranges, Mulatier and Erbeia [1991]).

Fiber-to-waveguide coupling efficiency also was the motivating factor for fabrication of phosphosilicate glass waveguides on silicon reported by Henry, Blonder and Kazarinov [1989]. In their technology a buffer silica layer of about 15 μm is grown through rapid oxidation of the silicon substrate under a high pressure steam. The phosphosilicate core layers ($4–5 \times 7\ \mu m^2$) are deposited by incorporating 6.5–8% of phosphorus in silica through low-pressure chemical vapor deposition (LPCVD) at 680°C. The process involves a chemical reaction between tetraethylorthosilane, ammonia, and phosphine. The cover ($\sim$5 μm) consists of phosphorus-doped ($\sim$2% P) silica layers, deposited through LPCVD at about 380°C from the same raw materials. Eventually, after the depositions are completed, the waveguide is annealed at about 1000°C to relieve strain and to densify the film. The measured fiber-to-fiber coupling losses for these phosphosilicate glass core waveguides at 1.3 and 1.5 μm are shown in fig. 13 (Henry, Blonder and Kazarinov [1989]).

Silicon-based waveguides suitable for optical coupling from laser diodes are based on silicon nitride core layers (Henry, Kazarinov, Lee, Orlowsky and Katz [1987], Henry, Blonder and Kazarinov [1989], Shani, Henry, Kistler, Orlowsky and Ackerman [1989]). These waveguides are characterized by a tightly confined modal field due to a relatively large index difference ($\Delta n \sim 0.55$) between the core and surrounding medium. A silica buffer layer of about 5 μm thickness, which is sufficient to reduce the leakage

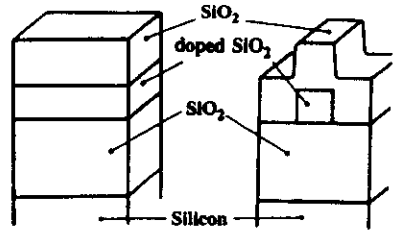

Fig. 12. Schematic of planar and channel waveguide geometries with phosphosilicate glass for optimum coupling to optical fibers. (Reproduced from Valette, Jadot, Gidon, Renard, Grand, Fournier, Grouillet, Philippe, Denis, Desgranges, Mulatier and Erbeia [1991] by permission

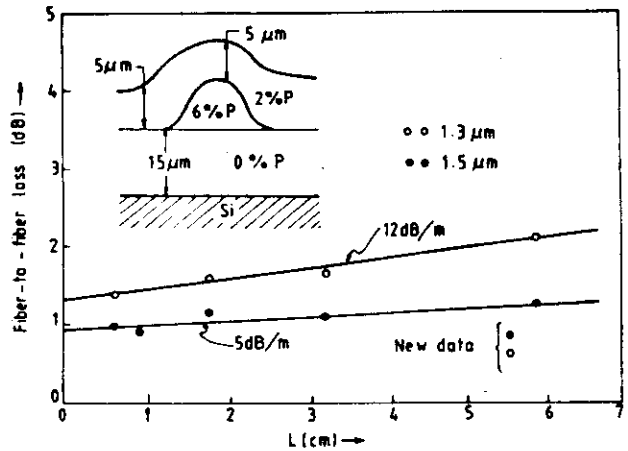

Fig. 13. Measured fiber-to-fiber loss at 1.3 and 1.5 μm through a phosphosilicate core glass waveguide with length of the waveguide; new data indicate more recent results on a waveguide, the cross-section of which is shown in the inset. (Reproduced by permission of IEEE from Henry, Blonder and Kazarinov [1989], © 1989 IEEE.)

loss, is realized through deposition of phosphorus-doped glass (~8% of P), followed by annealing at 1000°C or through high-pressure oxidation (about 2.45×10^6 Pa at 950°C). To form the core layers of silicon nitride ($n \sim 1.97$ at 1.2–1.6 μm), LPCVD is employed with dichlorosilane, ammonia, and oxygen as the raw materials (Henry, Blonder and Kazarinov [1989]). Two-dimensional confinement of guided light is achieved by chemical etching with hot (~174°C) phosphoric acid to form a mesa rib waveguide ($\sim 4 \times 0.12$ μm^2) on silicon nitride; the etch rate is about 0.1 nm/s (Henry, Kazarinov, Lee, Orlowsky and Katz [1987]). The core is covered with a plasma-deposited, 0.8 μm thick, silica superstrate. With these waveguides, losses less than 0.3 dB in the 1.3–1.6 μm range were reported. Absorption peaks at 1.4 and 1.52 μm associated with hydrogen in silica and silicon nitride layers similar to the ones that occur in optical fibers were identified. These peaks could be reduced substantially, however, by annealing the waveguides at 1100–1200°C. The loss spectrum of a 4 μm wide silicon nitride rib waveguide is shown in fig. 14; the inset shows a Bragg reflector grating (see § 4) on top of the waveguide (Henry, Blonder and Kazarinov [1989], Henry [1991]). Waveguide refractive indices must often be known to an accuracy of a few parts in 10^4. For example, for a Bragg filter based on a waveguide with a core-cladding index difference of about 0.006, a change of

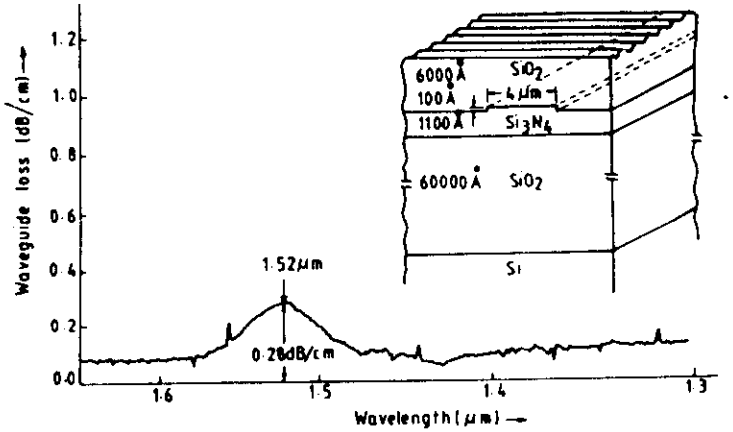

Fig. 14. Loss spectrum of a $SiO_2/Si_3N_4/SiO_2$ rib waveguide of 4 μm width. The inset shows a Bragg reflector grating developed on the cover. (Reproduced with permission of IEEE from Henry, Blonder and Kazarinov [1989], © 1989 IEEE.)

1 nm. Extensive experimental data for the refractive index dispersion of thermally deposited silica, phosphorus-doped silica, and silicon nitride glasses were reported by Lee, Henry, Orlowsky and Kometani [1988].

Fabrication of both planar and channel waveguides based on the composite structure $Si/SiO_2/Si_3N_4/SiO_2$ was also reported from France (Valette, Renard, Denis, Jadot, Fournier, Philippe, Gidon, Grouillet and Desgranges [1989], Valette, Jadot, Gidon, Renard, Grand, Fournier, Grouillet, Philippe, Denis, Desgranges, Mulatier and Erbeia [1991]). The silica buffer layer (~2 μm) is obtained by thermal oxidation of silicon, whereas the overlayer of silica is obtained through PECVD. The guiding layer of silicon nitride ($n = 2.014$ at 0.633 μm, and $n = 1.997$ at 0.8 μm) is relatively thin (typically, 0.08–0.22 μm) and is deposited by LPCVD. The fundamental mode spot size in these waveguides is small; it typically varies between 0.5 and 2 μm. The design key behind this technology is to produce a change in the effective index of the guided mode through a controlled dry ion etching of the silica overlayer. Figure 15a reproduces from Valette, Jadot, Gidon, Renard, Grand, Fournier, Grouillet, Philippe, Denis, Desgranges, Mulatier and Erbeia [1991] a curve depicting change in n_{eff} ($\equiv \Delta n_{eff}$), with the thickness of the silica overlayer as a variable. Physically the nature of the curve can be understood from the fact that varying thickness of the overlayer induces modification to the evanescent tail of the modal field distribution. For example, saturation of Δn_{eff} occurs when the silica overlayer thickness

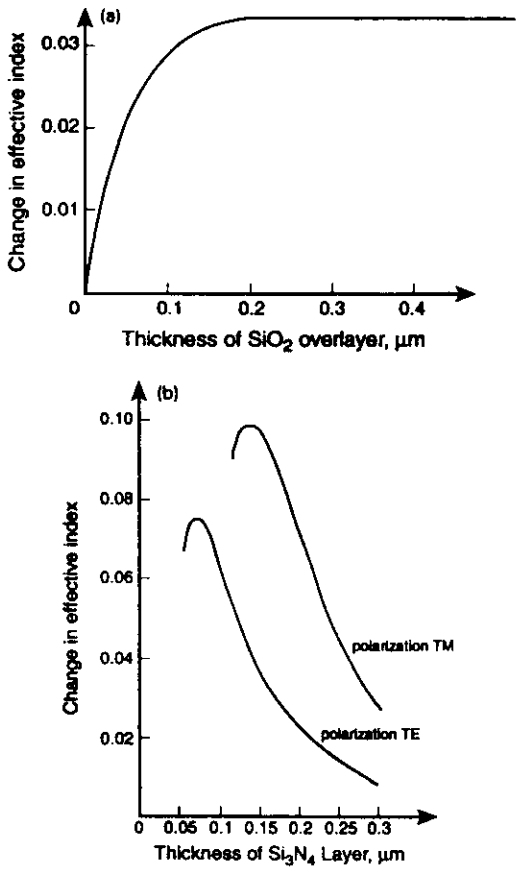

Fig. 15. (a) Theoretical change in the effective index of a single-mode $SiO_2/Si_3N_4/SiO_2$ waveguide as a function of thickness of the SiO_2 overlayer; (b) theoretical change in the effective index of the same waveguide with thickness of the Si_3N_4 core layer. (Both figures reproduced from Valette, Jadot, Gidon, Renard, Grand, Fournier, Grouillet, Philippe, Denis, Desgranges, Mulatier and Erbeia [1991] by permission of Kluwer Academic Publishers.)

exceeds the characteristic penetration depth of the mode's evanescent tail. Alternatively, modification of Δn_{eff} can be induced by using another dielectric of refractive index less than that of silica at the etched region. Futhermore, the change in n_{eff} with respect to a variation in the silicon nitride layer thickness is polarization sensitive, as shown in fig. 15b. The fundamental mode spot size in these waveguides is relatively small, and hence these waveguides are more suitable for coupling to laser diodes than to single-mode fibers.

The well-known flame hydrolysis deposition technology of fiber preform fabrication is the basis of an alternative approach to realize several guided-wave components on silicon (Kawachi [1990, 1991]). In this method (Kawachi, Yasu and Edahiro [1983]) a combination of flame hydrolysis deposition (FHD) and reactive ion etching (RIE) is employed to produce channel waveguides with modal field profiles matched to optical fibers. Raw materials in the form of a mixture of silicon tetrachloride ($SiCl_4$) and titanium tetrachloride ($TiCl_4$) or germanium tetrachloride ($GeCl_4$) and $SiCl_4$ are injected into an oxyhydrogen torch and react by flame hydrolysis to produce doped-silica soots, which get deposited on the silicon wafers. A large number of 7.62 cm silicon wafers (up to about 30) can be placed on a turntable of about 100 cm diameter to collect doped-silica particles. The refractive index of these synthesized glass particles can be controlled through variation in the $TiCl_4/GeCl_4$ flow rates. Initially, only $SiCl_4$ is fed into the flame to deposit silica soot to form the buffer layer before the core layers of doped silica are deposited. The deposited porous structure of buffer and core layers is then consolidated by heating in a separate electric furnace from about 1200 to 1300°C. A planar structure is thus formed. Typically, the buffer layer is about 20 μm thick and the core layer about 8 μm.

Various processing steps sequentially involved in this technology are shown in fig. 16. To form a ridge for channel waveguides, an overlayer of about 2 μm of amorphous silicon (a-Si) is deposited on top of the planar waveguide through magnetron sputtering. The ridge pattern was defined by conventional photolithography, followed by RIE of the overlayer with $CBrF_3$ gas. Subsequently, RIE with a mixture of C_2F_6 and C_2H_4 is carried out to etch out the deposited layers except the photolithographically defined ridge region until the buffer layer is exposed. The core ridge is thus formed and then covered by depositing a thick overlayer of silica through flame hydrolysis. The final product is a buried waveguide (Kawachi [1990]). The thick overlayer enables easy attachment of optical fiber arrays to the waveguide and dicing of the waveguide without damaging the core.

Typically, for a single-mode waveguide, core size is $8 \times 8\ \mu m^2$ and core-cladding index difference (Δn) is 0.25% (Kawachi [1990]). Transmission loss in these waveguides is about 0.1 dB/cm. For components that require high resistance to bending, small cores ($6 \times 6\ \mu m^2$) with a relatively high Δn (up to 0.75%) are also reported (Takato, Jinguji, Yasu, Toba and Kawachi [1988]). These waveguides exhibit a somewhat larger transmission loss of about 0.3 dB/cm. These numbers are for the cores made of titania-doped silica. Germania (GeO_2), whose melting temperature of 1086°C is lower than

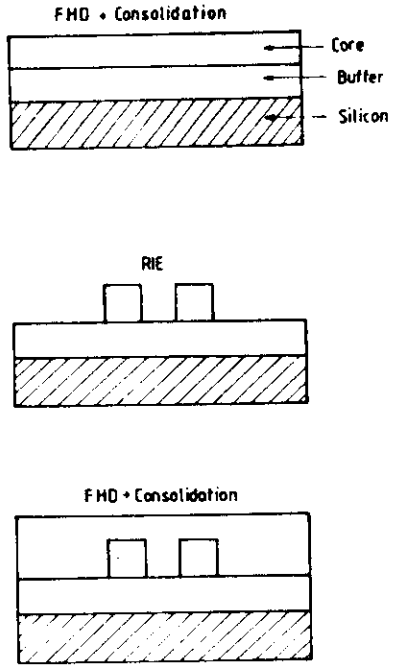

Fig. 16. Schematic of the flame hydrolysis deposition technology and its various intermediate steps. (After Takato, Jinguji, Yasu, Toba and Kawachi [1988], © 1988 IEEE.)

the value of 1850°C for titania, has been used to fabricate a long (~40 cm) single-mode waveguide having $\Delta n \simeq 0.75\%$ with fourteen 90° bends, each of 5 mm radius on a silicon wafer (Kominato, Ohmori, Okazaki and Yasu [1990], Kominato, Ohmori and Onose [1991]). Small amounts of phosphorus pentoxide (P_2O_5) and boron trioxide (B_2O_3), if added during deposition of both the core and the cladding, help to reduce the consolidation temperature of the deposited glass (Kominato, Ohmori, Okazaki and Yasu [1990]). Transmission loss, including the bend loss, was measured to be about 0.04 dB/cm at 1.55 μm (Kominato, Ohmori and Onose [1991]). Estimated loss in the straight part of the waveguide was about 0.01 dB/cm.

The FHD technique can be readily scaled up to produce highly multimode waveguides with cross-sections of about $40 \times 40\ \mu m^2$ and to realize integration of various optoelectronic components (Kawachi, Yasu and Edahiro [1983], Kawachi, Yamada, Yasu and Kobayashi [1985], Terui, Yamada, Kawachi and Kobayashi [1985]). Since mismatch in the thermal expansion coefficients between doped silica ($\simeq 0.5 \times 10^{-6}\ K^{-1}$) and silicon ($= 2.5 \times 10^{-6}\ K^{-1}$) is large, we might expect crack formation with such thick

silica layers. However, stress in silica waveguides is compressive, and this prevents cracking of the waveguides, although it leads to a birefringence of about 4×10^{-4} between the TM and TE modes (Kawachi [1990]).

Two different methods have been proposed to control the birefringence between the TE and TM modes in a silica-based waveguide on silicon. In one method a pair of grooves is etched (through RIE) symmetrically around the waveguiding ridge along its length in the cladding (Kawachi, Takato, Jinguji and Yasu [1987]). These grooves lead to a release of stress on the ridge; birefringence reduces to 0 as the ridge width decreases from about 500 to 50 μm (Kawachi [1990]). Alternatively, birefringence can be controlled by depositing a magnetron-sputtered 6 μm thick film of a-Si on top of the overcladding (Kawachi [1990]). The residual stress of the sputtered a-Si film modifies the birefringence of the waveguide. Once again, the magnitude of the resultant birefringence is determined by the width of the a-Si film. Birefringence increases to about 5.5×10^{-4} for an a-Si strip width of 50 μm, and then decreases to 2.5×10^{-4} as the strip width increases to about 200 μm (Kawachi [1990]). Microwave (2.45 GHz) plasma-assisted CVD at about 1000°C was also used to form germania-doped silica and silicon nitride waveguides on a silica substrate (Nourshargh, Starr and McCormack [1986], Nourshargh, Starr and Ong [1989]). In another recent investigation (Sun, Myers, Schmidt and Sumida [1991]), a germania-doped silica channel waveguide formed on silicon through FHD and RIE was transformed to a circular, cross-sectional channel waveguide by employing a selective etching of the waveguide in a buffered hydrofluoric acid (HF) solution (containing a mixture of 49% HF and 40% NH_4F solutions). In view of the circular cross-section of the core, the coupling loss from fiber-to-waveguide-to-fiber drops to about 0.5 dB from 1.8 dB, which is typical for a fiber-to-rectangular core-to-fiber coupling (Sun, Myers, Schmidt and Sumida [1991]).

Silicon in combination with silica is used to form multilayer ARRO waveguides, the functional principle of which was discussed in § 2. A second cladding of about 2 μm thickness is grown on the silicon wafer by thermal oxidation (fig. 9a). Subsequently, a thin (~0.1 μm) layer of poly-Si or titania or silicon nitride is deposited by CVD to form the highly reflecting layer. The silica core (~4 μm) is finally deposited on the top by LPCVD. Loss of about 0.4 dB/cm at 1.3 μm for TE modes has been reported (Duguay, Kokubun, Koch and Pfeiffer [1986]). The choice of materials for the first cladding depends on the wavelength. For wavelengths less than 0.9 μm, titania ($n \approx 2.1$) is the preferred material because poly-Si is highly absorbing at these wavelengths, whereas for wavelengths longer than 1.1 μm, poly-Si

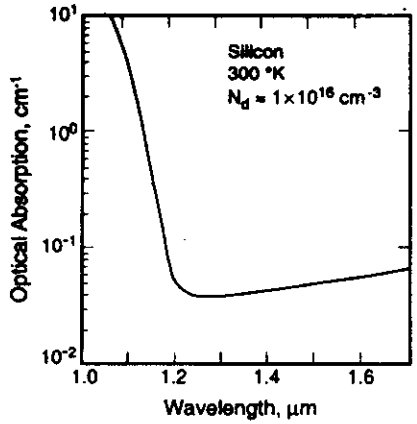

Fig. 17. Optical absorption spectrum of n-type crystalline silicon; donor concentration N_D is 10^{16} cm^{-3}. (Reprinted with permission of Solid State Technology from Soref and Lorenzo [1988].)

($n \sim 4.5$) is more suitable (Kokubun, Baba, Sasaki and Iga [1986]). On the other hand, silicon nitride is expected to be useful in both wavelength ranges (Pal, Singh, Ghatak and Bhattacharya [1990]). In a slightly different configuration (fig. 9c), the first cladding is replaced by a 0.3 μm layer of NA45 glass* of refractive index ~1.54 to provide total internal reflection in contrast to pure reflection that occurs in a normal ARRO waveguide (Baba and Kokubun [1989]). In this configuration, which is called an ARRO-B waveguide, all the layers are deposited by radiofrequency magnetron sputtering, and the measured losses for TE_0 and TM_0 modes were 0.5 and 0.7 dB/cm, respectively, at 0.633 μm (Baba and Kokubun [1989]).

All the silicon-based waveguides reported to date used silicon only as a support material. However, due to its high transparency between 1.2 and 1.6 μm (fig. 17), low-loss waveguide components in silicon are attractive for optical fiber systems. Significant work using silicon as a waveguide was reported by Soref and Lorenzo [1985, 1986, 1988], Soref and Bonnett [1987]), exploiting the fact that injection of free carriers reduces the refractive index of a semiconductor. However, the presence of free carriers also induces an increase in absorption coefficient. Free-carrier-induced decrease in the refractive index and increase in the absorption coefficient are given by (Moss [1959], Soref and Bonnett [1987], Lubberts, Burkey, Moser and Trabka [1981])

* A proprietory trade name is used to enable the readers to reproduce the experiment; other glasses might work as well or better.

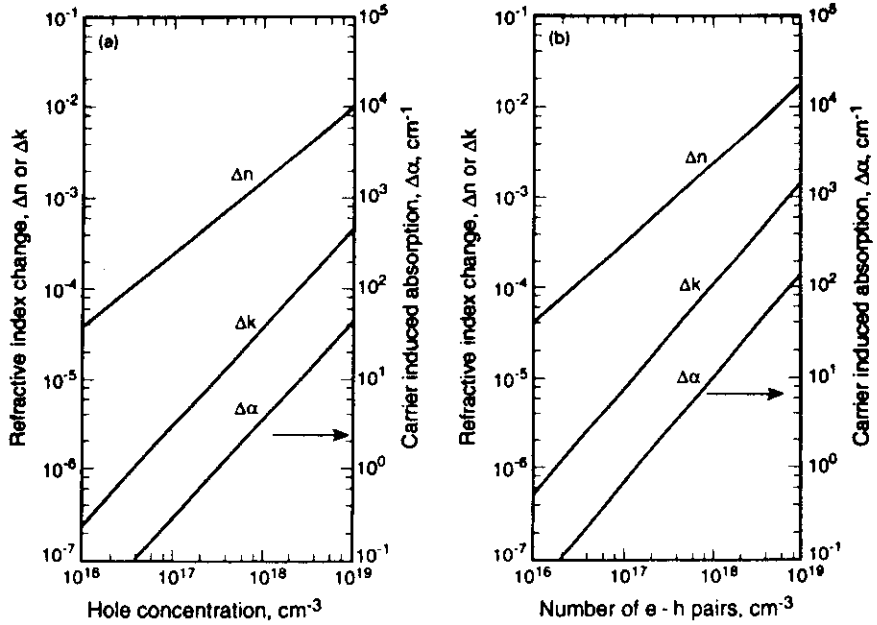

Fig. 18. Carrier-induced change in the complex refractive index $n + ik$ of silicon with: (a) hole concentration; (b) number of e–h pairs. (Reprinted with permission of Solid State Technology from Soref and Lorenzo [1988].)

$$\Delta n = -(q^2\lambda^2/8\pi^2c^2n\varepsilon_0)[N_e/m_{ce}^* + N_h/m_{ch}^*], \tag{3.1}$$

and

$$\Delta\alpha = (q^3\lambda^2/4\pi^2c^3n\varepsilon_0)[N_e/m_{ce}^{*2}\mu_e + N_h/m_{ch}^{*2}\mu_h], \tag{3.2}$$

where q, λ, ε_0, and n are electronic charge, optical wavelength, free-space permittivity, and refractive index of pure silicon. N_e, m_{ce}, and μ_e represent free-electron concentration, conductivity effective mass of an electron, and electron mobility, respectively; the corresponding quantities with h in the subscript represent the same characteristic quantities for holes. Free-carrier-induced changes in the real (Δn) and imaginary (Δk) parts of the refractive index, as well as the absorption coefficient ($\Delta\alpha$), are plotted as a function of carrier concentration in figs. 18a and b. Thus, optical waveguides can be formed by the epitaxial growth of a layer of lightly doped silicon on a heavily doped silicon substrate. The epilayer forms the core of an optical waveguide suitable for operation at 1.3 μm (Soref and Lorenzo [1985], Soref and Bonnett [1987]). To induce a sufficient change in the refractive index of silicon through carrier doping, carrier concentrations greater than 10^{16} cm^{-3} are required. Typically, for $N \sim 10^{18}$ cm^{-3}, Δn is about

-0.9×10^{-3} at 1.3 μm (Soref and Bonnett [1987]). Fabrication of several slab and channel waveguides with n on n^+, p on p^+, n on p^+, and p on n^+ have been reported. At 1.3 μm, these multimode waveguides exhibit loss ranging from 5 to 13 dB/cm in the slab and from 15 to 10 dB/cm in the rib channel geometry (Soref and Bonnett [1987], Hall [1987]).

Another method of forming optical waveguides in silicon involves the separation by implanted oxygen (SIMOX) technique (Hall [1987], Kurdi and Hall [1988]). Fabrication of planar waveguide by this technique was recently reported by Weiss, Reed, Toh, Soref and Namavar [1991]. Oxygen ions at a dose of 1.6×10^{18} cm^{-2} at 160 keV are implanted in silicon followed by thermal annealing for 6 h at 1300°C. Ion implantation leads to a 0.4 μm thick oxide layer buried under a 0.15 μm silicon layer. Subsequently, a 2 μm thick doped-silicon layer with a carrier concentration of about 10^{15} cm^{-3} is grown by CVD over the top surface. This layer of doped silicon forms the cover over the intermediate core of undoped silicon (Weiss, Reed, Toh, Soref and Namavar [1991]). Thus, the implanted silica layer essentially separates the core and substrate, both of which are made of silicon to prevent leakage loss. Loss measurements made at 1.15 and 1.523 μm with He–Ne lasers indicated a loss minimum of 8 dB/cm for the TE_0 mode at 1.15 μm (Weiss, Reed, Toh, Soref and Namavar [1991], Weiss and Reed [1991]).

Fabrication of single-mode waveguides in silicon through in-diffusion of Si–Ge alloys was also reported (Splett, Schmidtchen, Schüpert and Petermann [1990]). The process involved diffusion of Ge_xSi_{1-x} alloy into a well-defined section of the silicon wafer at 1200°C for 65 h; typically, $x = 0.5$. Single-mode ridge waveguides having $x = 0.01$ were fabricated through anisotropic etching with a mixture of 100 g of KOH and 100 mL of H_2O at 60°C. The best transmission loss was about 3 dB/cm at 1.3 μm (Splett, Schmidtchen, Schüpert and Petermann [1990]).

Fabrication of buried optical waveguides using electron beam irradiation of silica in a slab geometry was recently reported (Barbier, Green and Madden [1991]). An electron accelerating voltage of about 25 keV was used to irradiate the samples, leading to a waveguide depth of 7.5 μm. Lowest measured loss was about 0.3 dB/cm at 0.6328 μm.

§ 4. Guided-Wave Optical Components on Silicon

Although the technology of silicon-based integrated optics is relatively

reported. They include Fresnel lenses, beam splitters, dispersive mirrors, couplers, polarization devices, spectrum analyzers, displacement sensors, refractive index sensors, wavelength and frequency division multiplexers and demultiplexers, Bragg cells, optical switches, Y branches, X crosses, directional couplers, 8 × 8 star couplers, waveguide arrays, phase shifters, birefringence controllers, resonators, Bragg reflector lasers, and Bragg reflection filters. By means of photolithography two doped-silica FHD waveguides separated by only a few micrometers can be designed on silicon to form a directional coupler (fig. 7) (Kawachi [1990], Okamoto, Takahashi, Suzuki, Sugita and Ohmori [1991]). The intermediate region between the two cores is easily filled with cladding glass during the consolidation step of the FHD process. These couplers are polarization insensitive. Several such guided-wave optical beam splitters suitable for splitting, redirecting, tapping, and combining optical signals have been fabricated through FHD waveguides on silicon (fig. 19) (Kawachi [1990]). The excess loss due to coupling from fiber-to-waveguide-to-fiber in the Y configuration of the beam splitter is about 1 ± 0.5dB in the 1.2 to 1.6 μm wavelength range. In the directional coupler configuration (fig. 19b), high wavelength selectivity of the directional couplers allows the beam splitter to operate at 1.3 or 1.55 μm with an excess loss of less than 1 dB. Wavelength division multiplexers and demultiplexers

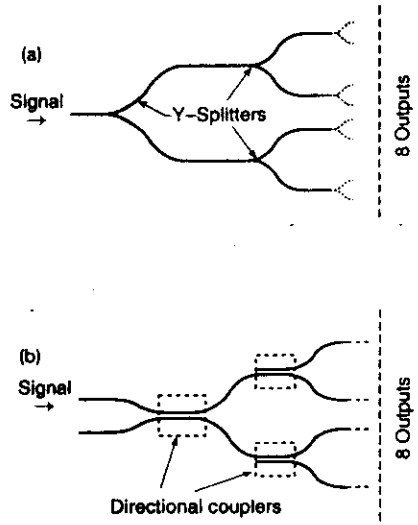

Fig. 19. Schematic of a silica-based, single-mode (1 × 8) optical waveguide beam splitter in two different configurations: (a) Y-shaped branch, (b) directional couplers. (After Kawachi [1990].)

based on directional couplers can be constructed either in a single coupler configuration or by combining two directional couplers along the z-direction in a Mach–Zehnder interferometer on silicon (Kobayashi, Kito, Yasu and Kawachi [1989], Kawachi [1990], Jinguji, Takato, Sugita and Kawachi [1990]). In the single-coupler geometry, which is more suitable for realizing large wavelength separation (1.3 and 1.5 μm), the coupler is designed to have zero coupling at one wavelength (λ_1) and 100% coupling at the second wavelength (λ_2). Thus, as shown in fig. 20a, light at λ_1 will exit through the output port of the first waveguide and λ_2 will exit through the output port of the second waveguide. In the second configuration two directional couplers are joined through two intermediate waveguide arms with a small path difference ΔL between them (fig. 20b). To obtain good wavelength multiplexing and demultiplexing efficiency for arbitrary combinations of λ_1 and λ_2, submicrometer accuracy is required in ΔL. This accuracy is readily attained through photolithography during the mask preparation (Kawachi [1990]).

The temperature coefficient of the refractive index of silica, dn/dT, is about 10^{-5}. Thus, a temperature increase of 6.5°C will induce a phase shift of π to the guided mode in a 10 mm silica waveguide. Typically the power consumption will be only 0.5 W. A thin-film chromium heater can be loaded on top of a single-mode buried silica waveguide in silicon (as shown in

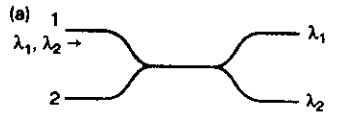

Single directional coupler configuration

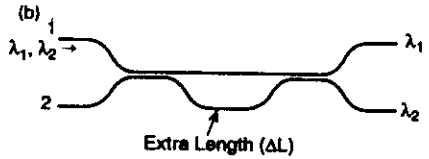

MZ Interferometer configuration

Fig. 20. Two different directional coupler configurations for realizing wavelength-division multiplexer or demultiplexer: (a) single directional coupler, (b) Mach–Zehnder interferometer. (After Kawachi [1990].)

fig. 21) to realize such an in-line thermo-optic phase shifter. Optical frequency division multiplexers or demultiplexers have been fabricated by loading a Mach–Zehnder waveguide interferometer in silica with such a thin-film chromium heater (Toba, Oda, Nosu and Takato [1989], Takato, Kominato, Sugita, Jinguji, Toba and Kawachi [1990]). As shown in fig. 21, two 3 dB waveguide couplers are combined through two waveguide arms with a path difference of ΔL between them. A thin-film heater is loaded on one arm to induce an additional phase shift and, hence, a corresponding additional optical path length difference between the two arms to obtain frequency tuning in the demultiplexer. The path length difference ΔL determines frequency spacing Δf through (Kawachi [1990])

$$\Delta f = \frac{c}{2n\,\Delta L}, \tag{4.1}$$

where n is the refractive index of the waveguide and c is the free-space velocity of light. An optical path difference (ΔL) of 17 mm will cause Δf to be about 6 GHz; Δf is related to wavelength spacing $\Delta\lambda$ through

$$\Delta f = -\frac{c}{\lambda^2}\Delta\lambda. \tag{4.2}$$

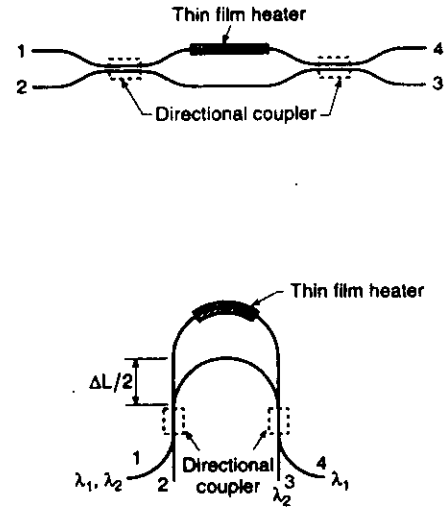

Fig. 21. Frequency division multiplexer or demultiplexer with thermo-optic phase shifter on a silica-based Mach–Zehnder waveguide interferometer. (After Takato, Jinguji, Yasu, Toba and

A value of Δf of 6 GHz amounts to a wavelength spacing of about 0.05 nm in the 1.55 μm wavelength band. Frequency tuning in these multiplexers or demultiplexers can be obtained through modulation of the optical path-length difference between the two arms of the interferometer by means of the phase shifter. This thermo-optic effect can also be used to perform switching operations in an otherwise passive silica waveguide, although the switching time is slow (~2 ms) (Takato, Jinguji, Yasu, Toba and Kawachi [1988], Kawachi [1990]). A thermo-optic switch is configured by combining two directional couplers through two intermediate waveguide arms as in the thermo-optic frequency division multiplexer. However, there is one difference. In contrast to loading one of the waveguides as in a frequency division multiplexer, both waveguide arms are loaded with thin-film heaters in a switch. In the absence of any electrical input to the phase shifters, the switch operates in the cross-state. When electrical power corresponding to a π phase shift is supplied to either of the phase shifters, the switch operates in the parallel state.

In an alternative scheme a photo-induced change in the refractive index of germania-doped silica has been used in an asymmetric Mach–Zehnder waveguide interferometer-based frequency division multiplexer to obtain frequency tuning (Hibino, Kominato and Ohmori [1991]). A 20 W Ar^+ ion laser is used to irradiate the waveguide for about an hour, which leads to a maximum refractive index change of about 4×10^{-5} at 1.3 μm. The frequency shift (Δf) due to laser irradiation relative to free spectral range ($f_s = 25$ GHz) of the multiplexer is described by (Hibino, Kominato and Ohmori [1991]),

$$\frac{\Delta f}{f_s} = 2\,\Delta n\,(L + \Delta L)\lambda, \tag{4.3}$$

where Δn is the photo-induced refractive index change in the lower arm of the asymmetric Mach–Zehnder interferometer, L is the length of the shorter waveguide between the two 3 dB couplers of the interferometer. Photo-induced change in the refractive index has also been observed in titania-doped silica waveguides (Hibino, Abe, Kominato and Ohmori [1991]). A maximum change in the refractive index induced by an Ar^+ laser was about 1×10^{-5} in a Mach–Zehnder waveguide interferometer in which the concentration of titania in the core was about 0.3 mol%. In another experiment, the laser-induced change in the refractive index of a silicon oxynitride–silica waveguide was used to tune the optical power coupling ratio to any arbitrary value in a directional coupler (Gleine and Müller [1991]). A large number

either in parallel or in series to form a variety of devices. Examples include 128 channel selective optical frequency division multiplexed filter (Takato, Sugita, Onose, Okazaki, Okuno, Kawachi and Oda [1991]), 8×8 matrix thermo-optic switch through sixty-four 2×2 switching units (Sugita, Okuno, Matsunagu, Kawachi and Ohmori [1990]), and 8-tap optical transverse filter (Kawachi [1991], Sasamaya, Okuno and Habara [1991]). Performance characteristics of a wide variety of FHD waveguide components including ring resonators on silicon were recently reviewed (Kawachi [1990, 1991]).

FHD silica ridge waveguides in which germania and phosphorus pentoxide are used as co-dopants have also been reported to generate the second harmonic of a Q-switched Nd–YAG laser pump at 1.064 μm (Kashyap, Ainslie and Maxwell [1989]). Frequency doubling is due to a nonlinearity similar to the quadrupole interaction known to occur in silica fibers (Österberg and Margulis [1986]). A 200-fold increase in the yield of the frequency-doubled radiation has been observed when the waveguide is seeded for about an hour with a 0.532 μm light.

Several other guided wave components and devices based on waveguides on silicon, such as the spectrum analyzer, Fresnel lenses and mirrors, Bragg cell, displacement sensor, and liquid refractive index sensors were reviewed by Valette, Jadot, Gidon, Renard, Grand, Fournier, Grouillet, Philippe, Denis, Desgranges, Mulatier and Erbeia [1991]. In the spectrum analyzer, 1.5 μm of ZnO, which is a piezoelectric material, is deposited by magnetron sputtering from a zinc target on top of a silicon nitride waveguide leading to the composite structure $Si/SiO_2/S_3N_4/SiO_2/ZnO$. Surface acoustic waves are generated and propagated through the ZnO film by feeding electrical signals to an interdigital transducer (IDT) finger laid on it, thereby creating a phase grating on the waveguide. The guided waves experience Bragg diffraction by this grating. Scanning the spatial locations of the diffracted light spot by means of a photodiode array can be correlated to the frequency content of the electrical signal feeding the ZnO piezotransducer. The theory of such acousto-optic devices has been described by Ghatak and Thyagarajan [1989]. Two different versions of such a spectrum analyzer, *in-line* and *folded* types, were reported (Valette, Lizet, Mottier, Jadot, Gidon and Renard [1984], Mottier, Valette and Jadot [1986], Valette, Mottier, Lizet and Gidon [1986]). Typical characteristics of these devices operating at 0.835 μm are shown in table 2. The displacement sensor is essentially a Michelson interferometer in which all the optical components, such as lenses, beam splitter, mirrors, and phase shifters, are integrated on the silicon wafer. The interfer-

TABLE 2
Integrated optical spectrum analyzer: performances of in-line and folded types (From Valette, Jadot, Gidon, Renard, Grand, Fournier, Grouillet, Philippe, Denis, Desgranges, Mulatier and Erbeia [1991].)

Device parameter	In-line type	Folded type
Bandwidth (MHz)	180	480
Resolution (MHz)	6	3 (1.5–2)*
Central freq. (MHz)	Acoustic mode	600–700**
Acoustic mode	Rayleigh classical	Sesawa
Integrated lenses	Fresnel lenses	Curved Fresnel lenses
Focal length (mm)	10	20
Resolved spots	20	160
Dynamic range (dB)	25 (30)	10–15 (25)
Access time	20 μs	5 μs (2)
Photodetector array	Serial-parallel CCD 2 × 10 pixels	Serial-parallel CCD 16 × 10 pixels
Optical source	HLP 1400 (0.835 μm)	HLP 1400 (0.835 μm)

* Numbers in parentheses indicate performances possible in the near future.
** Transducer array with 700 MHz central frequency leads to the generation of a third acoustic mode beyond 860 MHz.

wafer (Gidon, Valette and Schweizer [1985], Valette, Renard, Jadot, Gidon and Erbeia [1989], Valette, Renard, Jadot, Gidon and Erbeia [1990]). The working distance of this sensor is 10 cm, and it can make linear distance measurements with an accuracy of 0.1 μm. Furthermore, if a liquid of refractive index less than that of the cover silica layer is placed on the sensing arm of the interferometer, it will induce a phase change in the guided beam. As a result, a fringe shift in the interference pattern will occur, which can be correlated with the refractive index of the sample liquid (Valette, Renard, Jadot, Gidon and Erbeia [1990]).

Several optical components, such as Fresnel lenses, mirrors (plane, parabolic, and elliptical), polarization converters or dividers, and phase shifters, have been reported on oxidized silicon substrates through partial or complete etching of the silicon overlayer (Mottier and Valette [1981], Valette, Morque and Mottier [1982], Gidon, Valette and Mottier [1985], Valette, Renard, Denis, Jadot, Fournier, Philippe, Gidon, Grouillet and Desgranges [1989]). U-grooves are etched in silicon to achieve low-loss (<0.7 dB) connection between single-mode fibers and channel waveguides grown in silicon (Grand, Denis and Valette [1991]). The process uses RIE to create a slot of a width equal to the diameter of the fiber to be connected. This is followed by deep

to the groove with a glue (Grand, Jadot, Valette, Denis, Fournier and Grouillet [1990]). A set of four U-grooves are formed to construct a four-channel wavelength multiplexer or demultiplexer (fig. 22) (Valette, Gidon and Jadot [1987]). In this device a waveguide Fresnel mirror is incorporated on the silicon substrate to disperse and focus the four wavelengths (channel separation ≃20 nm around 1.5 μm) to four spatial locations at one edge of the substrate. The U-grooves are etched on these locations to form microguides and make optical coupling with the four optical fibers. Cross-talk between the channels is less than −15 dB (Grand, Jadot, Valette, Denis, Fournier and Grouillet [1990]). Recently, fabrication of a ringe resonator operating at 0.8 μm was also reported. A finesse of 48 ± 1.5 has been achieved at a propagation loss of 0.028 ± 0.009 dB/cm; the effective diameter of the ring is about 3 cm (Bismuth, Gidon, Revol and Valette [1991]).

A large number of novel components based on phosphosilicate or silicon nitride–core silica waveguides on silicon was reviewed by Henry, Blonder and Kazarinov [1989]. Examples include star couplers (Dragone, Henry, Kaminow and Kistler [1989], Dragone [1991], Dragone, Edwards and Kistler [1991]), polarization splitters (Shani, Henry, Kistler, Kazarinov and Orlowsky [1990]), four-channel Mach–Zehnder multiplexers (Verbeek, Henry, Olsson, Orlowsky, Kazarinov and Johnson [1988]), Bragg reflector lasers (Olsson, Henry, Kazarinov, Lee, Orlowsky, Johnson, Scotti, Ackerman and Anthony [1988]), and Bragg reflection filters (Henry, Shani, Kistler, Jewell, Pol, Olsson, Kazarinov and Orlowsky [1989a,b]). As shown in fig. 23 in their $N \times N$ star coupler geometry (N up to 40), an array of phosphosilicate

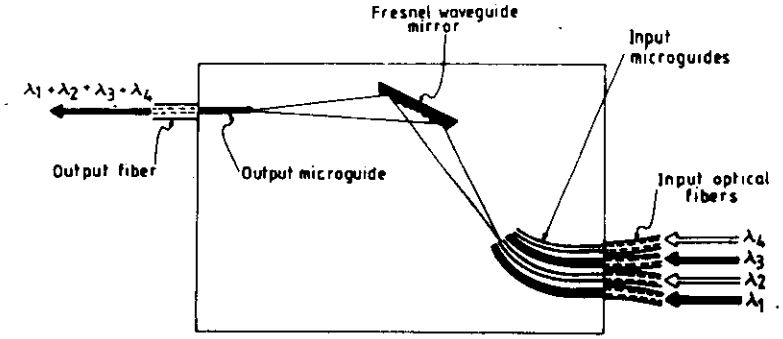

Fig. 22. Schematic of a wavelength division multiplexer or demultiplexer integrated with a waveguide Fresnel mirror. (Reproduced from Valette, Jadot, Gidon, Renard, Grand, Fournier, Grouillet, Philippe, Denis, Desgranges, Mulatier and Erbeia [1991] by permission of Kluwer Academic Publishers.)

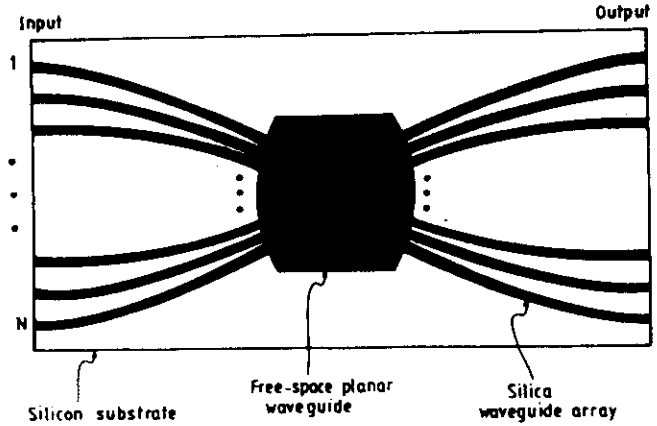

Fig. 23. Schematic of a $N \times N$ star coupler on silicon. (Reproduced with permission of IEEE from Henry, Blonder and Kazarinov [1989], © 1989 IEEE.)

glass cores merges into a free-space slab waveguide formed on the silicon substrate. The light injected by the array waveguides into the slab is collected by a corresponding array of waveguides on the other side of the slab. For a 19 × 19 star coupler, fiber-to-fiber loss was only about 3 dB more than the excess loss due to division by 19 (Henry, Blonder and Kazarinov [1989]). The polarization splitter consists of a Mach–Zehnder interferometer formed with phosphosilicate glass waveguides in which one of the arms has an additional 22 nm patch of silicon nitride (fig. 24) (Henry, Blonder and Kazarinov [1989]). The silicon nitride layer is added before deposition of the phosphosilicate glass. The silicon nitride layer is highly birefringent, and induces a phase shift to the TE polarization larger than the TM polarization.

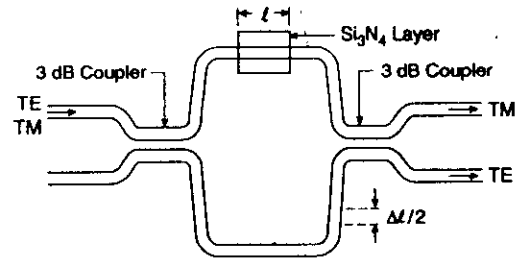

Fig. 24. Schematic of a polarization splitter based on a silica waveguide Mach–Zehnder interferometer, in which a patch of Si_3N_4 is introduced in one arm to produce a linear birefringence between the TE and TM modes. (Reproduced with permission of IEEE from Henry, Blonder and Kazarinov [1989], © 1989 IEEE.)

The length of the silicon nitride layer is adjusted to induce a 2π phase change in the upper arm so the TE polarization crosses over to the lower port. The TM polarization is made to undergo a phase change of π only in the upper arm by adjusting the additional length ΔL (fig. 24). Thus, TE polarization may exit through the lower port while the TM mode exits through the other output port. The insertion loss is in the range of 1.6 to 2.0 dB, whereas suppression of unwanted polarization is 14 to 21 dB. A polarization splitter that has an insertion loss of about 1.5 dB and uses a Y-branch waveguide made with phosphosilicate glass and silicon nitride cores was fabricated by Shani, Henry, Kistler, Kazarinov and Orlowsky [1990]. It is an adiabatic device based on an asymmetric Y-branch. A 7 μm phosphosilicate glass core is gradually tapered to a 5 μm waveguide 5 mm in length, which branches off adiabatically (over a length of 1 mm) into a pair of waveguides: a 55 nm silicon nitride core waveguide and a 7 μm phosphosilicate glass core waveguide. The TE mode can be made to branch to the nitride guide by an appropriate choice of the nitride layer thickness, which is birefringent, while the TM mode exits through the phosphosilicate glass waveguide. The silicon nitride waveguide eventually makes a transition to a phosphosilicate glass waveguide. Cross-talk for the unwanted polarization is in the range of −15 to −34 dB at 1.55 μm. A four-channel multiplexer with a channel separation of 7.7 nm was fabricated on silicon by combining three Mach–Zehnder interferometers formed with phosphosilicate glass waveguides in which fiber-to-fiber insertion loss is 2.5 dB (Verbeek, Henry, Olsson, Orlowsky, Kazarinov and Johnson [1988]). The multiplexer is almost polarization insensitive. The additional path length ΔL_1 is chosen to yield a channel spacing of 14.4 nm between λ_1 and λ_2 (fig. 25). The other wavelengths λ_3 and λ_4 are chosen with the same channel spacing. The third Mach–Zehnder

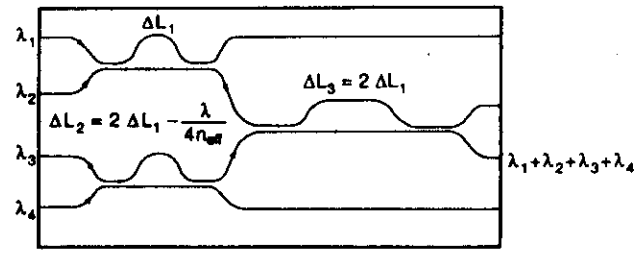

Fig. 25. A four-channel wavelength multiplexer based on Mach–Zehnder interferometric elements in a doped-silica waveguide on silicon. (Reproduced with permission of IEEE from Verbeek, Henry, Olsson, Orlowsky, Kazarinov and Johnson [1988], © 1988 IEEE.)

interferometer combines all the wavelengths into a single channel. All the variables ΔL_1, ΔL_2, and ΔL_3, which are required to a high precision in the multiplexer design, are controlled at the mask development stage. The fiber-to-fiber insertion loss is 2.5 dB.

High-resolution Bragg reflection filters that operate at 1.3–1.6 μm require line and spatial features of the grating to be about 0.25 μm. A spatial frequency-doubling lithography (SFDL) technique with an excimer laser in the deep ultraviolet region is used for patterning such periodic features on silicon waveguides (Olsson, Henry, Kazarinov, Lee and Orlowsky [1987], Henry, Blonder and Kazarinov [1989], Henry, Shani, Kistler, Jewell, Pol, Olsson, Kazarinov and Orlowsky [1989a,b]). The SFDL technique can be used to generate a number of gratings simultaneously on the same mask. In another set of experiments, holographic techniques are employed to pattern gratings of a period of about 0.5 μm on the top surface of a silicon nitride waveguide to form a *silicon chip Bragg reflector* (fig. 14) (Ackerman, Kwo, Silva and Wagner [1988]). When such a reflector is coupled to a laser diode, single-mode operation of the laser can be attained near the Bragg wavelength (Henry, Blonder and Kazarinov [1989], Olsson, Henry, Kazarinov, Lee, Orlowsky, Johnson, Scotti, Ackerman and Anthony [1988]). Under certain operating conditions, temperature variations can cause a great reduction in the line width of these lasers. Typically, $\Delta\nu$ is 1–50 MHz (Henry, Shani, Kistler, Jewell, Pol, Olsson, Kazarinov and Orlowsky [1989a,b]); in one experiment, $\Delta\nu$ was 110 kHz (Ackerman, Kwo, Silva and Wagner [1988]). In another version a 1.5 μm laser was coupled to an integrated optic quarter-wave shifted Bragg cavity to realize an ultra-narrow line width ($\Delta\nu \sim 135$ kHz) resonant optical reflection laser (Olsson, Henry, Kazarinov, Lee, Johnson and Orlowsky [1987]). Such a laser with $\Delta\nu$ as low as 10 kHz was reported by Ackerman, Dabura, Shani, Henry, Kistler, Kazarinov and Kwo [1990].

Electrorefraction or carrier-induced refractive index change in silicon has been used to realize an electro-optic switch in silicon (Soref and Lorenzo [1986, 1988], Soref and Bonnett [1987]). Electrorefraction, which is related to the well-known Franz–Keldysh effect of electro-absorption, arises due to electric field-induced tunneling between the valence and the conduction bands. On the other hand, a carrier injection of 10^{18} cm^{-3} can induce a change of 10^{-3} in the refractive index of silicon. An infrared light modulator has been fabricated by using such a carrier-induced change in the refractive index of silicon (Kanada, Fujisawa and Kikuiri [1986]). Fabrication of an optical power divider with two epitaxially grown, crossed silicon multimode

rib waveguides with a donor concentration (n_D) of about 9×10^{14} cm^{-3} on a heavily doped ($n_D \sim 3 \times 10^{19}$ cm^{-3}) silicon substrate to operate at 1.3 μm has also been reported (Soref and Lorenzo [1986]).

§ 5. Active Waveguides on Silicon

Considerable progress has been achieved in recent years on rare earth-doped fiber lasers and amplifiers (Urquhart [1988]). Fiber lasers with a variety of rare earth dopants such as neodymium, erbium, thulium, holmium, ytterbium, praseodymium, and samarium, and based on silica and fluorozirconate glasses as host, have already been reported (Digonnet [1990, 1993]). Since the materials involved in silica-based optical waveguides on silicon are very similar to those of low-loss optical fibers (Pal [1979]), it should be possible to realize active components like lasers and amplifiers in silica-based planar waveguides on silicon. Indeed, continuous wave lasing at a wavelength of 1.0515 μm was achieved by fabricating a neodymium-doped silica core ridge waveguide 20 μm wide on a silicon substrate by FHD and RIE (Hibino, Kitagawa, Shimizu, Hanawa and Sugita [1989]). Neodymium is incorporated into the silica waveguide by immersing the FHD soot glass consisting of a network of silica, boron, and phosphorus in an alcohol solution of 0.5% of $NdCl_3 \cdot 6H_2O$ before the sintering step. Neodymium ion concentration is estimated to be about 2000 ppm. A 6 μm wide ridge pattern is formed on the sintered core of a neodymium-doped phosphosilicate glass waveguide by RIE followed by deposition of silica overcladding by the FHD process. Light from a Ti:Al_2O_3 laser tuned into 0.8 μm wavelength and pumped by an Ar^+ laser is injected into a single-mode fiber, which is butt-joined to the neodymium-doped waveguide as the pump source. A second single-mode fiber is butt-joined to the other end of the waveguide to collect the guided light. The resonator is formed by depositing dielectric mirrors onto the fiber end faces. The lasing threshold is about 150 mW and the slope efficiency is 0.12% (Hibino, Kitagawa, Shimizu, Hanawa and Sugita [1989]). The FWHM of the emitted lasing peak wavelength of 1.0515 μm is about 0.12 nm, and the measured transmission loss at the lasing wavelength is 0.85 dB/cm.

Fabrication of a neodymium-doped silica waveguide laser with an 8 μm wide core was recently reported (Hattori, Kitagawa, Ohmori and Kobayashi [1991]). A commercially available laser diode emitting at 0.805 μm is used

end faces. The lasting threshold is only 25 mW at a slope efficiency of 1.2%. It was made possible by a careful analysis of the scattering loss induced by neodymium doping and dependence of the lasing threshold on the width of the core. Lasing (continuous wave) at two wavelengths around 1.589 and 1.604 μm were recently demonstrated with an erbium-doped phosphosilicate glass waveguide fabricated by following the same approach through FHD and RIE (Kitagawa, Hattori, Shimizu, Ohmori and Kobayashi [1991]). Erbium ion concentration is estimated to be 8000 ppm. A $Ti:Al_2O_3$ laser tuned into 0.98 μm and pumped by an Ar^+ laser is used as the pump source. Dielectric mirrors to form the resonator are deposited directly onto the waveguide end faces. The pump power required for lasing is about 49 mW with a slope efficiency of 0.81%. Transmission loss at 1.54 μm is about 0.82 dB/cm. In some earlier experiments, silicon diodes not in a waveguide configuration, after being implanted with erbium ions, had yielded emission of 1.54 μm radiation at room temperature (Ennen, Schneider, Pomrenke and Axmann [1983], Ennen, Pomrenke, Axmann, Eisele, Haydl and Schneider [1985]). This scheme of erbium ion implanted emission was consolidated in silica-based waveguides to realize optical emission at the 1.5 μm wavelength region (Polman, Lidgard, Jacobson, Becker, Kistler, Blonder and Poate [1990], Lidgard, Polman, Jacobson, Blonder, Kistler, Poate and Becker [1991]). In particular, fluorescence was observed at 1.54 μm from phosphosilicate-core silica glass waveguides on a silicon substrate by implanting 3.5 MeV erbium ions into the waveguide at an implantation fluence in the range of 10^{15} to 10^{16} ions/cm^2. Fluorescence lifetime is typically 10 ms, which is of the same order as that observed in erbium-doped fibers. The radiation at 488 nm from an Ar^+ laser is used as the pump. It should be possible to incorporate optically active rare earths in the silica network of an ARRO waveguide on silicon. Work is under way in our laboratory to realize a near-infrared source through such a scheme.

§ 6. Conclusions

Starting from the earliest experiments on silicon-based waveguides in the 1970s, we have described different technologic options and the status of components realized or reported to date, and the theory of propagation in optical waveguides, both in planar and rectangular geometries. The review should provide a comprehensive description for design, fabrication and estimation of silicon-based optical waveguides and associated passive and

Acknowledgements

This work was supported by the Indo–US Materials Science Collaboration Program. The writing of this review started at IIT, New Delhi; however, a major portion of it was written during my sabbatical year as Visiting Scholar at NIST, Boulder, Colorado. I am grateful to the Fulbright Foundation for providing travel support. Special thanks go to my host R. L. Gallawa for his keen interest, enthusiasm, and encouragement, and generosity of time and patience. His constructive criticisms have greatly improved the coherence of the review. I further thank A. K. Ghatak, N. Sanford, and G. P. Agrawal for very useful comments as reviewers for our internal editorial review board, and Matt Young and Don Larson for their helpful editorial suggestions. I had many interesting discussions on silicon-based integrated optics with my erstwhile student Hemant Singh at IIT Delhi. I thank Swagata Deb for her help in some of the numerical calculations on ARRO waveguides. Thanks are also due to Margalene Hartman for her editorial assistance.

References

Aarnio, J., S. Honkanen and M. Leppihalme, 1987, A novel semiconductor process for optoelectronic applications on silicon substrate, in: Proc. Eur. Conf. Optical Communications, ECOC'87, Helsinki, p. 235.

Ackerman, D.A., M.I. Dabura, Y. Shani, C.H. Henry, R.C. Kistler, R.F. Kazarinov and C.Y. Kwo, 1990, Compact hybrid resonant optical reflector lasers with very narrow linewidths, in: Topical Meeting on Integrated Photonics Res., Hilton Head, SC.

Ackerman, D.A., C.Y. Kwo, V.L. Silva and E.J. Wagner, 1988, Compact silicon chip Bragg reflector hybrid laser with 110 kHz line-width, in: 11th Int. Semiconductor Conf., Boston, MA.

Adams, M.J., 1981, An Introduction to Optical Waveguides (Wiley, Chichester).

Adams, R., Y. Shani, C.H. Henry, R.C. Kistler, G.E. Blonder and N.A. Olsson, 1991, Very low-loss phosphorus-doped silica-on-silicon waveguides measured using a ring resonator, in: Opt. Fib. Commun., OFC'91, San Diego, Paper TuF5, p. 22.

Aiki, K., M. Nakamura and J. Umeda, 1977, A frequency multiplexing light source with monolithically integrated distributed feedback diode lasers, IEEE J. Quantum Electron. **QE-13**, 220.

Alferness, R.C., and L.L. Buhl, 1982, Tunable electro-optic waveguide TE–TM converter/wavelength filter, Appl. Phys. Lett. **40**, 861.

Baba, T., and Y. Kokubun, 1989, New polarization-insensitive antiresonant reflecting optical waveguide (ARROW-B), IEEE Photonics Tech. Lett. **PTL-1**, 232.

Baba, T., and Y. Kokubun, 1990, High efficiency light-coupling from antiresonant reflecting optical waveguide to integrated photodetector using an antireflecting layer, Appl. Opt. **29**, 2781.

Baba, T., and Y. Kokubun, 1991, Scattering loss of antiresonant reflecting optical waveguides

Baba, T., Y. Kokubun and H. Watanabe, 1990, Monolithic integration of an ARROW-type demultiplexer and photodetector in the shorter wavelength region, IEEE J. Lightwave Tech. **LT-8**, 99.

Baba, T., Y. Kokubun, T. Sasaki and K. Iga, 1988, Loss reduction of an ARROW waveguide in shorter wavelength and its stack configuration, IEEE J. Lightwave Tech. **LT-6**, 1440.

Barbier, D., M. Green and S.J. Madden, 1991, Waveguide fabrication for integrated optics by electron beam irradiation of silica, IEEE J. Lightwave Tech. **LT-9**, 715.

Bean, K.E., 1978, Anisotropic etching of silicon, IEEE Trans. Electron. Dev. **ED-25**, 1185.

Bismuth, J., P. Gidon, F. Revol and S. Valette, 1991, Low-loss ring resonators fabricated from silicon based integrated optics technologies, Electron. Lett. **27**, 722.

Boyd, J.T., and C.L. Chen, 1976, Integrated optical silicon photodiode array, Appl. Opt. **15**, 1389.

Boyd, J.T., and C.L. Chen, 1977, Integrated optical waveguide and charge-coupled device image array, IEEE J. Quantum Electron. **QE-13**, 282.

Boyd, J.T., and S. Sriram, 1978, Optical coupling from fibers to channel waveguides formed on silicon, Appl. Opt. **17**, 895.

Boyd, J.T., S.H. Chang, C.L. Fan and D.A. Ramey, 1981, Integration of photodetectors and optical guided wave structures formed on silicon substrates, Proc. SPIE **272**, 98.

Boyd, J.T., R.W. Wu, D.E. Zelmon, A. Neumaan and H.A. Timlin, 1984, Planar and channel optical waveguides utilizing silicon technology, in: Proc. 1st Conf. Integrated Optical Circuit Engineering, Proc. SPIE **517**, 100.

Boyd, J.T., R.W. Wu, D.E. Zelmon, A. Neumaan, H.A. Timlin and H.E. Jackson, 1985, Guided wave optical structures utilizing silicon, Opt. Eng. **24**, 230.

Carney, J.K., and L.D. Hutcheson, 1987, GaAs-based integrated optoelectronic circuits: Design, development and applications, in: Integrated Optical Circuits and Components: Design and Applications, ed. L.D. Hutcheson (Marcel Dekker Inc., New York) p. 229.

Chang, C.L., and C.S. Tsai, 1983, Electro-optic analog to digital converter using channel waveguide Fabry–Pérot modulator array, Appl. Phys. Lett. **43**, 22.

Chen, C.L., and J.T. Boyd, 1981, Temperature independent thin film optical waveguide, Appl. Opt. **20**, 2280.

Chubachi, N., 1976, ZnO film for acousto-optic devices in nonpiezoelectric substrates, Proc. IEEE **64**, 772.

Digonnet, M.J., ed., 1990, Proc. Fiber Laser Sources and Amplifiers II, Sept. 18–19, San Jose, CA (Society of Photo Optical Instrumentation Engineers, Bellingham, USA).

Digonnet, M.J., ed., 1993, Rare Earth Doped Fiber Lasers and Amplifiers (Marcel Dekker, New York).

Dragone, C., 1991, An $N \times N$ optical multiplexer using a planar arrangement of two star couplers, IEEE Photonics Tech. Lett. **PTL-3**, 812.

Dragone, C., C.A. Edwards and R.C. Kistler, 1991, Integrated Optics $N \times N$ multiplexer on silicon, IEEE Photonics Tech. Lett. **PTL-3**, 896.

Dragone, C., C.H. Henry, I.P. Kaminow and R.C. Kistler, 1989, Efficient multichannel integrated optics star coupler on silicon, IEEE Photonics Tech. Lett. **PTL-1**, 241.

Duguay, A., Y. Kokubun, T.L. Koch and L. Pfeiffer, 1986, Antiresonant reflecting optical waveguides in SiO_2–Si multilayer structures, Appl. Phys. Lett. **49**, 13.

Dutta, S., H.E. Jackson and J.T. Boyd, 1980, Reduction of scattering from a glass thin film optical waveguide by CO_2-laser annealing, Appl. Phys. Lett. **37**, 512.

Dutta, S., H.E. Jackson and J.T. Boyd, 1981, Extremely low-loss glass thin-film optical waveguides utilizing surface coating and laser annealing, J. Appl. Phys. **52**, 3873.

Dutta, S., H.E. Jackson, J.T. Boyd, F.S. Hickernell and R.L. Davis, 1981, Scattering loss reduction in ZnO optical waveguides by laser annealing, Appl. Phys. Lett. **39**, 206.

Dutta, S., H.E. Jackson, J.T. Boyd, R.L. Davis and F.S. Hickernell, 1982, CO_2-laser annealing of Si_3N_4, Nb_2O_5 and Ta_2O_5 thin film optical waveguides to achieve scattering loss reduction,

Ennen, H., G. Pomrenke, A. Axmann, K. Eisele, W. Haydl and J. Schneider, 1985, 1.54 μm electroluminescence of erbium-doped silicon grown by molecular beam epitaxy, Appl. Phys. Lett. **46**, 381.

Ennen, H., J. Schneider, G. Pomrenke and A. Axmann, 1983, 1.54 μm luminescence of erbium-implanted III–V semiconductors and silicon, Appl. Phys. Lett. **43**, 963.

Falco, C., J. Botineau, A. Azema, M. De Micheli and D.B. Ostrowsky, 1983, Optical properties determination at 10.6 μm of thin semiconducting layers, Appl. Phys. Lett. A **30**, 23.

Findalky, T., 1985, Glass waveguides by ion exchange: A review, Opt. Eng. **24**, 244.

Ghatak, A.K., 1986, Electromagnetics of integrated optical waveguides, J. Inst. Electron. & Telecom. Eng. (India) **32**, 159.

Ghatak, A.K., and K. Thyagarajan, 1989, Optical Electronics (Cambridge University Press, Cambridge).

Ghatak, A.K., K. Thyagarajan and M.R. Shenoy, 1987, Numerical analysis of planar optical waveguides using matrix approach, IEEE J. Lightwave Tech. **LT-5**, 600.

Gidon, P., S. Valette and P. Schweizer, 1985, Vibration sensor using planar integrated interferometric circuit on oxidized Si substrate, in: Proc. 2nd Int. Conf. on Optical Fiber Sensors, Stuttgart, eds R.Th. Kersten and R. Kist (VDE-Verlag GmbH, Berlin) p. 187.

Gidon, P., S. Valette and P. Mottier, 1985, Integrated lenses on silicon nitride waveguides, Opt. Eng. **24**, 235.

Gleine, W., and J. Müller, 1991, Laser trimming of SiON components for integrated optics, IEEE J. Lightwave Tech. **LT-9**, 1626.

Goell, J.E., 1969, A circular harmonic computer analysis of rectangular dielectric waveguides, Bell Syst. Tech. J. **48**, 2133.

Goell, J.E., and R.D. Strandley, 1969, Sputtered glass waveguides for integrated optical circuits, Bell Syst. Tech. J. **48**, 3445.

Grand, G., H. Denis and S. Valette, 1991, New method for low cost and efficient optical connections between single-mode fibers and silica guides, Electron. Lett. **27**, 16.

Grand, G., J.P. Jadot, H. Denis, S. Valette, A. Fournier and A.M. Grouillet, 1990, Low loss PECVD silicon channel waveguides for optical communications, Electron. Lett. **26**, 2135.

Grand, G., J.P. Jadot, S. Valette, H. Denis, A. Fournier and A.M. Grouillet, 1990, Fiber pigtailed wavelength multiplexer/demultiplexer at 1.55 μm integrated on silicon substrate, in: Proc. 8th Ann. Eur. Fiber Optics Communication and Local Area Networks Conf., Munich, June 27–29 (IGI Europe, Boston, MA) p. 108.

Hall, D.G., 1987, Survey of silicon-based integrated optics, IEEE Computer Soc. Mag. (December) p. 25.

Hashizume, H., M. Seki and N. Nakoma, 1989, Polarization insensitive planar waveguide 1×4 branching device with good wavelength flattened characteristics by ion exchange, in: Optical Fiber Communication Conf., OFC'89, Houston, TX, paper WM1.

Hattori, K., T. Kitagawa, Y. Ohmori and M. Kobayashi, 1991, Laser-diode pumping of waveguide laser based on Nd-doped silica planar lightwave circuit, IEEE Photonics Tech. Lett. **PTL-3**, 882.

Henry, C.H., 1991, Integrated optics and hybrid optoelectronic devices on silicon, Tutorial Lecture, in: Optical Fiber Commun. Conf. OFC'91, San Diego, Feb. 18–22.

Henry, C.H., G.E. Blonder and R.F. Kazarinov, 1989, Glass waveguides on silicon for hybrid optical packaging, IEEE J. Lightwave Tech. **LT-7**, 1530.

Henry, C.H., R.F. Kazarinov, H.J. Lee, K.J. Orlowsky and L.E. Katz, 1987, Low-loss Si_3N_4–SiO_2 optical waveguides on silicon, Appl. Opt. **26**, 2621.

Henry, C.H., Y. Shani, R.C. Kistler, T.E. Jewell, V. Pol, N.A. Olsson, R.F. Kazarinov and K.J. Orlowsky, 1989a, Compound Bragg reflection filters made by high resolution deep ultraviolet stepper, in: Optical Fiber Communication Conf. OFC'89, Houston, TX, paper TuBB4.

Henry, C.H., Y. Shani, R.C. Kistler, T.E. Jewell, V. Pol, N.A. Olsson, R.F. Kazarinov and K.J. Orlowsky, 1989b, Compound Bragg reflection filters made by spatial frequency doubling lithography, IEEE J. Lightwave Tech. LT-7, 1379.

Hibino, Y., M. Abe, T. Kominato and Y. Ohmori, 1991, Photoinduced refractive-index changes in TiO_2-doped silica optical waveguides on silicon substrate, Electron. Lett. 27, 2294.

Hibino, Y., T. Kominato and Y. Ohmori, 1991, Optical frequency tuning by laser-irradiation in silica-based Mach–Zehnder-type multi/demultiplexers, IEEE Photonics Tech. Lett. PTL-3, 640.

Hibino, Y., T. Kitagawa, M. Shimizu, F. Hanawa and A. Sugita, 1989, Neodymium-doped silica optical waveguide laser on silicon substrate, IEEE Photonics Tech. Lett. PTL-1, 349.

Hickernell, F.S., 1979, An optical measure of the acoustic quality of ZnO thin films, Proc. IEEE Ultrasonics Symp., p. 932.

Hickernell, F.S., 1988, Optical waveguides on silicon, Solid State Technol. (November) p. 83.

Hickernell, F.S., R.L. Davis and F.V. Richard, 1978, The acousto-optic properties of thin film Si_3N_4, Ta_2O_5, ZnO, and 7059 glass on oxidized silicon substrates, in: Proc. IEEE Ultrasonics Symp., p. 60.

Hocker, G.B., and W.K. Burns, 1977, Mode dispersion in diffused channel waveguides by the effective index method, Appl. Opt. 16, 113.

Izutsu, M., H. Haga and T. Sueta, 1983, Picosecond signal sampling and multiplication by using integrated tandem light modulators, IEEE J. Lightwave Tech. LT-1, 285.

Jiang, W., J. Chrostowski and M. Fontaine, 1989, Analysis of ARROW waveguides, Opt. Commun. 72, 180.

Jinguji, K., N. Takato, A. Sugita and M. Kawachi, 1990, Mach–Zehnder interferometer type waveguide coupler with wavelength-flattened coupling ratio, Electron. Lett. 26, 1326.

Kanada, S., Y. Fujisawa and K. Kikuiri, 1986, Infrared light modulator of ridge type optical waveguide structure using effect of free carrier absorption, Electron. Lett. 22, 922.

Kashyap, R., B.J. Ainslie and G.D. Maxwell, 1989, Second harmonic generation in GeO_2 ridge waveguides, Electron. Lett. 25, 206.

Kawachi, M., 1990, Silica waveguides on silicon and their application to integrated-optic components, Opt. Quantum Electron. 22, 391.

Kawachi, M., 1991, Silica-based planar lightwave circuit technologies, in: Proc. Eur. Conf. Optical Communications, ECOC'91/IOOC'91, Paris, Invited Papers, p. 51.

Kawachi, M., T. Miya and Y. Ohmori, 1991, Silica based planar lightwave circuits for fiber-to-the-home applications, in: Optical Fiber Communication Conf. OFC'91, San Diego, paper TuG1, p. 26.

Kawachi, M., M. Yasu and M. Kobayashi, 1983, Flame hydrolysis deposition of SiO_2–TiO_2 glass planar optical waveguides on silicon, Jpn. J. Appl. Phys. 22, 1932.

Kawachi, M., M. Yasu and T. Edahiro, 1983, Fabrication of SiO_2–TiO_2 glass planar optical waveguides by flame hydrolysis deposition, Electron. Lett. 19, 583.

Kawachi, M., N. Takato, K. Jinguji and M. Yasu, 1987, in: Proc. Conf. Optical Fiber Communication/Integrated Optics OFC/IOCC'87, Reno, paper TuQ31.

Kawachi, M., Y. Yamada, M. Yasu and M. Kobayashi, 1985, Guided-wave optical wavelength division multi-demultiplexer using high-silica channel waveguides, Electron. Lett. 21, 314.

Kendall, D.L., 1979, Vertical etching of silicon at very high aspect ratios, Ann. Rev. Mater. Sci., p. 373.

Kitagawa, T., K. Hattori, M. Shimizu, Y. Ohmori and M. Kobayashi, 1991, Guided-wave laser based on erbium-doped silica planar lightwave circuit, Electron. Lett. 27, 334.

Knox, R.M., and P.P. Toulios, 1970, Integrated circuits for the millimeter through optical frequency range, in: Proc. of MRI Symp. on Submillimeter Waves, ed. J. Fox (Polytechnic Press, Brooklyn) p. 497.

Kobayashi, S., T. Kito, M. Yasu and M. Kawachi, 1989, in: Fall Nat. Conv. IECE, Japan, C-265.

Kokubun, Y., T. Baba, T. Sasaki and K. Iga, 1986, Low-loss antiresonant reflecting optical waveguide on Si substrate in visible-wavelength region, Electron. Lett. 22, 892.

Kokubun, Y., S. Tamura and T. Kondo, 1991, Spot-size transformer by ARROW-B waveguides, in: Topical Meeting on Integrated Photonics Research, Monterey, CA, Paper ThA2.

Kominato, T., Y. Ohmori and K. Onose, 1991, Characteristics of high silica single-tap ring resonator fabricated by planar lightwave circuit technology, in: Spring National Conv. IECE, Japan, C-144. In Japanese.

Kominato, T., Y. Ohmori, H. Okazaki and M. Yasu, 1990, Very low-loss GeO_2 doped silica waveguide fabricated by flame hydrolysis deposition method, Electron. Lett. 26, 327.

Koren, U., 1989, Optoelectronic integrated circuits, in: Optoelectronic Technology and Lightwave Communications Systems, ed. C. Lin (Van Nostrand Reinhold, New York).

Korotky, S.K., and R.C. Alferness, 1987, Ti–$LiNbO_3$ integrated optic technology: Fundamentals, design considerations, and capabilities, in: Integrated Optical Circuits and Components: Design and Applications, ed. L.D. Hutcheson (Marcel Dekker Inc., New York) p. 169.

Kumar, A., A.N. Kaul and A.K. Ghatak, 1985, Prediction of coupling length in a rectangular core directional coupler: An accurate analysis, Opt. Lett. 10, 86.

Kumar, A., M.R. Shenoy and K. Thyagarajan, 1984, Modes in anisotropic rectangular waveguides: An accurate and simple perturbation approach, IEEE Trans. Microwave Theory & Tech. MTT-32, 1416.

Kumar, A., K. Thyagarajan and A.K. Ghatak, 1983, Analysis of rectangular core dielectric waveguides: An accurate perturbation approach, Opt. Lett. 8, 63.

Kurdi, B.N., and D.G. Hall, 1988, Optical waveguides in oxygen implanted buried oxide silicon-on-insulator structures, Opt. Lett. 13, 175.

Lee, H.J., C.H. Henry, R.F. Kazarinov and K.J. Orlowsky, 1987, Low loss Bragg reflectors on SiO_2–Si_3N_4–SiO_2 rib waveguides, Appl. Opt. 26, 2618.

Lee, H.J., C.H. Henry, K.J. Orlowsky and T.Y. Kometani, 1988, Refractive index dispersion of phosphosilicate glass, thermal oxide, and silicon nitride films on silicon, Appl. Opt. 27, 4104.

Leonberger, F.J., C.E. Woodward and D.L. Spears, 1979, Design and development of high-speed electro-optic A/D converter, IEEE Trans. Circuits & Sys. CAS-26, 1125.

Lidgard, A., A. Polman, D.C. Jacobson, G.E. Blonder, R.C. Kistler, J.M. Poate and P.C. Becker, 1991, Fluorescence life time studies of MeV erbium implanted silica glass, Electron. Lett. 27, 993.

Lubberts, G., B.C. Burkey, F. Moser and E.A. Trabka, 1981, Optical properties of phosphorus-doped polycrystalline silicon layers, J. Appl. Phys. 52, 6870.

Marcatili, E.A.J., 1969, Dielectric rectangular waveguides and directional couplers for integrated optics, Bell Syst. Tech. J. 48, 2071.

Marcuse, D., 1974, Theory of Dielectric Optical Waveguides (Academic Press, New York).

Marx, G.E., M. Gottlieb and G.B. Brandt, 1977, Integrated optical detector array, waveguide, and modulator based on silicon technology, IEEE J. Solid-State Circuits SC-12, 10.

Matsuo, S., 1978, Selective etching of SiO_2 relative to silicon using CF_4 plasma, Jpn. J. Appl. Phys. 17, 235.

Matsuo, S., 1980, Selective etching of SiO_2 relative to silicon without undercutting by $CBrF_3$ plasma, Appl. Phys. Lett. 36, 768.

McWright Howerton, M., and T.E. Batchman, 1988, A multi-film waveguide photodetector using hydrogenated amorphous silicon, IEEE J. Lightwave Tech. LT-6, 1856.

Mergerian, D., E.C. Malarkey, R.P. Pautienus, J.C. Bradley, G.E. Marx, L.D. Hutcheson and A.L. Kellner, 1980, Operational integrated optical RF spectrum analyzer, Appl. Opt. 19, 3033.

Merz, J.L., Y.R. Yuan and G.A. Vawter, 1985, Photonics for integrated circuits and communications, Opt. Eng. 24, 214.

Miller, S.E., 1969, Integrated optics: An introduction, Bell Syst. Tech. J. 48, 2059.

Moss, T.S., 1959, Optical Properties of Semiconductors (Butterworths, London).
Mottier, P., and S. Valette, 1981, Integrated Fresnel lens on thermally oxidized Si substrate, Appl. Opt. **20**, 1630.
Mottier, P., S. Valette and J.P. Jadot, 1986, Broadband Bragg deflector for optical waveguides on Si-substrates, Opt. & Laser Technol. **18**, 89.
Neumaan, A., and J.T. Boyd, 1980, Phosphosilicate glass flow for integrated optics, J. Vac. Sci. & Technol. 17, 529.
Neumaan, A., and J.T. Boyd, 1981, Laser annealing of phosphosilicate glass, J. Vac. Sci. & Technol. **18**, 821.
Nissim, C., A. Beguin, R. Jansen and P. Laborde, 1989, Fabrication and characterization of buried single-mode waveguides and couplers made by ion-exchange in glass, Optical Fiber Communication Conf., OFC'89, Houston, TX, Paper WM2.
Nourshargh, N., E.M. Starr and J.S. McCormack, 1986, Plasma deposition of GeO_2/SiO_2 and Si_3N_4 waveguides for integrated optics, IEE Proc. J. **133**, 264.
Nourshargh, N., E.M. Starr and T.M. Ong, 1989, Integrated optic 1×4 splitter in SiO_2/GeO_2, Electron. Lett. **25**, 981.
Okamoto, K., 1991, Recent progress in high-silica planar lightwave circuits, in: Topical Meeting on Integrated Photonics Research, Monterey, CA, April 9–11, Paper ThE1.
Okamoto, K., H. Takahashi, S. Suzuki, A. Sugita and Y. Ohmori, 1991, Design and fabrication of integrated-optic 8×8 star coupler, Electron. Lett. **27**, 774.
Olsson, N.A., C.H. Henry, R.F. Kazarinov, H.J. Lee, B.H. Johnson and K.J. Orlowsky, 1987, Narrow linewidth 1.5 μm semiconductor laser with a resonant optical reflector, Appl. Phys. Lett. **51**, 1141.
Olsson, N.A., C.H. Henry, R.F. Kazarinov, H.J. Lee, K.J. Orlowsky, B.H. Johnson, R.E. Scotti, D.A. Ackerman and P.J. Anthony, 1988, Performance characteristics of 1.5 μm single frequency semiconductor laser with an external waveguide Bragg reflector, IEEE J. Quantum Electron. **QE-4**, 143.
Olsson, N.A., C.H. Henry, R.F. Kazarinov, H.J. Lee and K.J. Orlowsky, 1987, Relation between chirp and linewidth reduction in external reflector semiconductor lasers, Appl. Phys. Lett. **51**, 92.
Österberg, U., and W. Margulis, 1986, Dye laser pumped by Nd:YAG pulses frequency doubled in a glass optical fiber, Opt. Lett. **11**, 195.
Pal, B.P., 1979, Optical communication fiber waveguide fabrication: A review, Fib. Int. Opt. **2**, 195.
Pal, B.P., 1987, Lightwave propagation in optical waveguides, in: Fiber Optics and Instrumentation, ed. M.M. Butusov (Mashinistroenie Publisher, Leningrad). In Russian.
Pal, B.P., H. Singh, A.K. Ghatak and A.B. Bhattacharya, 1990, Design and fabrication of ARROW (antiresonant reflecting optic waveguide) on silicon, in: XXIII General Assembly, URSI, Praha, 28 Aug–5 Sept.
Papuchon, M., 1986, Integrated optics, J. Inst. Electron. & Telecom. Eng. (India) **32**, 171.
Papuchon, M., Y. Combemale, X. Mathieu, D.B. Ostrowsky, L. Reiber, A.M. Roy, B. Sejourne and M. Werner, 1975, Electrically switched optical directional coupler: COBRA, Appl. Phys. Lett. **27**, 289.
Peterson, K.E., 1982, Silicon as a mechanical material, Proc. IEEE **70**, 420.
Polman, A., A. Lidgard, D.C. Jacobson, P.C. Becker, R.C. Kistler, G.E. Blonder and J.M. Poate, 1990, 1.54 μm room temperature luminescence of MeV erbium-implanted silica glass, Appl. Phys. Lett. **57**, 2859.
Ramaswamy, R.V., and R. Srivastava, 1988, Ion-exchanged glass waveguides: A review, IEEE J. Lightwave Tech. **LT-6**, 984.
Rand, M.J., and R.D. Strandley, 1972, Silicon oxynitride films on fused silica for optical waveguides, Appl. Opt. **11**, 2482.

Sasamaya, K., M. Okuno and K. Habara, 1991, Coherent optical transversal filter using silica-based waveguides for high-speed signal processing, IEEE J. Lightwave Tech. **LT-9**, 1225.
Schmidt, R.V., and R.C. Alferness, 1979, Directional coupler switches, modulators and filters using alternating $\Delta\beta$ techniques, IEEE Trans. Circuits & Sys. **CAS-26**, 1099.
Shani, Y., C.H. Henry, R.C. Kistler, K.J. Orlowsky and D.A. Ackerman, 1989, Efficient coupling of a semiconductor laser to an optical fiber by means of a tapered waveguide on silicon, Appl. Phys. Lett. **55**, 2389.
Shani, Y., C.H. Henry, R.C. Kistler, R.F. Kazarinov and K.J. Orlowsky, 1990, Integrated optic adiabatic polarization splitter on silicon, Appl. Phys. Lett. **56**, 120.
Sodha, M.S., and A.K. Ghatak, 1977, Inhomogeneous Optical Waveguides (Plenum Press, New York).
Soref, R.A., and B.R. Bonnett, 1987, Electro-optical effects in silicon, IEEE J. Quantum Electron. **QE-23**, 123.
Soref, R.A., and J.P. Lorenzo, 1985, Single-crystal silicon: A new material for 1.3 and 1.6 μm integrated-optical components, Electron. Lett. **21**, 953.
Soref, R.A., and J.P. Lorenzo, 1986, All-silicon active and passive guided wave components for $\lambda = 1.3$ and 1.6 μm, IEEE J. Quantum Electron. **QE-22**, 873.
Soref, R.A., and J.P. Lorenzo, 1988, Silicon guided-wave optics, Solid-State Technol. (November) p. 95.
Soref, R.A., and K.J. Ritter, 1990, Silicon antiresonant reflecting optical waveguides, Opt. Lett. **15**, 792.
Splett, A., J. Schmidtchen, B. Schüpert and K. Petermann, 1990, Integrated optical channel waveguides in silicon using Si–Ge alloys, in: Proc. SPIE Conf. on Physical Concepts of Materials for Novel Optoelectronic Device Applications, Aachen, Oct. 28–Nov. 2.
Stutius, W., and W. Streifer, 1977, Silicon nitride films on silicon for optical waveguides, Appl. Opt. **16**, 3218.
Sugita, A., M. Okuno, T. Matsunagu, M. Kawachi and Y. Ohmori, 1990, Strictly non-blocking 8×8 integrated optical matrix switch with silica-based waveguides on silicon substrates, in: Proc. Eur. Conf. Optical Communications ECOC'90, Amsterdam, Paper WeG4, p. 1.
Sun, C.J., W.M. Myers, K.M. Schmidt and S. Sumida, 1991, Silica-based circular cross-sectioned channel waveguides, IEEE Photonic Tech. Lett. **PTL-3**, 238.
Takagi, A., K. Jinguji and M. Kawachi, 1991, Wavelength-flattened (3×3) coupler with silica waveguides on silicon, in: Optical Fiber Communications Conf. OFC'91, San Diego, Paper TuF4, p. 21.
Takato, N., K. Jinguji, M. Yasu, H. Toba and M. Kawachi, 1988, Silica based single-mode waveguides on Si and their application to guided-wave optical interferometers, IEEE J. Lightwave Tech. **LT-6**, 1003.
Takato, N., T. Kominato, A. Sugita, K. Jinguji, H. Toba and M. Kawachi, 1990, Silica-based integrated optic Mach–Zehnder multi/demultiplexer family with channel spacing of 0.01–250 nm, IEEE J. Select. Areas in Communication **8**, 1120.
Takato, N., A. Sugita, K. Onose, H. Okazaki, M. Okuno, M. Kawachi and K. Oda, 1991, 128-channel polarization-insensitive frequency-selective-switch using high-silica waveguides on Si, IEEE Photonics Tech. Lett. **PTL-2**, 441.
Taylor, H.F., 1978, Guided wave electro-optic device for logic and computation, Appl. Opt. **17**, 1493.
Terui, H., Y. Yamada, M. Kawachi and M. Kobayashi, 1985, Hybrid integration of laser diode and high-SiO_2 multimode optical channel waveguide on Si, Electron. Lett. **21**, 646.
Tewari, R., H. Singh and B.P. Pal, 1990, An accurate numerical technique for the analysis of ARROW waveguides, Opt. Technol. & Microwaves Lett. **3**, 305.
Thyagarajan, K., S. Diggavi and A.K. Ghatak, 1987, Analytical investigation of leaky and absorbing planar structures, Opt. Quantum Electron. **19**, 131.

Thylen, L., and L. Stensland, 1982, Lens-less integrated optic spectrum analyzer, IEEE J. Quantum Electron. **QE-18**, 381.

Toba, H., K. Oda, K. Nosu and N. Takato, 1989, 16-channel optical FDM distribution/transmission experiment utilizing multichannel frequency stabilizers and waveguide frequency selection switch, Electron. Lett. **25**, 574.

Urquhart, P., 1988, Review of rare-earth doped fiber lasers and amplifiers, IEE Proc. **135**, Part J, p. 385.

Valette, S., 1987, Integrated optics on silicon substrate: Application to optical communications, in: Proc. of Horizon de l'Optique 87, Marseille, June.

Valette, S., 1988, State-of-the-art of integrated optics technology at LETI for achieving passive optical components, J. Mod. Opt. **35**, 993.

Valette, S., J.P. Jadot, P. Gidon, S. Renard, S. Grand, A. Fournier, A.M. Grouillet, P. Philippe, H. Denis, E. Desgranges, L. Mulatier and C. Erbeia, 1991, Integrated photonic circuits on silicon, in: Novel Silicon Based Technologies, ed. R.A. Levy (Kluwer, Amsterdam) p. 173.

Valette, S., J. Lizet, P. Mottier, J.P. Jadot, P. Gidon and S. Renard, 1984, Integrated optical circuits archieved by planar technology on Si substrates: Application to optical spectrum analyzer, IEE Proc. **131**, Part H, p. 325.

Valette, S., P. Mottier, J. Lizet and P. Gidon, 1986, Integrated optics on silicon substrate: A way to achieve complex optical circuits, Proc. SPIE **651**, 94.

Valette, S., S. Renard, H. Denis, J.P. Jadot, A. Fournier, P. Philippe, P. Gidon, A.M. Grouillet and E. Desgranges, 1989, Si-based integrated optics technologies, Solid-State Technol. (February) p. 69.

Valette, S., S. Renard, J.P. Jadot, P. Gidon and C. Erbeia, 1989, Silicon based integrated optics technology for optical sensor applications, in: Proc. 5th Int. Conf. on Solid Sensors and Actuators, Transducer'89, Montrieux, Switzerland, June 25–30, p. 324.

Valette, S., S. Renard, J.P. Jadot. P. Gidon and C. Erbeia, 1990, Silicon-based integrated optics technology for optical sensor applications, Sensors & Actuators **A21–A23**, 1087.

Valette, S., P. Gidon and J.P. Jadot, 1987, New integrated optical multiplexer/demultiplexer realized on Si substrate, in: Proc. 4th Eur. Conf. on Integrated Optics, ECIO'87, Glasgow, eds C.D.W. Wilkinson and J. Lamb, p. 145.

Valette, S., A. Morque and P. Mottier, 1982, High performance integrated Fresnel lenses on oxidized Si substrates, Electron. Lett. **18**, 13.

Varshney, R.K., and A. Kumar, 1988, A simple and accurate modal analysis of strip loaded optical waveguides with various index profiles, IEEE J. Lightwave Tech. **LT-6**, 601.

Verbeek, B.H., C.H. Henry, N.A. Olsson, K.J. Orlowsky, R.F. Kazarinov and B.H. Johnson, 1988, Integrated 4-channel Mach–Zehnder multi/demultiplexer fabricated with phosphorus doped SiO_2 waveguides on Si, IEEE J. Lightwave Tech. **LT-6**, 1011.

Verber, C.M., R.P. Kenan and J.R. Busch, 1983, Design and performance of an integrated optical digital correlator, IEEE J. Lightwave Tech. **LT-1**, 256.

Weiss, B.L., and G.T. Reed, 1991, The transmission properties of optical waveguides in SIMOX structures, Opt. Quantum Electron. **QE-23**, 1061.

Weiss, B.L., G.T. Reed, S.K. Toh, R.A. Soref and F. Namavar, 1991, Optical waveguides in SIMOX structures, IEEE Photonics Tech. Lett. **PTL-3**, 19.

Welbourn, D., C. Beaumont and M. Nield, 1991, Directional couplers in a high-index silica waveguide, in: Topical Meeting on Integrated Photonics Research, Monterey, CA, April 9–11, Paper ThA3.

Willander, M., 1983a, Carrier-dependent parameters in a silicon optical waveguide, J. Appl. Phys. **56**, 4660.

Willander, M., 1983b, Surface recombination velocity in a silicon optical waveguide, Appl. Phys. A **31**, 45.

Yamada, Y., M. Kawachi, M. Yasu and M. Kobayashi, 1984a, Optical fiber coupling to high-silica channel waveguides with fiber guiding grooves, Electron. Lett. **20**, 313.

Yamada, Y., M. Kawachi, M. Yasu and M. Kobayashi, 1984b, Fabrication of a high silica glass waveguide optical accessor, Electron. Lett. **20**, 589.

Yao, S.K., D.B. Anderson and R.R. August, 1979, An update of integrated optics on Si substrates, in: Proc. Europ. Conf. on Optical Communications, ECOC'79, Amsterdam.

Zelmon, D.E., H.E. Jackson, J.T. Boyd, A. Neumaan and D.B. Anderson, 1983, A low scattering graded index SiO_2 planar optical waveguide thermally grown on silicon, Appl. Phys. Lett. **42**, 565.

PROGRESS IN FIBER OPTICS AND LIGHTWAVE COMMUNICATION TODATE:A RETROSPECTIVE

BISHNU P. PAL*
Physics Department
Indian Institute of Technology Delhi
New Delhi - 110016
INDIA

ABSTRACT

Low-loss high-silica fibers were first reported in 1970 and since then these glass fibers have proven to be the most viable transmission media for lightwave communication. Even though the first low loss fiber was a single-mode fiber, initial systems revolved around multimode fibers from the point of view of practical reasons like easier fiber to fiber splicing and coupling from off-the-shelf available LEDs. Since early 1980s, single-mode fibers became the preferred media for optical transmission and single-mode fibers overtook the multimode fibers for lightwave communication. Networks which operate with single-mode fibers at the 1.31 μm low-loss wavelength window are now taken for granted. Operations with advanced fiber designs at the silica fiber's lowest loss window of 1.55 μm are now gearing to take over the long-haul routes; these are contemplated to be based on erbium doped fiber amplifiers (EDFA) and dispersion shifted fibers. An alternative and promising scheme for this wavelength window involving use of already laid fibers optimized for 1.31 μm requires insertion of a dispersion compensating fiber(DCF) as an additional component in the link. In the immediate future, lightwave systems would operate with EDFA at the OC-48 level, which amounts to a bit rate of $\sim$ 2.5 Gb/s and are compatible with SDH (STM-16) networks. For WDM transmission with EDFAs, one would require a variety of in-line fiber components like wavelength selective couplers, and bandpass/bandstop filters to add/drop channels. Until recently, optical fibers were considered to be optically linear. However, with the introduction of EDFAs, which provide large and broadband ($\approx$ 30 - 35 nm) optical gains, a large number of WDM information channels can be transmitted and simultaneously provided gains across this broad gain spectrum of EDFAs. Furthermore, amplifier spacings could be much longer than the present day regenerator spacings. These two fall outs of EDFA namely, large optical power density and long interaction lengths have elevated optical fiber nonlinearities to an important design issue in lightwave systems. In this presentation we would aim to trace the evolutionary trends in lightwave communications seen along the above lines since the reporting of the first low-loss fibers a quarter century ago.

INTRODUCTION

Feasibility of laser-based optical telecommunication with glass fiber waveguides as the transmission media was predicted by Kao and Hockham from England [1] in 1966. Conventional glasses like window glasses at that time were characterized by transmission losses $\sim$ thousands of dB/km, which were considered prohibitively high for telecommunication. Their research with collected samples from fiber makers convinced them that high transmission losses in such fibers were attributable to impurities in silica glasses and not to silica itself. They worked out a proposal for optical telecommunication by propagating modulated laser beams through single-mode fibers formed out of purified glass so that transmission losses in them could be reduced to below 20 dB/km. Kao reported their finding at an IEE meeting in London in May, 1966 and observed that "....the experimental optical waveguide developed by Standard Telecommunication Laboratories has an information carrying capacity .... of one gigacycle, or equivalent to about 200 TV channels or more than 200,000 telephone channels. He described STL's device as consisting of a glass core about three or four micrometers in diameter, clad with a coaxial layer of another glass having a refractive index about 1% smaller than that of the core .... . Surface optical waves were propagated along the interface between the two types of glass" [2]. It took another four years before this prediction became a distinct possibility when an R & D team in Corning Glass Works Inc. in the USA led by Robert Maurer announced in September 1970 fabrication of a fused silica-based single-mode optical fiber wavelength with an attenuation at the He-Ne laser wavelength of 633 nm, which was less than the goal of 20 dB/km set by Kao and Hockham [3]. They achieved this breakthrough by following a route which was radically different from what many others notably the British Post Office Research Center in England had tried through purification of compound glass melt used for standard optics. The Corning method involved a vapour phase oxidation process through flame hydrolysis of high purity $SiCl_4$ with a few per cent of $TiCl_4$ vapour carried out at $\sim$ 1100°C. The resultant product namely, doped-silica glass in the form of *soots* (i.e. tiny particles of diameter $\sim$ 0.01 to 0.1 μm) were driven through a fused quartz tube, where some of these particles got collected on the inner wall of the tube. These deposited

---

* Facsimile: 011-686 2037/5039; e-mail: bppal@physics.iitd.ernet.in

soots were sintered into a transparent glass by means of a traversing (back-and-forth) burner, which was then collapsed to form a solid rod, what is now known as *preform*, and drawn into a fiber separately in another fiber drawing furnace [4,5]. This process was, however, inherently slow and typically required ~ 24 hours to form a preform suitable for drawing into a few kilometer long fiber; moreover, the process yielded only single-mode fibers. A number of variations of this basic process of vapour phase oxidation was subsequently developed by several other groups as proprietary process of the respective groups, including the Corning group. These were called modified chemical vapour deposition (MCVD), outside vapour deposition (OVD), plasma-enhanced MCVD (PMCVD), plasma-activated CVD (PCVD), vapour phase axial deposition (VAD) and plasma outside deposition (POD) [5,6]. These process improvements coupled with shift to longer operating wavelengths, where silica fibers exhibit inherently lower loss, led to a steady decrease with year in the transmission loss of high-silica fibers down to 0.2 dB/km at 1.55 μm in 1979 [7]. The lowest loss reported to-date was 0.154 dB/km in a state-of-the-art fiber [8], which is almost the theoretically achievable lowest loss in silica fibers. Simultaneously, life of GaAlAs semiconductor lasers with respect to cw operation at room temperature had also steadily increased from few hours in 1970 to several thousands of hours in the next few years. Semiconductor diode lasers have emerged as the most viable lightwave sources for lightwave communication. Improvements in the performance of these two key components in the 1970s have paved the way for rapid introduction of fiber optics in the communication networks [9]. However, due to factors like non-availability of fiber splicing machines suitable for single-mode fibers and apprehensions about high losses in coupling light to small cores of single-mode fibers, first generation fiber optic telephone links, which went public and operated at bit rates up to ~ 100 Mb/s, were all based on graded index multimode fibers of core diameter ~ 50 μm. Ever since, the applications of lightwave communications in the telecommunication industry around the world have been wide spread. Optical fibers have become the transmission media of choice in almost all areas of communication be it undersea cable systems, terrestrial longhaul networks, trunklines linking switching offices in metropolis or subscriber loop systems serving end customers. More recently CATV industry has been deploying fibers for trunking and distribution. Fiber based local area networks have been introduced to extend computer networking capability. Approximately, 60 million kilometers of fibers have been installed around the world as of 1995. In North America alone, the market for fiber optic cables has been projected to grow annually @ 17% - from $ 2.2 billion in 1994 to $ 4.8 billion in 1999. In the last nine years, undersea cable suppliers have installed an amount of fiber cables, which *nearly equalled* all of the copper cables installed over the 37 years from 1950 to 1987. Rarely since the discovery of transistors, have we noticed such a fantastic growth rate of a new technology. Double digit growth rate is continuing unabated. According to Charles Kao[10], three major attributes of fiber optics are its almost infinite *BW*, nearly zero cost and nearly zero loss - which make these optical fibers the ideal choice for broadband - ISDN networks. Indeed, these optical fibers have quietly become the backbone of much-hyped information super-highway information super highway. To meet the demands of information super highway research continues to explore efficient use of vast information BW of low-loss single-mode fibers. Although the demand for higher transmission capacity and longer transmission length was the key driving force for this phenomenal growth rate, it was *improvements in certain fiber characteristics which essentially dictated the technology development in terms of newer generations of lightwave communication.*

FIRST GENERATION SYSTEMS

The first generation lightwave systems operating with AlGaAs semiconductor light sources (LDs and LEDs) emitting at wavelengths around 0.82 μm in conjunction with multimode graded index core fibers and silicon photodiodes were commercially introduced in 1977-78. They operated at a bit rate ~ 50-100 Mb/s and enabled a *bit-rate-distance product* [*BL* ~ 500 (Mb/s)-km] with repeater spacings of the order of 8-10 km. This distance approximately corresponded to spacings between the exchanges typically encountered within metropolis throughout the world and thus repeaterless metropolitan area networks (MAN) could be contemplated. This implied immediate decrease in installation and maintenance costs associated with conventional coaxial systems due to elimination of repeaters, which were otherwise spaced every 2 kilometers or so. The choice of the operating wavelength (~ 0.82 μm) was dictated by the ready availability of commercial grade light sources (which could be directly modulated) and efficient detectors based on silicon. Added to it, the transmission loss around this wavelength in high-silica fibers also exhibited relatively low loss ~ 3-4 dB/km [11]. However, the bit-rate was limited to ~ 100 Mbit/s in practice due to intermodal dispersion[12,13]. Although theoretical model for optimum profiled multimode fibers, which were fabricated to follow the following so called power-law refractive index profile

$$n^2(r) = n_1^2 [1 - 2\Delta (r/a)^q], \quad r/a < 1$$

$$= n_1^2 [1-2\Delta], \quad r/a \geq 1 \qquad (1)$$

predicted a much larger *BL product* (~ 10 Gb/s - km), extremely precise control of the graded core profile shape parameter q was called for to achieve such high bandwidth.

In Eq. (1), a is the fiber core radius and Δ represents relative core-cladding index difference [$\approx (n_1 - n_2)/n_1$]. The parameter Δ is kept around 1 % in graded core multimode fibers for two reasons. Firstly, it ensures low transmission loss for the signal and secondly it helps to reduce pulse dispersion. A value of ~ 2 - 2Δ for q would represent an optimum profile fiber in which intermodal dispersion is minimum [14]. Theoretical estimates have shown that a deviation by ~ 1 % from this value of optimum q leads to almost *four* times increase in intermodal dispersion thereby resulting in *four* times decrease in *BL* product (see Fig. 1).

SECOND GENERATION SYSTEMS

In 1975, in an important paper the Southampton University Group from England had reported that material dispersion in silica vanishes at a wavelength of 1.276 μm [15]. Material dispersion coefficient (D_m, which is proportional to $d^2n/d\lambda^2$) in silica is ~ -90 ps/(nm-km) at λ ~ 0.85 μm, it reduces to < 0.1 ps/(nm-km) at 1.3 μm and increases again to ~ 20 ps/(nm-km) at 1.55 μm. It was latter found that this wavelength of zero material dispersion (λ_{ZMD}) shifts to a longer wavelength when silica is doped with index modifiers like GeO_2, P_2O_5 to enhance Δ as shown in Fig. 2 [16]. This realization of vanishing material dispersion led to a worldwide effort since mid-1970s to develop InGaAsP based lasers for cw operation at room temperatures and detectors to exploit this low dispersion window, where achievable loss is also below 1 dB/km. These developments indeed came through by late 1970s. Since chromatic dispersion, which is proportional to source spectral width, is almost negligible at about 1.31 μm, this window allowed LEDs as a more reliable substitute for LDs in systems with moderate speed and distance requirements. For subscriber-loop applications, these systems operated at bit rates up to ~ 200 Mb/s.

THIRD GENERATION SYSTEMS

A laboratory experiment in 1981 demonstrated 2 Gb/s error free transmission through a 44 km long single-mode fiber at 1.31 μm [17]. This was possible because of negligible *total chromatic dispersion*, which is a combination of *material* and *waveguide* dispersions at 1.31 μm in this fiber. Dispersion coefficient or dispersion parameter, D is usually expressed in ps/(nm-km). Since material and waveguide dispersion coefficients are of opposite sign at wavelengths longer than λ_{ZMD}, they cancel at some wavelength λ_{ZD} ($> \lambda_{ZMD}$); λ_{ZD} corresponds to the wavelength at which the total chromatic dispersion crosses the x-axis in D vs λ curve and this wavelength is called the *zero dispersion wavelength* (see Fig. 3). Low-loss fusion fiber splicers for single-mode fibers also started becoming available about this time. These developments coupled with the unpredictable nature of the bandwidth of concatenated multimode fibers triggered an intense interest to deploy single-mode fibers in mid-1980s [18]. By 1987, third generation lightwave systems with zero dispersion single-mode fibers operating at 1.31 μm with single-channel repeaterless transmission at 1.7 Gb/km rate upto 50 km started appearing in the market. In Fig. 4, theoretical maximum transmission bandwidth of an ideal step index single-mode fiber is displayed [19]. The curves are labelled for sources of different spectral widths ($\Delta\lambda$). For $\Delta\lambda \approx 0$ i.e. source for $\Delta\lambda <$ signal BW, the maximum bit rate $(B_{max})^3.L$ = constant for λ's near λ_{ZD} = 1.31 μm, while away from λ_{ZD} it follows the relations $(B_{max})^2.L$ = constant. If the source $\Delta\lambda$ > signal bandwidth, maximum bit rate B_{max} satisfies $(B_{max})^2.L$ = constant near λ_{ZD}, which modifies to $B_{max}.L$ = constant away from λ_{ZD}. These relations along with Fig. 5 allow scaling of maximum transmission distance for various data rates. Although, extremely high bit rate transmission was achievable in third generation systems, maximum link length/repeater spacings was limited by transmission loss. Loss spectrum of a typical good quality commercial grade single-mode fiber currently available in the market is shown in Fig. 5. It can be seen that loss is minimum at 1.55 μm.

FOURTH GENERATION SYSTEMS

It was indeed demonstrated in 1979 by the NTT team from Japan that the lowest loss is achievable (limited by Rayleigh scattering) at 1.55 μm in silica fibers by reporting fabrication of a fiber with 0.2 dB/km loss at this wavelength [7]. This had triggered an intense R & D interest to shift operating wavelength from 1.31 μm to 1.55 μm in order to exploit this lowest loss

window. However, commercial introduction of fourth generation systems based on operation at 1.55 μm had to wait almost another 10 years. This was mainly because conventional fibers optimized for the 1.31 μm window exhibited excessive chromatic dispersion [$\sim$ + 18-20 ps/(nm-km)] at 1.55 μm. Conventional fibers are characterized by a step refractive index (known as *matched index clad*) or *depressed index cladding* (DIC); these are shown in Fig. 6. Typically, chosen Δ and $2a$ are $\leq$ 0.3% and $\geq$ 8.7 μm, respectively which lead to a resultant mode field diameter (MFD) of 9.5 μm at 1.31 μm (10.5 μm at 1.55 μm) and cut-off wavelength (λ_c) of 1260 nm, while chromatic dispersion at the wavelength of 1.31 μm is targeted to be < 3.5 ps/(nm-km). DIC fibers, on the otherhand, are characterized by two additional profile variables: Δ and $2b$, which allow greater flexibility in optimising fiber designs. Waveguide dispersion in a DIC fiber can be appropriately tuned by adjusting Δ and Δ' to yield chromatic dispersion ($\leq$ 3.2 ps/(nm-km) over the range $1285 \leq \lambda_0$ (nm) ≤ 1330 with $\lambda_{ZD} = 1310 \pm 10$ nm [20]. Typically, $\Delta = 0.37\%$, $\Delta' = 0.12\%$, $2a = 8.3$ μm, $b/a = 6.5$ and λ_c is less by about 100 nm from matched clad fiber having identical core parameters [21]. Zero dispersion slope (S_0) in both the fiber varieties are 0.09 ps/(nm^2-km). At 1.55 μm, these two differently designed fibers, typically exhibit 0.19 dB/km and 0.2 dB/km transmission loss, respectively.

In mid-1980s, it was realized that a considerable advantage in terms of pushing repeater spacings to much longer distances can be achieved if the fiber designs could be so tailored to shift λ_{ZD} to coincide with the lowest loss wavelength of 1.55 μm. The most common types of laser diodes available for operation at 1.55 μm are *Fabry-Perot* (FP) and *Distributed Feedback* (DFB) lasers based on InGaAsP semiconductors. FP lasers are characterized by broader spectral width (FWHM = 2 to 5 nm) than DFB lasers (cw spectral width « 1 nm). However, due to chirping and mode hoping etc. at high modulation rates ($\geq$ 2 Gb/s) DFB lasers can exhibit dynamic spectral widths $\sim$ 1 to 2 nm. Further, DFB lasers can cost anywhere from $ 7000 to $ 2000/device depending on volume and features while FP lasers are priced well below $ 1000/device. In view of these factors, *the choice* of dispersion-tailored fibers in conjunction with FP lasers seems to be the *best near-term option* for optimum use of the 1.55 μm wavelength window.

Broadly, the dispersion tailored fibers are classified as dispersion-shifted (DS-SM) and dispersion-flattened (DF-SM) fibers as shown in Fig. 7. Typical dispersion spectra (material and waveguide dispersion) of these fibers along with that of a conventional dispersion unshifted fiber are shown in Fig. 8. The magnitude of waveguide dispersion can be enhanced to achieve negligible dispersion at 1.55 μm through a variety of alternative designs (shown in Figs. 9 and 10). Typically, chromatic dispersion coefficient is $\leq$ 2.7 ps/(nm-km) with $S_0 \sim 0.08$ ps/(nm^2-km) in a DS-SM fibers whereas it is $\leq$ 2 ps/(nm-km) in a DF-SM fiber over the range 1.3 to 1.55 μm while maintaining inherent scattering loss low ($\sim$ 0.21 dB/km at 1.55 μm). Fourth generation systems at 2.4 Gb/s became commercial in 1990 with potentials to work at bit rates in excess of 10 Gb/s with careful design of sources and receivers and use of dispersion shifted fibers. In a report released by Corning Glass in late 1994, worldwide use of dispersion-shifted fiber has been estimated to have increased approximately 2.5 times on a normalized volume basis (with respect to estimated 1991 DS-SM fiber volume) during the three year period 1991-94. This trend persisted and is likely to persist even for the coming years. Till recently, optical fibers were primarily meant to serve the role of transmission media in long-haul and trunk routes, however, with interactive services (e.g. ISDN) and wideband CATV booming on the horizon, fibers should steadily move closer to the businesses (FTTB) and to the homes (FTTH).

FIFTH GENERATION SYSTEMS AND NETWORK UPGRADES

The telecommunication industry has all along played a crucial role in stimulating growth in the fiber optics industry. In the decade (January 1984 - January 1994) since A T & T's divestiture of its local telephone companies, the number of telephone calls handled by A T & T on an average business day had jumped from 37.5 million to 150 million, number of calls handled on the busiest holiday was 42.4 million (X'mas day) in 1984 and went up to 106.2 million in 1994 (Mother's day), and the transmission facilities have increased from 590 million to 2 billion circuit miles [22]! Optical fibers are now being used in almost all segments of telecommunications. In this scenario, in the late 1980s typical state-of-the art repeaterless transmission distances were about 40-50 kms @ 560 Mb/s transmission rate. Since maximum launched optical power was below 100 μW, it was difficult to improve system lengths beyond this specifications and use of electronic repeaters became inevitable. At a repeater, the so called 3R-regeneration functions (*reshaping, retiming, reclocking*) are performed. However, these complex functions are expensive and require unit replacement in case of network capacity upgradation in terms of higher bit transmission rates. Since these units are required to convert photons to electrons and back to (regenerated) photons, often at modulation rates approaching the limits of current electronic switching technology, a bottleneck was encountered in the late

1980s. *What was needed was an optical amplifier to bypass this electronic bottleneck.*

In 1986, the Southampton University Group reported success in incorporating rare earth trivalent erbium ions into host silica glass during fiber fabrication [23]. Erbium is a well known lasing species characterized by strong fluorescence at 1.55 μm. In another subsequent paper [24], the same group demonstrated that excellent noise and gain performance is feasible in a large part of the 1.55 μm window using erbium-doped otherwise standard silica fibers. The concept of optical amplification in fiber is almost as old as the laser itself. Today erbium-doped fiber amplifiers (EDFA) looks like an outstanding breakthrough, but it is really an old idea. In 1964, Koester and Snitzer [25] had demonstrated a gain of 40 dB at 1.06 μm in an 1 meter long Nd-doped fiber side pumped with flash lamps. The motivation at that time was to find optical sources for communication but development of semiconductor lasers in subsequent years pushed fiber lasers to the background. The operation of an EDFA is very straightforward. The electrons in the 4*f* shell of the erbium ions are excited to higher energy states by absorption of energy from a pump. Absorption bands as well as absorption and emission spectra around the 1550 nm low loss window of silica fibers for an erbium-doped silica fiber are shown in Fig. 11. Out of these various absorption bands most suitable as pump for obtaining amplification of 1.55 μm signals are the 980 nm and 1480 nm wavelengths due to absence of the detrimental excited state absorption (ESA). Efficient high power quantum well lasers are available at both these wavelengths. Typical pump powers required in an EDFA range from 20 to 100 mW. As shown in Fig. 12 the pump is injected to the erbium-doped fiber through a WDM device based on a wavelength selective four-port fused fiber coupler. Configurations may include combinations of co-and/counter-propagating pumps. Simultaneous pumping from both ends can improve both high-power and low-noise performance [26,27]. Absorption of pump energy by the erbium ions leads to *population inversion* of these ions from the ground state ($4I_{15/2}$) to either $4I_{11/2}$ (980 nm) or $4I_{13/2}$ (1480 nm) excited states; $4I_{13/2}$ level effectively acts as a storage of pump power from which the incoming weak signals may stimulate emission and experience amplification. Stimulated events are extremely fast and hence the amplified signal slavishly follows the amplitude modulation of the input signal. EDFAs are accordingly *bit rate transparent*. Optical isolators prevent the amplifier from oscillating if spurious reflections are present. EDFAs are new tools that system planners now almost routinely use for designing networks. EDFAs can be incorporated in a fiber link with insertion loss ~ 0.1 dB and almost full population inversion is achievable at the 980 nm pump band. Practical EDFAs with output power of around 100 mW (20 dBm), 30 dB small signal gain, and a noise figure of < 5 dB are now available commercially. They can be used either as a *power amplifier* to boost the signal power immediately after the source or as *in-line repeater* along the communication link or as a *preamplifier* at the receiver end [see Fig. 13]. In a 10 Gbit/s transmission experiment, a record receiver sensitivity of 102 photons per bit was attained in a two-stage composite EDFA having a noise figure of 3.1 dB [28]. In practice, noise figure typically range from 3.5 to 5 dB. Several characteristics of these doped fibers e.g. refractive index profile, Δ, core-composition, core diameter, erbium ion concentration etc. are required to be weighted from the point of view of gain, noise figure, and output power because each depends *intimately* on the combination of fiber length and pump intensity [29]. A typical small signal gain as a function of input pump power is shown in Fig. 14. An important figure of merit for optical amplifiers is the slope of gain versus pump power curve expressed in dB/mW. The best performance numbers reported have been 11 dB/mW for 0.98 μm pumping and 5.9 dB/mW for 1.48 μm pumping. In a system containing a chain of EDFAs (e.g. in trans-oceanic links) amplified spontaneous emission (ASE) generated (due to random emission of photons by metastable state ions) at each amplifier accumulates and gets further amplified by subsequent EDFAs. Accumulated ASE noise is proportional to the gain of each EDFA and the number of EDFAs. If the total system length is L and EDFA spacings is l_A ⇒ the number (m) of EDFAs is L/l_A and the EDFA gain equals $(G_{sys})^{1/m}$, G_{sys} being the total link transmission margin (or loss) [26]. However, ASE photocurrent increases slowly with l_A upto a distance of ~ L_{eff}, which is known as the effective attenuation length of the fiber. $L_{eff} = [1 - \exp(-\alpha' L)]/\alpha'$, with α' representing the attenuation coefficient in nepers/length of the fiber material and L is the length of the actual fiber. For $\alpha' L \gg 1$, L_{eff} is ~ $1/\alpha'$; for a fiber having 0.22 dB/km loss, L_{eff} is 20 km [26]. Calculations have shown that required optical power at the output of each amplifier in an amplified transmission system (containing a chain of EDFAs) rises steeply when l_A exceeds L_{eff} [26]. Consumption of fiber amplifiers in North America alone totalled over $ 119 million by 1995. Annual consumption of fiber amplifiers is expected to show an average growth rate of 17.8% per year to reach $ 269 million in 1999.

WAVELENGTH DIVISION MULTIPLEXED (WDM) SYSTEMS

The already embedded installed fibers under the ground, almost totally, are of the conventional type having dispersion minimum at λ = 1.31 μm. These fibers are characterized by a relatively high loss ~ 0.35-0.4 dB/km. Thus the regenerator spacing in these systems are essentially limited by fiber loss to a nominal figure of 40 km. Upgrading the transmission

capacity say, from low data rates (e.g. 1.5 and 45 Mbit/s) to higher rates (~ 1.7 Gbit/s) through electronic multiplexing will involve replacement of all regenerative repeaters, which is a costly proposition. Several dual channel 1.31/1.55 μm WDM systems have been installed notably in the US for capacity upgradation. These systems, though, did not require replacement of existing regenerators, expensive DFB lasers with low chirp were required to be used because conventional 1.31 μm optimized fibers [$D \leq 3.5$ ps/(nm-km)] exhibit a chromatic dispersion of ~ +17-18 ps/(nm-km) at 1.55 μm. A very important feature of EDFAs is that they exhibit a smooth gain versus wavelength curve (especially in case the fiber is doped with Al) almost 30-35 nm wide [see Fig. 11(b)]. Thus multichannel operation through WDM within this gain spectrum is feasible, each wavelength channel being simultaneously amplified by the same EDFA. "Relatively long life time of the excited state (~ 10 ms) leads to slow gain dynamics and therefore minimal crosstalk between WDM channels [26]." System designers are now contemplating use of four, eight or more wavelengths per fiber. Pirelli Cable in a recent experiment has demonstrated a *four-fold* increase in number of simultaneous conversations from 30,000 to 120,000 over a single-fiber through WDM combined with EDFA at the wavelengths of 1533 nm, 1543 nm, 1550 nm, and 1557 nm. This amounted to almost 300% increase in simultaneous conversations. Capacity increase by 700% through further innovation is on card! Since cross-talk is almost absent between the channels, more wavelength channels can be added at a future date thereby offering flexibility to make the network responsive to future demands. A T & T Bell laboratories have demonstrated a successful laboratory scale experiment in which 40 Gbit/s repeaterless transmission over 1420 km of single-mode fiber was achieved! This trend setting experiment of enormous transmission (56.8 terabit/s-km) was made possible by employing WDM with 16 independent laser diodes, each modulated at 2.5 Gbit/s and with 14 EDFAs located at 96 to 123 km spacings [30]. One important feature of this experiment with so many channels involved deployment of a *Pre-emphasis* (also referred to as the *Robin-Hood gain*) technique in the system. It was necessitated by the fact that in a long chain of amplifiers, the gain may not be flat with each wavelength channel. The pre-emphasis technique ensured that signal to noise ratio for all the 16 wavelengths at the receiving end are same. Input channels ranged between 9 and 0 dBm and the pre-emphasis technique equalized the 17 to 18 dB output *signal-to-noise* ratio of all the 16 channels. Thus bit error rate performance of each of the 2.5 Gbit/s channel remained same. Transmitters consisted of 8 DFB lasers and 8 external cavity lasers (wavelengths ~ 1549-1561 nm) with 0.8 nm channel spacings. Furthermore dispersion compensation technique was exploited to achieve this success. Half of the fiber segments consisted of conventional single-mode fibers having zero dispersion at 1.31 μm while the rest half were of dispersion shifted fibers with zero dispersion at 1.55 μm. When the signal wavelength $> \lambda_{ZD}$, it experiences positive dispersion and if it is $< \lambda_{ZD}$, the signal will experience negative dispersion. Since dispersion is *additive*, different fiber segments with positive and negative dispersion leads to effective cancellation of dispersion over the entire link. All segments having dispersion of identical sign may lead to excessive dispersion. In practice, a rough balance is required.

At the OFC'96 early this year, several experimental results involving WDM technology and architecture to achieve very high transmission capacity have been reported during the Post-deadline session. Notable amongst these were the 1.1 Tbit/s transmission experiment through 55 LD's, each operating @ 20 Gbit/s and ranging in wavelengths from 1531.70 nm to 1564.07 nm with a channel separation of 75 GHz (0.6 nm) [31]. It involved transmission over 150 km of a 1.31 μm zero-dispersion fiber through use of pre-emphasis, wideband EDFAs and a dispersion compensating fiber (DCF's) to neutralize the positive chromatic dispersion of ~ 17-18 ps/(nm-km) at the operating wavelengths. In another high capacity transmission experiment [32], 1 Tbit/s WDM transmission was achieved through 55 km of a non-zero dispersion fiber (50 channels each at 20 Gbit/s). Fifty channels were generated by polarization multiplexing outputs from 25 LDs ranging in wavelengths from 1542 nm to 1561.2 nm with a channel spacing of 100 GHz.

Considering that most of the already laid fibers were optimized for 1.31 μm window, an alternate school of thought explored the feasibility of having a fiber amplifier which will efficiently work at this window. Such fiber amplifiers have indeed become commercially available only recently. These are known as *Praseodymium-doped fluoride* fibers. However, these are based, not on silica, but on ZBLAN (fluorides of Zn, Ba, La, Al, and Na) as the host materials. These amplifiers are called PDFFAs. BT laboratory researchers have successfully demonstrated a 5 Gb/s transmission without regeneration with commercial (HP make) PDFFA through 100 km of 1.3 μm optimized fibers [33]. The pump wavelength was 1047 nm based on a Nd-YLF laser pumping scheme, in which Nd-YLF laser was pumped by a 800 nm GaAs LD. This engineered device was mounted in a standard rack unit of 42x9.6x38 cm^3. On the debit side these amplifiers cost ~ $ 60,000/unit in contrast to $ 20,000 to $ 40,000 cost of an EDFA.

While research and field trials with PDFFA continue, as an alternative route, use of the highly matured EDFA technology is very attractive to "mine" the large inherent BW in the already embedded fibers. However, as already stated such 1310 nm

optimized fibers exhibit almost 5 times more positive dispersion (+ 17 ps/km-nm) at 1550 nm and hence to reap the benefit of EDFAs, upgrading to 1550 nm of the already installed links necessarily requires some dispersion compensation scheme. Consequently, a variety of dispersion compensation techniques both active and passive have been attempted and reported in the literature. Some of the passive dispersion compensation techniques that have been proposed/demonstrated involve use of: a fiber Gires-Tournois interferometric filter, bulk gratings, fiber gratings, wavelength dependent coupling in multicore waveguide structures, large negative waveguide dispersion of the LP_{11}-mode of a two-mode fiber or a single-mode dispersion compensating fiber (DCF) with a large negative waveguide dispersion. Out of these many options, use of a DCF appears to be very attractive [34]. A dispersion compensation scheme using optical fibers involves use of a compact reel holding a specified length of specially designed DCF which provides a dispersion opposite to that of the fiber in the link and thus canceling any accumulated dispersion. System experiments have been reported to demonstrate viability of such upgrade schemes in which dispersion and loss of a 1310 nm optimized fiber link were compensated by use of a DCF followed by EDFA or vice versa. An important figure of merit in the design of such a DCF is known to be dispersion per unit loss expressed in units of ps/(nm-dB). Its importance arises from the fact that unless care is taken through suitable design of the refractive index profile, attainment of a large negative dispersion may entail greatly increased excess loss due to absorption, scattering or macro and microbending. Recent investigations have shown that by a proper choice of the transverse refractive index profile, it is possible to design fibers with dispersion coefficients as large as -4000 ps/(nm-km) [35]. These values are one order of magnitude greater than what is presently reported in the literature. Such large dispersion values are very interesting since using such fibers it is possible to compensate for the accumulated dispersion in 50 km of 1300 nm optimized fibers by using only about 200 m of the dispersion compensating fiber. Since for a practical implementation, the fiber should possess other characteristics such as low scattering loss, low bend induced loss, mode field diameter consistent with the 1300 nm optimized fibers etc. a proper optimization of the fiber profile would be needed to achieve the optimal DCF.

Another issue which becomes important with the insertion of a DCF in a fiber link is the splice loss arising from the jointing of DCF to the signal carrying standard single-mode fiber or an EDFA. In a recent paper we have proposed use of an erbium-doped dispersion compensating fiber (EDDCF), which can compensate loss and dispersion simultaneously. Such a scheme eliminates the need for additional splicing of the DCF to an EDFA or vice versa (if they are used as two discrete components), thereby making the compensator more compact [36].

NONLINEAR OPTICAL EFFECTS IN FIBER TRANSMISSION [12, 26, 27, 36-38]

Silica in its bulk form, is a poor nonlinear medium. However, in the form of a fiber, *power confinement* could be quite high due to its *small cross-sectional area* and *very long interaction lengths*; these two factors may lead to large intensities and hence nonlinear effects. In the present lightwave systems, even though single spans are ~ 40 km, nonlinear effects are not observable. However, with the introduction of EDFAs, which provide broadband gains and enable multichannel transmission, regenerator spacings could be much longer than the present day regenerator spacings. These two fall-outs of EDFA, have elevated optical fiber nonlinearities to an important system design issue. Broadly, nonlinearities in silica fibers could be grouped into two categories. *Stimulated scatterings*, which result in *signal attenuation* and the second category arises from *intensity dependent refractive* index of the fiber, which leads to self-phase modulation (SPM), cross-phase modulation (XPM) and four-wave mixing (FWM). In contrast to elastic scattering like Rayleigh scattering, in which scattered light remains unchanged in frequency, stimulated scatterings are inelastic and involves transfer of some of the signal energy to the medium. Thus the scattered light undergoes a *down-shift* in frequency. Two dominant types of such scattering that occur in silica fibers are the *Brillouin* (SBS) and *Raman scatterings* (SRS). The threshold power for SRS (P_{th}^{SRS}) in a single-span fiber link, at 1.55 μm is typically about 570 mW. In practical term, since launched power is below 10 mW, SRS does not contribute to signal attenuation. However, in EDFA-based multichannel systems, it could cause signal-to-noise ratio degradation. An order of magnitude estimate of P_{th}^{SRS} has been made for an amplified chain to be ~ 4W divided by number of amplified spans between regenerators. Due to SRS, the incident light gets downshifted in frequency through parametric interactions with optical phonons of the material. In a WDM system, lower frequency signals can draw power through SRS from higher frequency channels, which may lead to cross-talks and degradation of SNR in the high frequency channels [26,27]. According to [39] as quoted in [26], to keep system performance degradation due to SRS to an acceptable level, one must have

$$[NP_0] \cdot [(N-1)\,\delta\nu] \cdot L_{eff} < 10^4 \text{ W-GHz-km}, \qquad (2)$$

where N is the number of channels, P_0 is the power per channel in watts, $\delta\nu$ is the channel separation in GHz, and L_{eff}

represents total effective length in kilometers. Above inequality sets an upper bound to the number of channels for acceptable performance.

In SBS, the backward propagating light scattered by acoustic waves in fiber grows at the expense of the forward propagating signal [27]. SBS is independent of the number of channels. Although, the threshold power for SBS is typically about 10 mW for single-span system, SBS is not of much concern in amplified WDM systems.

Most dominant of the three nonlinear effects due to intensity dependent refractive index is the FWM and this is analogous to intermodulation in electrical systems [27]. Nonlinearity induced mixing of two frequencies ω_1 and ω_2 may modulate the refractive index at the difference frequency $\omega_2 - \omega_1$, which leads to creation of sidebands at $(2\omega_2 - \omega_1)$ and $(2\omega_1 - \omega_2)$. These sidebands may grow at the expense of original waves and result in crosstalk between them. FWM effects depend on channel separation and fiber dispersion [see Fig. (15)]; increase in either of these will reduce FWM efficiency. In a WDM system containing N channels, the number of sidebands created by the FWM process is $N^2(N - 1)/2$ [39]. In case of equispaced channels, FWM may lead to power transfer between channels and result in intolerable power depletion from certain channels. If the channel spacings are unequal, the generated frequencies will lie intermediate between the primary channels and may introduce noise through interchannel interference. An estimate of the limiting power per channel allowed by various nonlinear phenomena in a multichannel WDM fiber transmission system at 1.55 μm is shown in Fig. 16. It is apparent that to contain FWM, which is a major trouble shooting nonlinear effect in an amplified multichannel link, launched power per channel should be limited to below 1 mW.

If we consider nonlinearity and dispersive nature of a fiber together, one can show that under certain conditions an optical pulse can propagate undistorted in shape and intensity through such a nonlinear dispersive medium. These are called solitary waves and *solitons* are special solitary waves, which can exist in a silica fiber due to interplay between SPM and anomalous dispersion. An important attribute of solitons is that they propagate undistorted through ultra long lengths of fibers. Using soliton technology, in a recent experiment, researchers from the Lucent Technologies of Bell laboratories have demonstrated soliton transmission up to 8 X 20 Gbit/s with BER $< 10^{-9}$ over recirculated fiber path lengths ranging from 19 - 9.6 Mm [40].

CONCLUSION

Evolutionary trends over the last 25 years seen in lightwave communication technology is described. Extensive use of 1.55 μm window with multichannel transmission through EDFAs appear to be imminent in high density, high bandwidth longhaul routes. Repeaterless transmission over transoceanic distances ($\sim$ 9000 km) with a chain of EDFAs seems quite feasible and within the reach of current technology. Dispersion compensation and pre-emphasis techniques are expected to be extensively exploited by system designers to "mine" and upgrade embedded networks through the WDM technology.

REFERENCES

1. C.K. Kao and G.A. Hockham, "Dielectric-fiber surface waveguides for optical frequencies," Proc. IEE, Vol. 133, pp. 1151-1158, 1966.

2. Laser Focus, April 1966 issue.

3. F.P. Kapron, D.B. Keck, and R.D. Maurer, "Radiation losses in glass optical waveguides," App. Phys. Letts., vol. 17, pp. 423-425, 1970.

4. R.D. Maurer, "Glass fiber for optical communication," Proc. IEEE, vol. 61, pp. 452-462, 1973.

5. B.P. Pal, "Optical communication fiber waveguide fabrication: A review," Fib. Int. Opt., vol. 2, pp. 195-252, 1979.

6. H. Karstensen, "Fabrication techniques of optical fibers," Chapter 9 in B.P. Pal (Ed.) "*Fundamentals of fiber optics in telecommunication and sensor systems*," John Wiley, New York and Wiley Eastern, New Delhi, 1992.

7. T. Miya, Y. Terunume, T. Hosaka, and T. Miyashita, "An ultimate low-loss single-mode fiber at 1.55 μm,"

Electron. Lett., vol. 15, pp. 106-108, 1979.

8. H. Yokota, H. Kanamori, Y. Ishigawa, G. Tanaka, S. Tanaka, H. Tanada, M. Watanabe, S. Suzuki, K. Yano, M. Hoshikawa, and H. Shimba, "Ultra-low-loss pure silica core single-mode fiber and transmission experiment," Opt. Fib. Commn. Conf. (OFC '86), PD3-1, p. 11, 1986.

9. T. Li, "Optical fiber communication: The state-of-the-art," IEEE Commun. vol. 26, pp. 946-955, 1978.

10. C.K. Kao, "The backbone of the future network," Optoelectronics and Communication Conf.(OECC'96), Chiba, Japan July 16-19, 1996.

11. B.P. Pal, "Evolution of fiber optics - A brief survey," Chapter 1 in *Fundamentals of fiber optics in telecommunication and sensor systems*, B.P. Pal (Ed.), John-Wiley, New York and Wiley Eastern, New Delhi, 1992.

12. B.P. Pal, "Optical transmission: Fiber optics," Chapter 4 in "*Perspective in optoelectronics*", S.S. Jha (Ed.), World Scientific, Singapore, 1995.

13. D. Gloge, A. Albanese, C.A. Barrus, E.L. Chinnock, J.A. Copeland, A.G. Dentai, T.P. Lee, T. Li, and K. Ogawa, Bell Syst. Tech. J., vol. 59, "Hig speed digital lightwave communication using LEDs and PIN photodiodes at 1.3 μm," pp. 1365 - 1382, 1980.

14. B.P. Pal, "Transmission characteristics of telecommunication optical fibers," Chapter 4 in "*Fundamentals of fiber optics in telecommunication and sensor systems*," B.P. Pal (Ed.), John Wiley, New York and Wiley Eastern, New Delhi, 1992.

15. D.N. Payne and W.A. Gambling, "Zero material dispersion in optical fibers," Electron. Letts. vol. 11, pp. 176-178, 1975.

16. D.L. Franzen, "Single-mode fiber Measurements", OFC'90 Tutorial, San Francisco, Calif., 1990.

17. J.I. Yamada, S. Machida, and T. Kimura, "2 Gbit/s optical transmission experiments at 1.3 μm with 44 km single-mode fiber," Electron. Lett., vol. 17 pp. 479-480, 1981.

18. C.M. Lemrow, "Trends and developments in optical fibers," Outside Plant Magazine, Practical Communications, Inc., Corning Glass Works (USA), 1985.

19. T. Li, "Advances in lightwave systems research," A T & T Tech. J., vol. 66, pp. 8-18, 1987.

20. B.P. Pal, "Optical fibers for lightwave communication: Design issues," in the book *Fiber optics and applications* by A.K. Ghatak, B. Culshaw, V. Nagarajan and B.D. Khurana (Eds.), VIVA Publishers, New Delhi, 1995.

21. D. Kalish and L.G. Cohen, "Single-mode fibers from research and development to manufacturing," A T & T Tech. J., vol. 66, pp. 19-32, 1987.

22. "10 year Retrospective" in the journal: Lightwave, January, 1994.

23. R.J. Mears, L. Reekie, S.B. Poole, and D.N. Payne, "Low- threshold tunable cw and Q-switched fiber laser operating at 1.55 μm," Electron. Lett., vol. 22, pp. 159-160, 1986.

24. R.J. Mears, L. Reekie, I.M. Jauncy, and D.N. Payne, "Low noise erbium-doped fiber amplifier operating at 1.54 μm," Electron. Lett., vol. 23, pp. 1026-1027, 1987.

25. C.J. Koester and E. Snitzer, "Amplification in a fiber laser," App. Opt., vol. 3, pp. 1182- 1184, 1964.

26. T. Li, "The impact of optical amplifiers on long-distance lightwave telecommunications," Proc. IEEE, vol. 81, pp. 1568-1579.

27. T. Li and C.R. Giles, "Optical amplifiers in lightwave telecommunications," Chapter 9, in *Perspective in Optolectronics*, S.S. Jha(Ed), World Scientific, Singapore, 1996.

28. R.I. Laming, A.H. Gnauck, C.R. Giles, M.N. Zervas, and D.N. Payne, "High sensitivity optical preamplifier at 10 Gbit/s employing a low noise composite EDFA with 46 dB gain," in Post-deadline session, Opt. Amp. and their Applications, OSA Topical Meeting, washington, DC, Paper PD13, 1992.

29. E. Desurvire, *Erbium doped fiber amplifier: Principle and applications*, Wiley-Interscience, New York, 1994.

30. A.R. Chraplyvy, et al., "1420-km transmission of sixteen 2.5 Gbit/s channels using silica-based EDFA repeaters," Optolectronics Conference'94, Chiba, Japan, Paper PD-1, 1994.

31. H. Onaka, H. Miyata, G. Ishikawa, K. Ohtsuka, H. Ooi, Y. Kai, S. Kinoshita, M. Seino, H. Nishimoto, and T. Chikama, "1.1 Tbit/s WDM transmission over a 150 km 1.3 μm zero dispersion single-mode fiber," OFC'96, San Jose, Paper PD-19, 1996.

32. A.H. Gnauck, R.W. Tkach, F. Forghievi, R.M. Derosier, A.R. McCormick, A.R. Chraplyvy, J.L. Zyskind, J.W. Sulhoff, A.J. Lucerno, Y. Sun, R.W. Jopson, and C. Wolf, "One terabit/s transmission experiment," *ibid*, 1996.

33. T.J. Whitley et al. "5 Gbps transmission over 100 km of optical fiber using directly modulated DFB laser and an engineered 1.3 μm Pr^{3+}-doped fluoride fiber power amplifier," Proc. OSA OAA'94, Brackenbridge, CO, Paper Wb1, 1994.

34. D.W. Howtof, G.E. Berkey, and A.J. Antos, "High figure of merit dispersion compensating fiber," OFC'96 Post deadline Paper No. PD6, San Jose, 1996.

35. K. Thyagarajan, R.K. Varshney, P. Palai, A.K. Ghatak, and I.C. Goyal, "A novel design of a dispersion compensating fiber," IEEE Photon. Tech. Letts., in press, 1996.

36. P. Palai, K. Thyagarajan, and B.P. Pal, "Erbium-doped dispersion compensating fiber for simultaneous compensation of loss and dispersion," submitted for publication, 1996.

37. G.P. Agrawal, *Nonlinear Fiber Optics*, Academic Press, New York, 1989.

38. A.R. Chraplyvy, "Limitations of lightwave communications imposed by optical fiber nonlinearity," J. Lightwave Tech., vol. 8, pp. 1548-1554, 1990.

39. A.R. Chraplyvy, "Fiber nonlinearities," Tutorial Sessions, OFC'93, San Jose, Paper WE, 1993.

40. L.M. Mollenaur, P.V. Memyshev, and M.J. Neubelt, "Demonstration of soliton WDM transmission at up to 8X10 Gbit/s, error free over transoceanic distances," OFC'96, San Jose, Paper PD22, 1996.

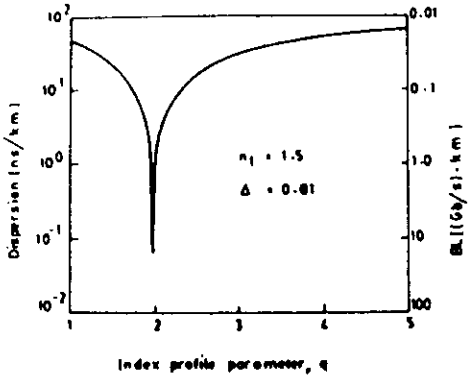

Fig. 1: Dispersion (or BW x length) vs index profile shape parameter for a multimode fiber (adapted from G.P. Agrawal, Copyright 1992, John Wiley and Sons, Inc.).

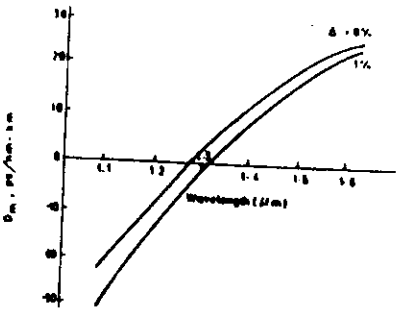

Fig. 2: Material dispersion vs wavelength for germano-silicate glass (after [16].

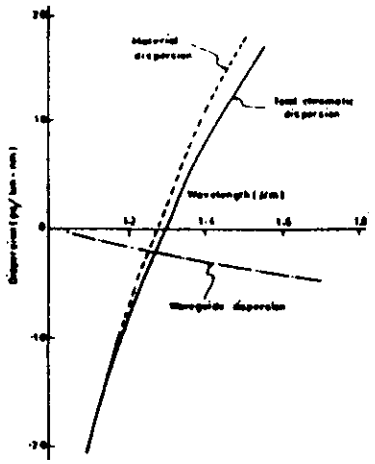

Fig. 3: Components of dispersion spectra for a single-mode fiber (after [16]).

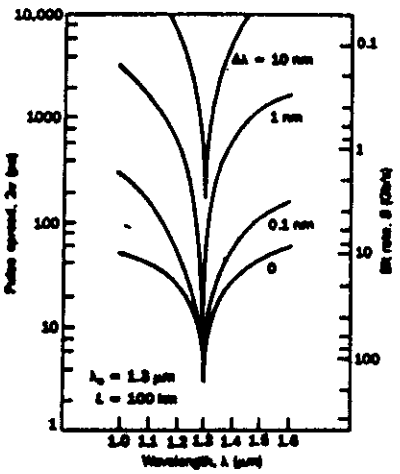

Fig. 4: Pulse spread (and bit rate) vs wavelength around λ_{ZD} for different source spectral widths (adapted from [19]).

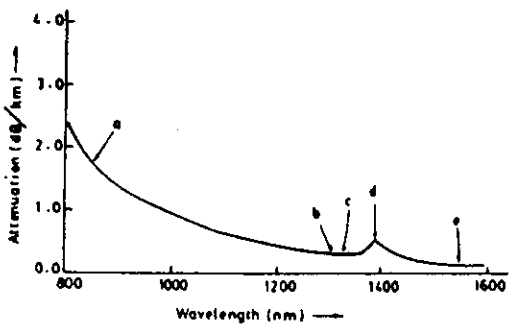

Fig. 5: Typical attenuation spectra of a commercial single-mode fiber; a: 1.81 dB/km @850 nm, b: 0.35 dB/km @ 1300 nm, c: 0.34 dB/km @1310 nm, d: 0.55 dB/km @ 1380 nm, and e: 0.19 dB/km @1550 nm (adapted from Product information of Corning Glass).

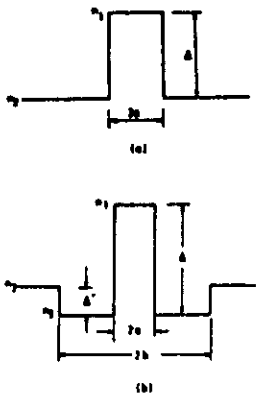

Fig. 6: Refractive index profiles of a) matched clad and b) depressed index clad fiber, $\Delta = (n_1 - n_3)/n_1$; $\Delta' = (n_2 - n_3)/n_2$.

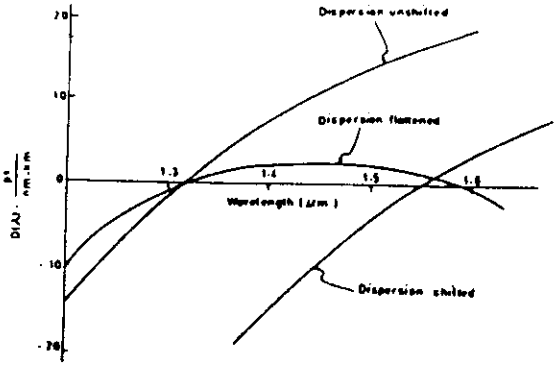

Fig. 7: Dispersion classes of single-mode fiber.

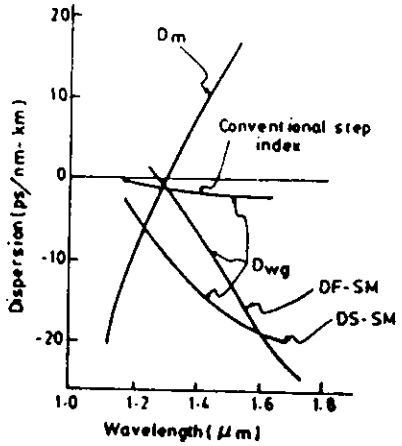

Fig. 8: Material (same for all) and waveguide dispersion components of various single-mode fiber designs (after [21]).

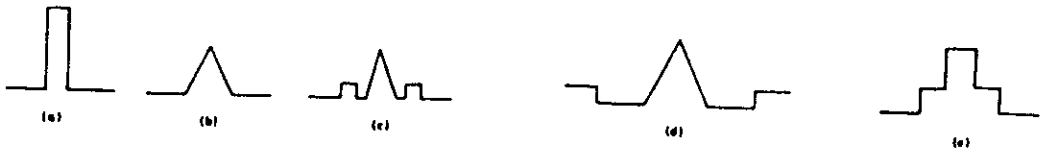

Fig. 9: Various designs of dispersion shifted fibers.

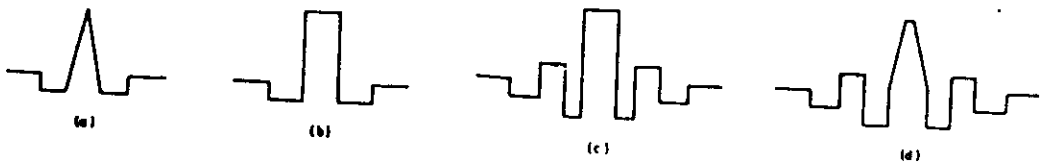

Fig. 10: Various designs of dispersion flattened fibers.

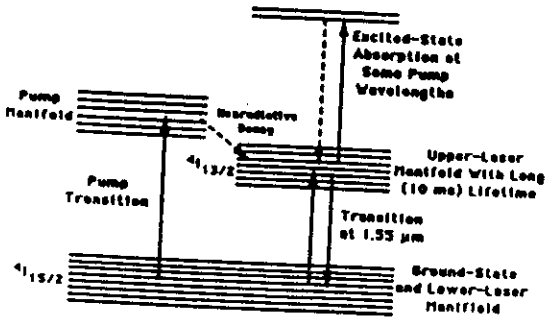

Fig. 11: a) Energy level diagram of the three-level transition at 1.55 μm in Er:silica (adapted from M.J.F. Digonnet(Ed), *Rare earth doped fiber lasers and amplifiers*, Marcel Dekker, N.Y., 1993.

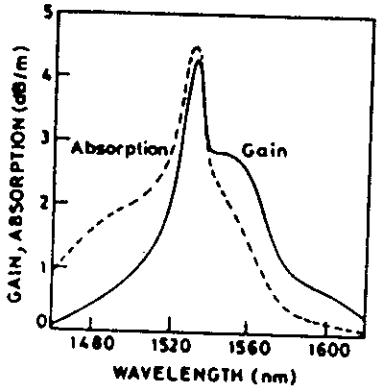

Fig. 11: b) absorption and emission spectra of an EDF (notice the broad band gain).

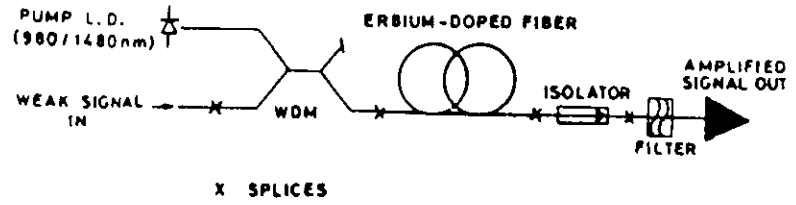

Fig. 12: EDFA configuration (adapted from N.K. Dutta and J.R. Simpson, Optical Amplifiers in Prog. Opt., vol. XXXI, ed. E. Wolf, Elsevier Science Pub., 1993).

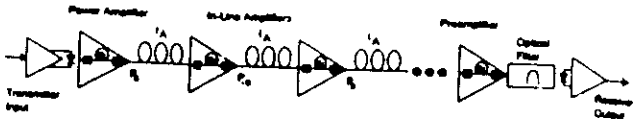

Fig. 13: EDFA with power amplifier, in-line amplifiers and pre-amplifier (adapted from [27]).

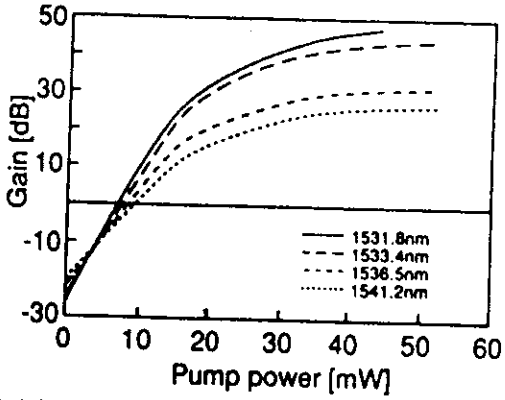

Fig. 14: Gain vs pump (975.5 nm) power for various wavelengths in an EDFA (after W.J. Miniscalco et al, Proc. OFC'90, Paper PA2, 1990).

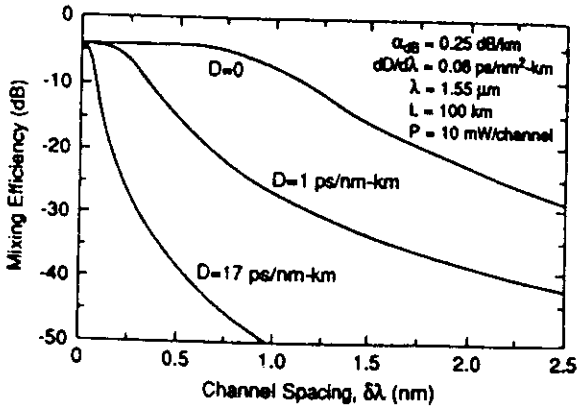

Fig. 15: Relative side-band powers or mixing efficiency due to FWM for two channels vs channel spacing for various values of D (adapted from [27]).

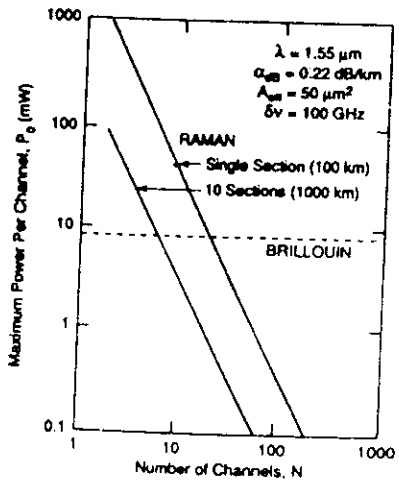

Fig. 16: Power limitations due to SRS and SBS for a multichannel WDM system (adapted from [27, 39].